The Renormalization Group Flow Analysis for a Cosmological Sector of Spin Foam Models

Dissertation

zur Erlangung des Doktorgrades

an der Fakultät für Mathematik,

Informatik und Naturwissenschaften

Fachbereich Physik

der

Universität Hamburg

vorgelegt von

Giovanni Rabuffo

Hamburg
2018

Abstract

Spin Foam Models (SFM) provide a non-perturbative and background independent path integral formulation of Quantum Gravity. The models are built on a lattice which represents spacetime and serves as a tool to control the d.o.f. of geometry. In fact, a given discretization can be thought as a scale at which we look at spacetime, while its refinement resembles a shift towards UV regimes. In the light of this interpretation, a SFM state sum is understood as an effective theory for the available degrees of freedom provided by the lattice. Then, the Wilsonian renormalization group approach stands out as an ideal tool to organize and describe the flow of the theory along a scale of complexity of the base lattice.

While many promising results have been achieved in SFM, the dynamics of these models is still hard to solve and most calculations are performed on extremely coarse discretizations. In order to get access to finer lattices we reduce the path integral state sum to certain symmetric configurations of geometry. This allows a numerical evaluation of some geometric observables on coarser and finer discretizations. Their comparison defines the renormalization group flow of the model in the parameter space. Notably, we find a fixed point with one attractive and two repulsive directions in the three-dimensional parameter space of the asymptotic Euclidean EPRL-FK Spin Foam Model. In such point, the expectation value of the observables do not depend on the lattice complexity. The existence of a fixed point opens the way to study another open problem of SFM, i.e. the continuum (infinite refinement) limit.

Zusammenfassung

Spin-Schaum Modells ermöglichen eine nicht-perturbative Pfadintegral Formulierung der Quantengravitation unabhängig von Hintergrund. Diese Modelle werden auf einem Gitter konstruiert, welches die Raumzeit repräsentiert und als Hilfsmittel dient um die Freiheitsgrade der Geometrie zu kontrollieren. Tatsächlich kann eine bestimmte Diskretisierung als Größenordnung auf welcher wir die Raumzeit betrachten, verstanden werden. Eine Verfeinerung bedeutet eine Verschiebung in den ultraviolett Bereich. In Anbetracht dieser Interpretation kann eine Spin-Schaum Zustandssumme als eine effektive Theorie für die durch das Gitter vorgegeben verfügbaren Freiheitsgrade verstanden werden. Daraus ergibt sich der Ansatz der Wilsonschen Renormierungsgruppe als ideales Hilfsmittel um den Fluss der Theorie in die Richtung einer Größenordnung an Komplexität des Grund-Gitters zu organisieren und zu beschreiben.

Während viele vielversprechende Ergebnisse mit Spin-Schaum Modellen erreicht wurden, ist die Dynamik dieser Modelle immer noch schwer zu lösen und die meisten Berechnungen werden auf extrem groben Diskretisierungen durchgeführt. Um eine feinere Gitterauflösung zu erreichen, reduzieren wir die Zustandssumme des Pfadintegrals auf gewisse symmetrische Konfigurationen der Geometrie. Dies erlaubt eine numerische Auswertung von einigen geometrischen Observablen auf gröberen und feineren Diskretisierungen. Der Vergleich von diesen definiert den Fluss der Renormierungsgruppe des Modells im Parameterraum. Bemerkenswerterweise finden wir einen Fixpunkt mit einer attraktiven und zwei repulsiven Richtungen im dreidimensionalen Parameterraum eines asymptotisch euklidischen EPRL-FK Spin-Schaum Modell. In einem solchen Punkt hängt der Erwartungswert der Observablen nicht von der Gitterkomplexität ab. Die Existenz eines solchen Fixpunktes öffnet einen neuen Weg um anderen offene Probleme des Spin-Schaum Modells wie das kontinuierliche Limit (unendliche Verfeinerung) zu studieren.

This thesis is based on the publications:

- B. Bahr, S. Klöser, G. Rabuffo, *Towards a Cosmological subsector of Spin Foam Quantum Gravity*, , Phys. Rev. D96 (2017) 086009, `arXiv:1704.03691`.

- B. Bahr, G. Rabuffo, *Deformation of the EPRL spin foam model by a cosmological constant*, Phys. Rev. D97 (2018) 086010, `arXiv:1803.01838`.

- B. Bahr, G. Rabuffo, S. Stainhaus, *Renormalization in symmetry restricted spin foam models with curvature*, `arXiv:1804.00023v2`.

Ai miei genitori e a mia sorella Claudia.

Contents

CONTENTS

Chapter 1

Introduction

Identifying a theory which is able to predict how nature behaves at the smallest distances of the Planck scale 10^{-35}m has puzzled generations of theoretical physicists. A solution to this riddle is expected to shed a new light on modern physics, whose boundaries are currently posing more questions than solutions. The great experimental achievements of the last years, especially the discovery of the Higgs boson at LHC [1] and the detection of the gravitational waves at the LIGO laboratories [2], have signed a historical decade and provided yet another confirmation of the well established Standard Model (SM) for particle physics and of the theory of General Relativity (GR).

Based on the principles of Quantum Mechanics and Special Relativity, and formulated as a Quantum Field Theory (QFT), the SM has indeed achieved the classification of all known fundamental particles and the description of electromagnetic, weak and strong fundamental forces in an organic framework [3]. These forces are the effect of dynamical gauge fields which mediate the interactions of elementary particles, also described as quantum fields.

Unanimously praised by scientists for its extraordinary elegance, to the point of being considered the most beautiful theory in physics, GR fuses the concepts of space and time into a single entity: spacetime. In the light of this paradigm shift, the gravitational force is described in a geometric framework as the curvature of spacetime. The theory has a record of staggering predictions concerning, among others, the passage of time (think gravitational time dilation [4]) and the propagation of light (see the gravitational lensing effect [5]).

These theories are so 'correct' that the best experimental tests in the history of physics e.g., the measure of the magnetic moment of the electron [6], confirm predictions made by the SM, while GR has by now entered our everyday life and its effects can be best appreciated when we get lost and we rely on our GPS [7].

Despite the success these theories do not come without critiques, open

problems and missing pieces. The Standard Model of particle physics, for example, raises conceptual questions of naturalness [8] i.e., it does not offer a clear explanation about how Nature chose the parameters of the model, including the cosmological constant. Also, the lacking description of dark matter and dark energy, among others, is hinting to a necessity of a physics beyond the Standard Model [9].

The gravitational singularities contemplated by GR could suggest that, in its current formulation, the theory is insufficient to describe what happens at extreme densities. A primordial singularity appears for example in the Big Bang theory, the prevailing cosmological model for the universe forged on Einstein's field equations [10]. A new understanding of the nature of such singularity might explain the observed high homogeneity among causally disconnected regions of space [11]. This is also known as the horizon problem. The most popular solution relies on the paradigm of a cosmic inflation [12], conjecturing an exponential expansion which stretched the primordial quantum fluctuations across the universe. A clear mechanism responsible for inflation is unknown [13]. Other singularities appear at the center of black holes. The mystery deepens around these spacetime regions, where a clear understanding of the microscopic mechanism underlying their thermodynamics is lacking [14].

Alongside these aspects, there is a desire for unification of all four fundamental forces, beyond the partial unification of electromagnetic, weak and strong forces in the SM [15].

A hope is that these open problems will find a new creative engine in the framework of a theory which unifies General Relativity with Quantum principles. These two realms, however, seem to avoid each other like oil and water. In the eyes of a theoretical physicist, this single reason is enough to feel uncomfortable and motivated to search for a solution to the problem of Quantum Gravity (QG). Many research sectors have emerged to confront this challenge.

The most conservative attitude remains within the realm of quantum field theory and studies the quantum properties of gravitational perturbations around a fixed background spacetime geometry. The major problem of this approach is that it results in a nonrenormalizable theory [16, 17]. A reason why the problems related to renormalization deserve attention is that their solutions may alter the properties of the classical action and affect the physics in remarkable ways [18]. Among other things, we know that renormalization predicts that various symmetries of the classical action must be dropped, because they are anomalous. The axial anomaly is what makes the neutral pion decay into two photons [19]. Even more, renormalization predicts that the coupling constants are not actually constants, but ultimately depend on the energy scale i.e., they are *running couplings*.

The nonrenormalizable divergences arising from the Einstein-Hilbert action

cannot be turned into a running of a finite set of couplings. Instead, the more one enters into the quantum regime, the more the theory generates new couplings. In practical terms, having a nonrenormalizable theory means that to confirm it we need to test an infinite number of coupling constants: this might be the sad conclusion of it [18].

Remaining within the realm of quantum field theory, a change of attitude towards certain fundamental assumptions e.g., about the locality of the interactions [20], may unlock new sectors that are still rather unknown. A simple way to achieve renormalizability in quantum gravity is, for example, by extending the Einstein-Hilbert action by means of higher-derivative terms [21]. However, local higher-derivative theories have a serious weakness: they are not unitary. Recent advancements in this field have overcome this problem by introducing a novel quantization prescription which makes higher derivative theories unitary [22, 23]. Recent results from the Planck mission seem to indicate that the best models of inflation are governed by an action including higher derivative terms [24].

The main limit of this conservative approach is the fact that it adopts perturbative methods and it is background dependent. In other words, it treats the gravitational field as a small perturbation around a fixed background geometry. In this sense, this is not after all the most conservative approach since it 'betrays' one of the essential principles of GR, which is the independence from any background structure. In fact, according to Einstein's interpretation, spacetime is not an absolute entity with respect to which motion is defined. Rather, it is a dynamical object and motion can only be defined in relative terms.

Then, in the language of QFT, the gravitational field as a whole (not just as a perturbation) is nothing more than a new field. Its gauge symmetry is the invariance under arbitrary differentiable coordinate transformations. Its vacuum is not empty space, it is just nothing. Matter and gauge fields should not be defined *on* spacetime, but in a relational framework as an integrated interaction *with* the gravitational field.

A different approach to the problem of quantum gravity is offered by String Theory, which studies the quantum field theory of finite-size nonlocal objects called strings [25]. Particles are identified with different oscillation modes (or quantum states) of the string. Surprisingly, one of these vibrational states corresponds to the graviton i.e., the particle which mediates the gravitational force. A theory of gravity is then naturally incorporated within this framework. At ordinary low energies, this theory roughly corresponds to GR, while at high energies it is modified. Also Yang-Mills gauge theories (like the SM) are included, however it is not yet understood how the $U(1) \times SU(2) \times SU(3)$ gauge group of the Standard Model is singled out. The potential description of gravity and all other forces in a unified mathematical framework makes

String theory a candidate for a 'theory of everything'. The consistency of String Theory requires, or predicts, the existence of supersimmetry and of ten or more spacetime dimensions. Among the main drawbacks, is the fact that there exists a huge 'landscape' of possible false string vacua, which raises technical as well as philosophical questions [26, 27]. Another criticism to string theory is that it is not *manifestly* background independent [28].

In this work we analyze another candidate theory, which has gathered attention in recent years, and attempts a formulation to quantum gravity which is explicitly background independent and non-perturbative. This goes by the name of Spin Foam Theory or Spin Foam Models (SFM) [29, 30]. Here, the gravitational field is treated in the same way as a fundamental quantum field i.e., according to the framework of quantum mechanics, made of probabilities, uncertainty principles, Hilbert spaces and so on. In this work we are concerned with the study of pure quantum gravity in the absence of matter fields. Spin foam models provide a covariant formulation for Loop Quantum Gravity (LQG) [31, 32], and it connects with several other approaches to quantum gravity such as Quantum Regge Calculus [33] , Group Field Theory [34] and Dynamical Triangulation [35], to name but a few.

1.1   An overview of Spin Foam Models

Spin Foam Models (SFM) provide a non-perturbative and background independent path integral formulation of Quantum Gravity. These models are built on a fiducial discretization of spacetime, which serves as a tool to control the d.o.f. of the gravitational field. More precisely, a spin foam is characterized by an allocation of quantum labels on a *reticulum* which plays the role of a representative for spacetime, and can be pictured as its skeleton. The labels encode the information about the geometry. Freezing their value one establishes a 'geometric configuration' which is a quantum state of the theory.

The reticular structure differs substantially e.g., from those of Lattice Gauge Theories. A first differentiation factor, compared to standard theories built on a lattice, is that here there is no definition of lattice spacing involved. Indeed, as we already pointed out, we are not seeking for a background structure on which to describe the dynamics of some field. We want the spacetime reticulum to be itself a dynamical object.

The way SFM achieve this purpose is by defining the dynamics in terms of a path integral over spacetime geometries. Roughly speaking, to get from a geometric state A to a state B, spacetime walks through all its possible configurations with a certain weight associated. In some sense this corresponds to summing over all lattice spacings (precisely, over all quantum labels).

While the 'spacings' vary, the complexity of the reticulum is kept fixed

in the number of its constituent nodes and links. The choice of a reticulum corresponds to a truncation of the theory to a certain accuracy. To capture more details of spacetime, we can use a finer reticulum which carries more degrees of freedom. In the light of this interpretation, a spin foam state sum can be understood as an effective theory for the available d.o.f. provided by the lattice. Then, the Wilsonian renormalization group (RG) approach stands out as an ideal tool to organize and describe the flow of the theory along a scale of complexity of the base lattice [36].

The idea behind Wilsonian renormalization is that the physics of a system at large scales should be independent of most microscopic (UV) details, and predictions should involve only a small portion of all the degrees of freedom of the system. Simply put, we do not need all the details about the water molecules to describe water flowing in a stream.

This approach is used in the context of QG e.g., by the Asymptotic Safety program [37]. In a QFT setting, an energy scale is defined by integrating out the high momentum (UV) modes above a certain cut-off. This operation defines an effective action which can be used to make predictions about experiments performed in a regime less energetic than the scale. The coupling constants defining this effective action depend themselves from the scale i.e., they are running couplings. In some rare point of the parameter space, it can happen that the couplings do not depend on the energy scale anymore. In these *fixed points*, independently of how many degrees of freedom we restore in the theory, the couplings do not run anymore i.e., they are scale independent.

Similar techniques are employed in the context of Lattice gauge theories, where a scale is defined by fixing a value for the lattice spacing which enforces a (UV) cut-off i.e., a smallest distance under which we forget about the degrees of freedom and work with an effective theory.

In the background independent context of SFM, there is no length scale to use as a (UV) cut-off since configurations with different geometries are being summed over. This means that on the same graph both low and high curvature (i.e., energy) states occur in the sum over states. This, as we have already mentioned, is a central feature of GR, in that geometry itself becomes a variable. Therefore, in the spin foam context the RG formalism needs to be adapted so to be independent of the spacetime background structure [38]. When we talk about renormalization in SFM we refer to what happens to the theory when we build it on finer or coarser reticles.
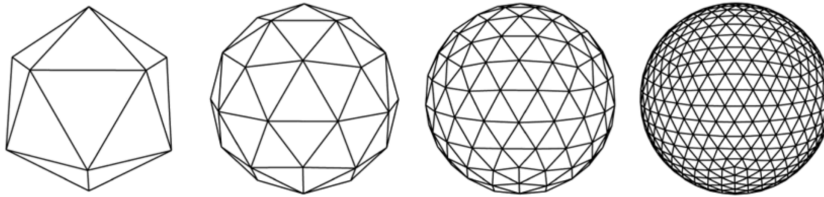
Figure 1.1: The RG flow interpolates between a scale with few degrees of freedom defined by coarse lattices and one which carries more information defined by finer reticulums.

In this sense, the renormalization group does not 'flow' with an energy scale interpolating between IR and UV regimes. Neither it flows on a scale defined by the lattice spacing since we have seen that there is none (or, more precisely, there are infinite of them summed over). It will instead flow in a scale defined by the complexity of the lattice, which we can roughly identify with the number of its nodes. A fixed point in this context indicates a region of the parameter space where the parameters are independent of the complexity of the base reticulum. The existence of a fixed point in SFM could lead towards an advancement in the thorny question of the *continuum* limit of spin foams i.e., the limit of infinite refinement of the base reticulum [1]. The final goal of this work is the definition and the analysis of the renormalization group of a specific SFM, and the search of its fixed points.

1.2   Structure of the Thesis

In Chapter 2, we focus our attention on the classical theories of gravitation, which provide the groundwork for developing the quantum theory.

In Chapter 3 we review the canonical and the covariant formulations of Loop Quantum Gravity. Depending on the quantization procedure, the covariant approach defines distinct Spin Foam Models.

In Chapter 4, we study the Euclidean formulation of the EPRL-FK spin foam model [2]. This is one of the most acclaimed SFM and is the subject of study in the rest of this work. In the same chapter we also consider an ad-hoc deformation of the model so to couple a cosmological constant term. The reported calculation is based on a recent publication of the author and collaborators [41]. The results of this section is used in the following chapters, however

---

[1] One must be careful not to confuse this with the *classical limit*, which is instead the limit where we get back to a low energy regime. The classical limit can be defined on each finite reticulum separately. Starting from a finite size reticulum one finds discrete GR in the classical limit. A missing piece of the LQG puzzle is a proof that, starting from a infinitely refined graph (continuum limit), one recovers standard GR in the classical limit. This goal can be achieved only if we understand the continuum limit of SFM.

[2] After its authors Engle, Pereira, Rovelli and Livine [39], and Freidel and Krasnov [40].

the details of the calculation are not fundamental for the understanding of the work. The reader is free to move on to the next chapter.

While many promising results have been achieved in SFM, the dynamics of these models is still hard to solve and most calculations are performed on extremely coarse discretizations. In order to get access to finer lattices, in Chapter 5 we reduce the path integral state sum to certain symmetric configurations of geometry which resembles the evolution of a flat homogeneous and isotropic universe. First, we compute the (semi)classical limit of the EPRL-FK spin foam state sum in the symmetry restricted setting. These approximations open the path to a numerical evaluation of the expectation values of geometric observables on different lattices and, ultimately, provide a setup for treating the renormalization of the EPRL-FK spin foam model (in Chapter 6). In the second part of Chapter 5, we investigate the classical dynamics associated to our reduced model in the three cases of vacuum, coupling with a cosmological constant, and with dust particles. From the discrete action we obtain the classical equations of motions and we find that in all cases, the corresponding Friedmann-Lemaitre-Robertson-Walker dynamics is recovered in the limit of fine lattices. Thus, the symmetry reduction adopted defines a cosmological sector of the EPRL-FK model. This section shows a large intersection with computations done in the context of cosmological modeling with discrete gravity. All the results presented in this chapter are an original work of the author and collaborators published in [42].

In Chapter 6, we review the concept of background independent renormalization for Spin Foam Models. Then, based on a recent work of the author and collaborators [43], we study the renormalization group flow of the approximated model obtained in the previous chapter (the EPRL-FK spin foam model, symmetry reduced, deformed by a cosmological constant, and used in its asymptotic limit). The reduction of degrees of freedom allows a numerical evaluation of certain geometric observables on coarser and finer discretizations. Their comparison defines the renormalization group (RG) flow in the parameters (α, Λ, G) of the model. Remarkably, we find the indications of a fixed point showing one repulsive and two attractive directions. In such point, the expectation value of the observables do not depend on the lattice complexity. Thus, its the existence opens the way to study another open problem of SFM, i.e. the continuum (infinite refinement) limit.

In Chapter 7 we conclude with an overview of the results.

Chapter 2

Classical Theories of Gravity

In this chapter we discuss the formalism of smooth curved surfaces and introduce the classical principles of General Relativity (GR).

In the first part, we study some of the main formulations of GR. Namely, after the standard metric approach is discussed, we explore the action formulations in the tetrad formalism as well as in terms of a constrained topological 'BF-theory'. Next, we move to the description of the Hamiltonian approach in the Arnowitt-Deser-Misner (ADM) formalism as well as in terms of the Ashtekar variables.

In the second part, a discrete formulation of gravity which goes by the name of Regge Calculus is studied. The Regge action, defining the classical dynamics of the discrete spacetime surface, will show up often in this work, primarily in the (semi)classical limit of the quantum theory. Also, we introduce the concepts of 2-complex and graph, basic discrete structures which respectively form a skeleton for spacetime and its boundary geometry. On their bones we distribute the smooth variables of BF-theory and those of the Ashtekar formulation. This provides the classical groundwork from which we build and develop the quantum theory in Chapter 3.

2.1   General Relativity

Classical General Relativity describes the spacetime structure as a four dimensional differentiable manifold $\mathcal{M}$. On this object we are interested in defining concepts which are independent of the choice of a reference frame. This property ensures that the *general covariance* principle is respected and we can study the physics of gravitational fields in arbitrary coordinate systems. On a differentiable manifold we can define tensor calculus and formulate the physical laws as tensorial equations. Although one can define vectors and tensors as abstract geometric entities, in the following we use an equivalent but more practical approach. Intuitively, to each point $p \in \mathcal{M}$ we can associate a *tan-*

gent space T_p and a *cotangent space* T_p^*, which are both real, four-dimensional vector spaces isomorphic to each other. Given a chart of coordinates x^μ, at each point we can set up a basis $\{\partial_\mu\}$ for T_p and a basis $\{\mathrm{d}x^\mu\}$ for T_p^* , with $\mu = 0, 1, 2, 3$. Then any abstract vector $\boldsymbol{v} \in T_p$ and 1-form $\boldsymbol{\omega} \in T_p^*$ can be written as a linear combination of elements of the respective basis

$$\boldsymbol{v} = v^\mu \partial_\mu, \qquad \boldsymbol{\omega} = \omega_\mu \mathrm{d}x^\mu.$$

The coefficients v^μ and ω_μ are respectively the components of the vector $\boldsymbol{v}$ and of the 1-form $\boldsymbol{\omega}$. Here, we treat the components v^μ and ω_μ as fundamental objects, denoting them respectively as *contravariant* and *covariant vectors*.

Under a change of frame $x^\mu \to x'^\mu(x)$, the differentials $\mathrm{d}x^\mu$ transform as

$$\mathrm{d}x^\mu \to \mathrm{d}x'^\mu = \frac{\partial x'^\mu}{\partial x^\nu} \mathrm{d}x^\nu.$$

In general, a contravariant vector is defined as a set of four numbers that, under a generic change of frame, transform as the differential of the coordinates

$$A^\mu \to A'^\mu = \frac{\partial x'^\mu}{\partial x^\nu} A^\nu.$$

Conversely, we define a covariant vector as a quantity that transforms with the inverse

$$A_\mu \to A'_\mu = \frac{\partial x^\nu}{\partial x'^\mu} A_\nu.$$

We call *tensor of rank* (p, q) an object $T^{\mu_1 \cdots \mu_p}_{\nu_1 \cdots \nu_q}$ with p *contravariant* indices and q *covariant* indices, which transforms as

$$T^{\mu_1 \cdots \mu_p}_{\nu_1 \cdots \nu_q} \to T'^{\mu_1 \cdots \mu_p}_{\nu_1 \cdots \nu_q} = \frac{\partial x'^{\mu_1}}{\partial x^{\rho_1}} \cdots \frac{\partial x'^{\mu_p}}{\partial x^{\rho_p}} \frac{\partial x^{\sigma_1}}{\partial x'^{\nu_1}} \cdots \frac{\partial x^{\sigma_q}}{\partial x'^{\nu_q}} T^{\rho_1 \cdots \rho_p}_{\sigma_1 \cdots \sigma_q}.$$

The relative distance between events i.e., spacetime points on $\mathcal{M}$, is specified by the *metric tensor* $g_{\mu\nu}$. It defines the *line element* i.e., the square of the infinitesimal displacement as

$$\mathrm{d}s^2 = g_{\mu\nu} \mathrm{d}x^\mu \mathrm{d}x^\nu. \tag{2.1}$$

Applying the metric tensor and its inverse to a generic tensor, we can switch from contravariant to covariant indices and vice versa

$$V_\mu = g_{\mu\nu} V^\nu, \qquad V^\mu = g^{\mu\nu} V_\nu, \qquad T_{\mu\nu} = g_{\mu\rho} g_{\nu\sigma} T^{\rho\sigma}, \quad \text{etc...}$$

In a mathematical language, the *equivalence principle* states that, given a spacetime point, it always exists an *inertial frame of reference* i.e., a coordinate patch in which $\mathrm{d}s^2$ assumes the Minkowskian form

$$\mathrm{d}s^2 = \eta_{\mu\nu} \mathrm{d}x^\mu \mathrm{d}x^\nu.$$

Nevertheless, in a curved space it is not possible to change $g_{\mu\nu}$ into $\eta_{\mu\nu}$ throughout all spacetime points via a coordinate transformation.

In order to compare geometries at different spacetime points, one requires an unambiguous way to '*parallel transport*' objects along curves in $\mathcal{M}$. This is achieved by introducing a *connection* on $\mathcal{M}$, determined by a set of functions of the coordinates $\Gamma^{\rho}_{\mu\nu}$ called *Christoffel symbols*, which vanish in an inertial frame of reference. In terms of these objects one can define the covariant derivative ∇_{μ}, which acts on tensors as

$$
\begin{aligned}
\nabla_{\mu}V^{\nu} &= \partial_{\mu}V^{\nu} + \Gamma^{\nu}_{\rho\mu}V^{\rho}, \\
\nabla_{\mu}V_{\nu} &= \partial_{\mu}V_{\nu} - \Gamma^{\rho}_{\nu\mu}V_{\rho}, \\
\nabla_{\mu}T^{\rho\sigma} &= \partial_{\mu}T^{\rho\sigma} + \Gamma^{\rho}_{\nu\mu}T^{\nu\sigma} + \Gamma^{\sigma}_{\nu\mu}T^{\rho\nu}, \\
&\cdots
\end{aligned}
\tag{2.2}
$$

The covariant derivative generalizes the derivative operator on curved spaces so to be independent of the the choice of coordinate system.

The commutator of two covariant derivatives

$$
(\nabla_{\rho}\nabla_{\nu} - \nabla_{\nu}\nabla_{\rho})V_{\mu} = R^{\sigma}_{\mu\rho\nu}V_{\sigma},
\tag{2.3}
$$

defines the Riemann tensor

$$
R^{\sigma}_{\mu\rho\nu} = \partial_{\rho}\Gamma^{\sigma}_{\mu\nu} - \partial_{\nu}\Gamma^{\sigma}_{\mu\rho} + \Gamma^{\sigma}_{\rho\lambda}\Gamma^{\lambda}_{\mu\nu} - \Gamma^{\sigma}_{\nu\lambda}\Gamma^{\lambda}_{\mu\rho},
\tag{2.4}
$$

which encodes the information about the *curvature* of spacetime. In fact, if we parallel transport a vector along an infinitesimal closed path γ, its variation is proportional to the product of the Riemann tensor and the area of the surface enclosed by γ. Contracting the Riemann tensor with the metric tensor we obtain the Ricci tensor $R_{\mu\nu} = R^{\rho}_{\mu\rho\nu}$ and a further contraction produces the scalar curvature $R = g^{\mu\nu}R_{\mu\nu}$.

On a manifold one can also define the concept of *torsion* which formally measures how tangent vectors rotate when they are parallel transported. In its original formulation, GR adopts the torsionless assumption, which is reflected in the symmetry of the Christoffel symbols in the lower indices in any coordinate basis

$$
\Gamma^{\rho}_{\mu\nu} = \Gamma^{\rho}_{\nu\mu}.
\tag{2.5}
$$

Also we demand that parallel transported vectors maintain the value of their scalar product. This property is called *metric compatibility* and mathematically is represented by the vanishing of the covariant derivative of the metric tensor

$$
\nabla_{\mu}g_{\nu\rho} = 0.
\tag{2.6}
$$

With these assumptions, the only torsionless, metric compatible connection is the Levi-Civita connection, and the Christoffel symbols can be expressed in terms of the metric tensor as

$$\Gamma^{\rho}_{\mu\nu} = \frac{1}{2}g^{\rho\lambda}(\partial_\mu g_{\nu\lambda} + \partial_\nu g_{\mu\lambda} - \partial_\lambda g_{\mu\nu}). \tag{2.7}$$

General Relativity is a theory which describes the dynamics of the spacetime manifold and it comes with different formulations.

2.1.1 Standard Formulation

A theory of gravitation can be formulated by using the metric tensor as a dynamical variable. We assume that its dynamics is regulated by a variational principle based on an action functional S, which is invariant under diffeomorphisms

$$x^\mu \to x'^\mu = x^\mu + \xi^\mu,$$

where $\xi^\mu(x)$ are four local parameters. To define such a functional, we must integrate scalar quantities, using the invariant measure $\mathrm{d}^4 x \sqrt{-g}$, where we have defined the determinant of the metric tensor $g = \det(g_{\mu\nu})$.

In its original formulation the dynamics of the metric tensor is encoded in the Einstein-Hilbert action

$$S_{\text{Einstein−Hilbert}}[g_{\mu\nu}] = \frac{1}{16\pi G} \int \sqrt{-g}R[g_{\mu\nu}], \tag{2.8}$$

where G is the gravitational constant with dimension $[G] = -2$ in units of mass. [1]

The Einstein equations of motion for a gravitational field coupled to bosonic matter are

$$R_{\mu\nu} - \frac{1}{2}g_{\mu\nu}R = 8\pi G T_{\mu\nu}, \tag{2.9}$$

where $T_{\mu\nu}$ is the covariant version of the energy-momentum tensor which describes the density and flux of energy and momentum in spacetime.

2.1.2 Tetrad Formalism

The *tetrad* is a collection of four linearly independent one-forms e^I_μ that provides a local isomorphism between a general reference frame and an inertial

---

[1]In principle one could include in the action infinite invariant terms $1, R^2, R_{\mu\nu}R^{\mu\nu}, R^3, \cdots$. These include a cosmological constant term as well as terms which are more than quadratic in the derivatives of the metric tensor. In what follows we stick to the classical formulation and ignore all these terms. Nonetheless, in Chapter 6 we will modify the theory at the quantum level so to re-introduce a cosmological constant term.

one, characterized by the flat metric δ_{IJ} [2], so that we can recast the metric tensor in the form

$$g_{\mu\nu}(x) = \delta_{IJ} e^I_\mu(x) e^J_\nu(x).$$

This is why the tetrads are sometimes described as the square root of the metric. The new indices $I = 0, 1, 2, 3$ are then internal flat indices and come together with an additional invariance under a local gauge group G e.g., $SO(3,1)$ in the Lorentzian theory or $SO(4)$ in the Euclidean one. We can interpret geometrically the tetrads as the linear map that, for each point $p \in \mathcal{M}$, sends the tangent space T_p in the flat space. Then, given a vector $\boldsymbol{v}$ in p, the tetrads are the matrices $e^I_\mu(x)$ that transform the components V^μ (i.e., contravariant vectors) into new components V^I by

$$V^I = e^I_\mu(x) V^\mu.$$

The inverse of the tetrad is a collection of four linearly independent vectors e^I_μ such that

$$e^I_\mu e^\mu_J = \delta^I_J, \qquad e^I_\mu e^\nu_I = \delta^\nu_\mu. \tag{2.10}$$

Then, any tensor can be decomposed using internal or spacetime coordinates related by the tetrads and their inverse i.e.,

$$T^{I_1 \cdots I_p}_{J_1 \cdots J_q} = e^{I_1}_{\mu_1} \cdots e^{I_p}_{\mu_p} e^{\nu_1}_{J_1} \cdots e^{\nu_q}_{J_q} \, T^{\mu_1 \cdots \mu_p}_{\nu_1 \cdots \nu_q}. \tag{2.11}$$

Related to the local gauge symmetry there is a connection ω^{IJ}_μ which is used to define the covariant derivative ∇_μ on any object that transforms under the local gauge group. For example,

$$\nabla_\mu V^I = \partial_\mu V^I + \omega^I_{\mu J} V^J. \tag{2.12}$$

The components $\omega^I_{\mu\ J}$ are related to the coefficients $\Gamma^\rho_{\mu\nu}$ of the Levi-Civita connection via

$$\partial_\mu e^I_\nu + \omega^I_{\mu J} e^J_\nu - \Gamma^\rho_{\mu\nu} e^I_\rho = \nabla_\mu e^I_\nu = 0, \tag{2.13}$$

where $\nabla_\mu e^I_\nu$ is the total covariant derivative of the tetrad i.e., the one acting on both spacetime and internal group indices. Its vanishing corresponds to the condition of compatibility of the connection $\omega^I_{\mu\ J}$ with the internal metric i.e., $\nabla_\mu \eta^{IJ} = 0$. One can easily check this by writing $\eta^{IJ} = e^I_\mu e^J_\nu g^{\mu\nu}$ and using the metric compatibility (2.6). Under this condition, $\omega^I_{\mu\ J}$ is the unique *spin connection* that we can write as a function of the tetrads.

---

[2]For the moment we keep the flat metric generic. Depending whether we are studying the Lorentzian theory or the Riemannian, we should pick up the Minkowski metric η_{IJ} or the positive defined Euclidean metric.

Moving from the coordinate basis to the differential form notation [3], we write $e^I = e^I_\mu \mathrm{d}x^\mu$ and $\omega^{IJ} = \omega^{IJ}_\mu \mathrm{d}x^\mu$. Then, the curvature is defined as the 2-form

$$F^{IJ} \equiv \nabla\omega^{IJ} \equiv \mathrm{d}\omega^{IJ} + \omega^I_K \wedge \omega^{KJ}, \qquad (2.14)$$

where we used the exterior derivative d, the wedge product $\wedge$ and the covariant derivative ∇ associated to the connection. In coordinates we write $F^{IJ} = F^{IJ}_{\mu\nu}\mathrm{d}x^\mu \wedge \mathrm{d}x^\nu$ with

$$F^{IJ}_{\mu\nu} = \partial_\mu \omega^{IJ}_\nu - \partial_\nu \omega^{IJ}_\mu + \omega^I_{\ \mu\ K}\omega^{KJ}_\nu - \omega^I_{\ \nu\ K}\omega^{KJ}_\mu. \qquad (2.15)$$

These are related to the Riemann tensor via

$$R^\mu_{\nu\rho\sigma} = e^\mu_I e^J_\nu F^I_{\mu\nu J}. \qquad (2.16)$$

The action (2.8) can be rewritten in the Palatini first order formulation i.e., using tetrads and connection as independent dynamical variables, as

$$\begin{aligned}
S_{\text{Palatini}}[e,\omega] &= \frac{1}{16\pi G} \int \epsilon_{IJKL}\ e^I \wedge e^J \wedge F^{KL}[\omega] \\
&= \frac{1}{16\pi G} \int *(e \wedge e) \wedge F[\omega],
\end{aligned} \qquad (2.17)$$

where ϵ_{IJKL} is a completely antisymmetric object such that $\epsilon^{0123} = 1 = -\epsilon_{0123}$, and $*$ is the hodge dual operator. One can check that the equations of motion for ω^{IJ} enforce the vanishing of torsion i.e.,

$$T^I = \nabla e^I = \mathrm{d}e^I + \omega^I_K \wedge e^K = 0. \qquad (2.18)$$

In fact, writing this equation in coordinates and using (2.13), one can check that it corresponds to the symmetry of the Christoffel symbols $\Gamma^\rho_{\mu\nu}$ in the lower indices (2.5). Equation (2.18) is uniquely solved by the spin connection $\omega[e]$ which, based on (2.13), is a function of the tetrad.

The equations of motion for the tetrad e^I, evaluated on-shell requiring (2.18), return the vacuum Einstein equations (2.9), corresponding to the vanishing of curvature $F[\omega[e]] = 0$.

It is possible to add a topological 'Holst' term to the Palatini action so that we get the more general

$$S_{\text{Holst}}[e,\omega] = \frac{1}{16\pi G} \int \left(*(e \wedge e) + \frac{1}{\gamma} e \wedge e \right) \wedge F[\omega], \qquad (2.19)$$

where γ is called Barbero-Immirzi parameter. The first term in the parentheses defines the Palatini action. The second is a topological sector in the sense

---

[3]Refer to [44] for an introduction.

that it does not alter the classical equations of motion. In fact its variation with respect to the tetrads vanishes if there is no torsion i.e., as long as we are on-shell [4]. Nevertheless, as we will see in the next chapter, the topological term gives a substantial contribution in the quantum domain and the Barbero-Immirzi parameter will play a crucial role in the definition of LQG and Spin Foam Models.

2.1.3 Gravity as Constrained BF-Theory

The theory of gravitation that we have studied above can be related to a rather general set of topological field theories which go by the name of BF-theory. On a D-dim manifold the dynamical variables are a connection 1-form $\omega(x) = \omega_a^I(x)\mathrm{d}x^a \tau_I$ and a $(D-2)$-form $B(x) = B_{a_1,\cdots,a_{D-2}}^I(x)\mathrm{d}x^{a_1} \wedge \cdots \wedge \mathrm{d}x^{a_{D-2}} \tau_I$, both with values a the Lie-algebra $\mathfrak{g}$ with generators τ_I. For the moment, we just require the corresponding gauge group G to be a generic finite dimensional Lie group. The BF action is

$$\begin{aligned} S_{\mathrm{BF}}[B,\omega] &= \int \langle B, F[\omega] \rangle \\ &= \int \delta_{IJ} B^I \wedge F^J[\omega] \\ &= \int B \wedge F[\omega], \end{aligned} \qquad (2.20)$$

being $F[\omega] = \nabla\omega$ the curvature of the connection. The B field acts as a Lagrange multiplier which enforces the curvature F of the connection to vanish i.e.,

$$\frac{\delta S_{\mathrm{BF}}}{\delta B} = 0 \quad \Rightarrow \quad F[\omega] = 0. \qquad (2.21)$$

On-shell, in absence of boundary, the equations of motion for ω are instead

$$\frac{\delta S_{\mathrm{BF}}}{\delta \omega} = 0 \quad \Rightarrow \quad \nabla B = 0 \quad \Rightarrow \quad \mathrm{d}B = 0. \qquad (2.22)$$

Let ϕ be a generic $\mathfrak{g}$-valued $(D-3)$-form. The action (2.20) is invariant under a gauge symmetry $\tilde{B} \equiv B + \nabla\phi$. In fact, using the Bianchi identity $\nabla F = 0$ and the vanishing of boundary, by partial integration we get

$$\int \langle \tilde{B}, F \rangle = \int \langle B, F \rangle + \int \langle \nabla\phi, F \rangle = \int \langle B, F \rangle. \qquad (2.23)$$

Locally, a general solution of the equations of motion (2.22) is $B = \mathrm{d}\phi$ and it is always possible to gauge transform this solution into $B = 0$. Since we can

---

[4]One can check this by using the Bianchi identity $\epsilon^{\mu\nu\rho\sigma} R_{\mu\nu\rho\delta} = 0$.

gauge away any local degrees of freedom, BF is called a topological field theory.

In three dimensions BF-theory with gauge group SU(2) is equivalent to GR, which is indeed a topological theory in $3d$. The B-field is a 1-form and we can define a metric as $g_{ab} = \delta_{ij}B_a^i B_b^j$, where $i = 1, 2, 3$ are indices associated to the generators J_i of the Lie algebra of SU(2). The equations of motion for B imply that ω is the Levi-Civita connection of g_{ab} and the equations of motion of ω impose the flatness of the metric [45].

In four dimensions instead, GR can be written as a topological BF-theory with constraints e.g., on the B field. Let us focus on the Euclidean theory with local gauge group $SO(4)$ or, rather, its double cover $\text{Spin}(4) \simeq \text{SU}(2) \times \text{SU}(2)$. The B-field is an element in the algebra $\mathfrak{spin}(4) \simeq \mathfrak{su}(2) \oplus \mathfrak{su}(2) \simeq \mathbb{R}^4 \wedge \mathbb{R}^4$. In the light of the last isomorphism, the B-field is also a *bivector* (see Appendix A). Then we can write its internal components B^{IJ} using indices $I, J = 0, 1, 2, 3$.

The constraints are formally implemented by adding to the set of variables a Lagrange multiplier tensor λ_{IJKL} with indices in the internal space such that $\lambda_{IJKL} = \lambda_{KLIJ} = -\lambda_{JIKL} = -\lambda_{IJLK}$ and satisfying $\epsilon^{IJKL}\lambda_{IJKL} = 0$. Writing explicitly the Lie algebra indices the resulting Plebanski action is

$$S_{\text{Plebanski}}[B, \omega, \lambda] = \int B^{IJ} \wedge F_{IJ}[\omega] + \lambda_{IJKL}B^{IJ} \wedge B^{KL}, \qquad (2.24)$$

and the *simplicity constraints* imply

$$B^{IJ} \wedge B^{KL} \propto \epsilon^{IJKL}, \qquad (2.25)$$

or, in the dual version and using spacetime coordinates (see [30])

$$\epsilon_{IJKL}B_{\mu\nu}^{IJ}B_{\rho\sigma}^{KL} \propto \epsilon_{\mu\nu\rho\sigma}. \qquad (2.26)$$

As it was shown in [46], this quadratic expression has two solutions

$$B = \pm * (e \wedge e) \quad \text{and} \quad B = \pm(e \wedge e), \qquad (2.27)$$

which define a *gravitational* and a *topological sector* given that, once substituted in (2.24) they respectively recover the Palatini action and the Holst term of (2.19).

In fact, if these two sectors are related via the Barbero-Immirzi parameter in a way such that we can write

$$(16\pi G)B \equiv *(e \wedge e) + \frac{1}{\gamma}e \wedge e, \qquad (2.28)$$

then it is clear that BF action (2.20) reduces to the Holst-Palatini (2.19).

There exists also a boundary formulation for the condition (2.28). Let us consider a manifold with a 3d spacelike boundary $\partial \mathcal{M} = \Sigma$. Here the invariance under 4d rotations is broken down to an invariance under local $SO(3)$ rotations. In other words, on the boundary we have the freedom of choosing a gauge fixing that induces this group breaking. It is convenient to work in the time gauge defined by requiring that the normal to all the tangent vectors in Σ is a time-like unit vector $n_I = (1, 0, 0, 0)$ i.e., the local boundary corresponds to a spatial surface at fixed time. The 2-form B^{IJ} can be projected on this boundary and decomposed as $K^I = n_J B^{IJ}$ and $L^I = n_J (*B)^{IJ} = \epsilon^{IJKL} n_J B_{KL}$. These vectors have no time component i.e., $n_I K^I = n_I L^I = 0$. In other words the B-field bivector is reduced in the time gauge to two vectors on the boundary

$$K^i = B^{i0} \qquad \text{and} \qquad L^i = \frac{1}{2} \epsilon^i_{jk} B^{jk}, \tag{2.29}$$

with $i = 1, 2, 3$. One can check that the imposition (2.28) implies that on the boundary Σ is satisfied the condition

$$\vec{L} \equiv \frac{1}{\gamma} \vec{K}. \tag{2.30}$$

We will come back to this formula in the next section where the formulation of the constraints will be a hot topic.

2.1.4 Hamiltonian formulation in ADM variables

Let us now continue our fly over classical formulations of GR but now in the Hamiltonian formalism, which provides a road to quantization as done in non relativistic quantum mechanics and also in relativistic field theory [5]. Eventually, this will be the basis of the canonical formulation of LQG.

The canonical analysis of GR is based on a 3+1-decomposition of the space-time manifold into a foliation $\mathcal{M} = \Sigma_t \times \mathbb{R}$ in terms of hypersurfaces Σ_t, labeled by a real parameter t.

Each spatial slice Σ_t is equipped with its own Riemannian structure. Let us call n_μ the unit vector normal to all the vectors tangent to Σ_{t_0}. The induced metric $q_{\mu\nu}$ on Σ_t can be uniquely determined by demanding that $q_{\mu\nu} n^\nu = 0$ and $q_{\mu\nu} s^\nu = g_{\mu\nu} s^\nu$ for any vector s^ν spanning the tangent space of Σ_t. Then, one has

$$q_{\mu\nu} = g_{\mu\nu} + n_\mu n_\nu, \quad n_\mu n^\mu = -1. \tag{2.31}$$

---

[5]For a detailed introduction on the Hamiltonian analysis of GR and of covariant systems in general see for example [47]. There, one can also find an explicit derivation of the formulas appearing in the next two subsections

The diffeomorphism which maps Σ_{t_0} into Σ_{t_0+t} is generated by a *time-evolution* vector field $t = t^\mu \nabla_\mu$. This defines the direction of time derivatives and is normalized such that $t^\mu \nabla_\mu t = 1$. A choice of t_μ satisfying the above requirements is not unique, and allows for some arbitrariness. A convenient choice of reference system is made in terms of the Arnowit-Deser-Misner (ADM) variables.

One introduces a function $N \equiv n_\mu t^\mu$ and a vector field $N_\mu \equiv h_{\mu\nu} t^\nu$ so that the time vector field can be decomposed into the spatial and normal parts as

$$t^\mu = N n^\mu + N^\mu. \tag{2.32}$$

In this coordinates one has

$$t^\mu = (1, 0, 0, 0), \quad N^\mu = (0, N^a), \quad n_\mu = (-N, 0, 0, 0), \quad n^\mu = (\frac{1}{N}, -\frac{N^a}{N}). \tag{2.33}$$

The ADM variables are the spatial 3-metric q_{ab}, the *lapse* function N and the *shift* vector field N_a, where $a = 1, 2, 3$ are space indices that behave like regular indices in a curved space. They have a clear interpretation: let us stand on Σ_t at a point $x^\mu = (t, x^a)$. The distance that separates us from any other point in Σ_t is determined by the spatial 3-metric q_{ab}. Now, if we move by $N dt$ in the direction of the time-like vector n^μ normal to all tangent vectors in Σ_t, we end up on Σ_{t+dt} at a point $y'^\mu = (t + dt, y^a)$. If we further shift on the Σ_{t+dt} surface by $N_a dt$ we arrive to the point $x'^\mu = (t + dt, x^a)$ which in our coordinates is the time evolution of x^μ. Thus the lapse function $N = N(x^\mu)$ determines how the proper time $d\tau = N dt$ elapses for an observer moving from Σ_t to Σ_{t+dt}. The shift vector field $N_a = N_a(x^\mu) = x^a - y^a$ measures instead the spatial shift on Σ_{t+dt}.

One can rewrite the manifold structures in the ADM variables. The full spacetime metric reads

$$g_{\mu\nu} = \begin{pmatrix} N^a N_a - N^2 & N_a \\ N_b & q_{ab} \end{pmatrix}. \tag{2.34}$$

The extrinsic curvature of Σ_t reads

$$K_{ab} = \frac{1}{2N}(\dot{q}_{ab} - \nabla_a N_b - \nabla_b N_a), \tag{2.35}$$

being ∇_a the spatial covariant derivative. This can also be regarded as an *evolution equation* for the spatial metric.

The ADM decomposition is particularly useful since no time derivatives of N and N_a appear in the action and hence they correspond to non-propagating fields that enforce constraints. In other words they play the role of Lagrange multipliers. Therefore all the dynamics of the gravitational field is contained in the 3-metric q_{ab} and its conjugate momentum

$$\pi^{ab} = \frac{\sqrt{q}}{16\pi G}(K^{ab} - K^c{}_c q^{ab}), \tag{2.36}$$

where $q = \det(q_{ab})$. They satisfy the canonical Poisson brackets

$$\{q_{ab}(t,x), \pi^{cd}(t,y)\} = \frac{1}{2}(\delta_a^c\delta_b^d + \delta_b^c\delta_a^d)\delta^{(3)}(x-y),$$
$$\{q_{ab}(t,x), q_{cd}(t,y)\} = 0, \tag{2.37}$$
$$\{\pi^{ab}(t,x), \pi^{cd}(t,y)\} = 0.$$

The action with ADM variables takes then the totally constrained form

$$S_{\text{ADM}}(N, N_a, q, \pi) = \frac{1}{16\pi G}\int \mathrm{d}t \int \mathrm{d}^3 x(\pi^{ab}\dot{q}_{ab} - NC(\pi,q) - N^aC_a(\pi,q)). \tag{2.38}$$

The *Hamiltonian constraint* is

$$C(\pi, q) = (16\pi G)G_{abcd}\pi^{ab}\pi^{cd} - \frac{\sqrt{q}R[q]}{16\pi G}, \tag{2.39}$$

where we defined the Wheeler-DeWitt metric $G_{abcd} = \frac{1}{2\sqrt{q}}(q_{ac}q_{bd} + q_{ad}q_{bc} - q_{ab}q_{cd})$ and $R[q]$ is the Riemann curvature scalar on Σ_t. The *diffeomorphism constraint* reads

$$C_a(\pi, q) = -2q_{ac}\nabla_b\pi^{bc}. \tag{2.40}$$

The equations of motion for lapse and shift respectively enforce these constraints i.e.,

$$C(\pi, q) \overset{!}{=} 0, \qquad C_a(\pi, q) \overset{!}{=} 0. \tag{2.41}$$

The Hamiltonian of GR in the ADM variables is

$$H = \frac{1}{16\pi G}\int \mathrm{d}^3 x(NC + N^aC_a), \tag{2.42}$$

and it vanishes when the constraint equations are satisfied. Thus, strictly speaking, in such system time is not a physical quantity but a free parameter. Then, evolution must be interpreted in a relational way. Explicitly, the 6 degrees of freedom of q_{ab} are halved by the diffeomorphism constraint and the dynamics is encoded in the Hamiltonian constraint, as a relation among the remaining 3 degrees of freedom. Eventually, at each point in space one has 2 degrees of freedom as expected.

Starting from (2.37) one can also show that the constraints satisfy the following relations [48] [6]

$$\{C_a(x), C_b(y)\} = C_a(y)\partial_b^{(x)}\delta(x-y) - C_b(x)\partial_a^{(y)}\delta(x-y),$$
$$\{C_a(x), C(y)\} = C(x)\partial_a^{(x)}\delta(x-y), \tag{2.43}$$
$$\{C(x), C(y)\} = C^a(y)\partial_a^{(x)}\delta(x-y) - C^a(y)\partial_a^{(y)}\delta(x-y).$$

---

[6]Notice that this does not constitutes a Lie algebra. In fact, raised and lowered spacetime indices imply a dependence on the metric tensor.

These Poisson brackets vanish on the constraint surface, which catalogs the constraints as *first class*. The Poisson brackets of the constraints with the dynamical variables q_{ab} and π^{cd} generate infinitesimal gauge transformations. The Hamiltonian constraint C associated to the lapse function generates time reparametrizations. The diffeomorphism constraint C_a associated to the shift function gives rise to changes of spatial coordinates. Points in the phase space related by these transformations are physically equivalent.

2.1.5   Hamiltonian formulation in Ashtekar variables

There exists a change of variables that makes the Hamiltonian formulation of GR very close to that of SU(2) gauge theory, apart from the unavoidable fact that the Hamiltonian is a fully constrained one. This turns out to be quite useful in that it makes possible the use of tools borrowed from Yang-Mills theories.

In each point of the Cauchy surface Σ_t a reference frame is specified by the triads e_a^i, where $i = 1, 2, 3$ are internal indices which behave like indices of flat-space. The spatial 3-metric q_{ab} can be expressed in terms of the triads as

$$q_{ab} = \delta_{ij} e_a^i e_b^j. \tag{2.44}$$

The dynamics on a slice Σ_t is invariant under local SO(3) transformations of the triad or, more generally, under its double cover SU(2). The new dynamical variables are the *densitized triad*

$$E_i^a = \det(e) e_i^a = \frac{1}{2} \epsilon_{ijk} \epsilon^{abc} e_b^j e_c^k, \tag{2.45}$$

and a $\mathfrak{su}(2)$-connection on Σ_t called *Ashtekar connection*

$$A_a^i = \Gamma_a^i + \gamma K_a^i, \tag{2.46}$$

where $\Gamma_a^i = \Gamma_a^i[e]$ is the torsionless spin connection associated to the triad, γ is the Barbero-Immirzi parameter already introduced in the tetrad formulation of GR while K_a^i is related to the extrinsic curvature K_{ab} of Σ_t and to the densitized triad via

$$K_a^i = \frac{K_{ab} E_j^b \delta^{ij}}{\sqrt{\det E}}, \tag{2.47}$$

with $\det E = \det(E_k^c)$.

Let us notice that, on a spatial slice, the metric is fully specified by the densitized triad. Then, any geometric quantity in space can be written in

terms of E_i^a. For example, the area of a surface S on Σ_t with local coordinates σ_1, σ_2 and normal unit vector n_a is a functional [7]

$$\alpha(S) = \int_S \mathrm{d}^2\sigma \sqrt{E_i^a E^{bi} n_a n_b}.$$ (2.50)

Also, given a region $R \subset \Sigma_t$ we can write its volume as

$$V(R) = \int_R \mathrm{d}^3x \sqrt{g} = \int_R \mathrm{d}^3x \sqrt{|\frac{1}{3!}\epsilon_{abc}\epsilon^{ijk}E_i^a E_j^b E_k^c|}.$$ (2.51)

We will come back to these expressions in the quantum theory, where areas and volumes will become operators and the solution of their eigenvalue problem will show that in the quantum regime geometric quantities come in discrete levels.

The pair (A_a^i, E_i^a) forms a set of canonically conjugated variables fulfilling the Poisson brackets

$$\{A_a^i(x), E_j^b(y)\} = 8\pi G\gamma \delta_j^i \delta_a^b \delta(x, y),$$
$$\{A_a^i(x), A_b^j(y)\} = 0,$$ (2.52)
$$\{E_i^a(x), E_j^b(y)\} = 0.$$

Once again, the general covariance of the theory is manifest in the totally constrained form of the dynamics of the Ashtekar variables. The action can be written as

$$S_{\text{Ashtekar}}(N, N_a, A, E) = \frac{1}{16\pi G}\int \mathrm{d}t \int \mathrm{d}^3x(\dot{A}_a^i E_i^a - NC - N^a C_a - A_0^i C_i).$$ (2.53)

The Hamiltonian and the diffeomorphism constraints take the form

$$C = \frac{E^{aj}E^{bk}}{\sqrt{\det E}}\left(\epsilon_{ijk}F_{ab}^i - 2(1+\gamma^2)K_{[a}^i K_{b]}^j\right),$$
$$C_a = E_k^b F_{ba}^k - (1+\gamma^2)K_a^i C_i,$$ (2.54)

---

[7]In fact, the area in terms of the 3-metric is

$$\alpha(S) = \int_S \mathrm{d}\sigma_1\mathrm{d}\sigma_2 \sqrt{\det\left(q_{ab}\frac{\partial x^a}{\partial \sigma^u}\frac{\partial x^b}{\partial \sigma^v}\right)}, \qquad u, v = 1, 2$$ (2.48)

With few manipulations, using the relations $q_{ab}q_{cd} - q_{ac}q_{bd} = \frac{1}{2}\epsilon_{ace}\epsilon_{bdf}qq^{ef}$ and the definition of the normal unit vector to the surface $n_e = \epsilon_{eab}\frac{\partial x^a}{\partial \sigma^1}\frac{\partial x^b}{\partial \sigma^2}$, we obtain

$$\alpha(S) = \int_S \mathrm{d}\sigma_1\mathrm{d}\sigma_2 \sqrt{gg^{ab}n_a n_b} = \int_S \mathrm{d}\sigma_1\mathrm{d}\sigma_2 \sqrt{e^2 e_i^a e^{bi} n_a n_b} = \int_S \mathrm{d}^2\sigma \sqrt{E_i^a E^{bi} n_a n_b}.$$ (2.49)

being

$$F_{ab}^i = \partial_a A_b^i - \partial_b A_a^i + \epsilon_{jk}^i A_a^j A_b^k, \tag{2.55}$$

the curvature of the Ashtekar connection, and

$$C_i = \nabla_a E_i^a = \partial_a E_i^a + \epsilon_{ijk} A_a^j E^{ak}, \tag{2.56}$$

the first class *Gauss constraint* generating the infinitesimal transformations associated to the additional SU(2) gauge freedom.

This Hamiltonian formulation of GR will be the starting point to define the Canonical formulation of LQG in the next Chapter.

2.2 Discrete Gravity

Born as a tool for performing complex relativistic calculations, discrete gravity has been proved a convenient instrument in the development of a conceptually consistent quantum theory of gravitation. For example, the standard construction of the quantum theory developed in Chapter 3 relies on a operational discretization of the spacetime manifold. This corresponds to a substantial cut of geometrical degrees of freedom. We should then expect that, once we have defined our quantum model, the theory we obtain taking the classical limit does not exactly resemble GR but rather a discrete version of it. The following section is thus dedicated to the discrete formulations of gravity.

2.2.1 Regge Calculus

In order to simplify the study of general relativity, and in particular the calculation of the solutions of the Einstein field equations, Tullio Regge developed in the early sixties a mathematical formalism which now goes by the name of *Regge Calculus* [49]. The original idea was to develop a formulation of General Relativity avoiding the use of co-ordinates. A strategy to do so is by approximating the smooth geometry of spacetime using discrete building blocks whose metric is internally flat. For the moment we consider the signature to be Euclidean, however the formulation supports a Lorentzian signature as well. Let us consider a general D-dimensional surface whose geometry is described by a metric $g_{ij}(x)$ with $i, j = 1, \cdots D$. Intuitively we would expect that such surface can be arbitrarily well approximated by a growing number of D-dimensional polyhedra glued through their faces [8](see the 2d example in Figure 2.1). Upon refinement, this approximation does not look exact if we focus on the small details, however the broad picture will be quite satisfactory.

---

[8]Along the work we often refer to some fixed dimensional examples to get the reader familiar with jumping back and forth into imagining different dimensions so to facilitate the comprehension of the work.
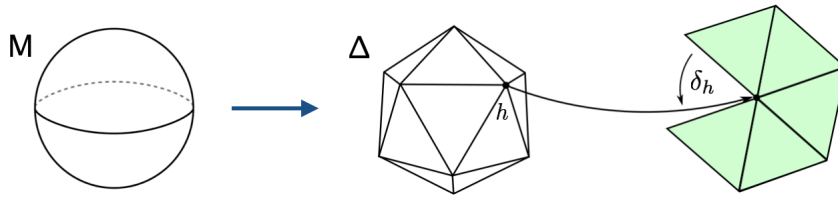
Figure 2.1: Approximation of a smooth 2-dimensional manifold $\mathcal{M}$ by a triangulation Δ. The metric degrees of freedom are carried by the sides lengths. The curvature is distributional, peaked on the 0-dimensional hinges h and equivalent to the deficit angle δ_h.

The easiest way to perform such approximation is by means of a simplicial discretization. Formally a *D-simplex* σ is defined as the convex hull of its $n + 1$ vertices v_i i.e.,

$$\sigma = \left\{ x = \sum_{i=0}^{n} \lambda_i v_i \Big| \sum_{i=0}^{n} \lambda_i = 1 \text{ and } \lambda_i \geq 0 \; \forall i \right\}. \tag{2.57}$$

Let us notice that at any point of the manifold one needs $D(D+1)/2$ numbers to fix the metric $g_{ij}(x)$. This corresponds also to the number of side lengths l_{ij} which uniquely identify a D-simplex, the l_{ij} being defined as the Euclidean distance between v_i and v_j. We can then approximate the surface in a local neighborhood around a point x with a D-simplex σ. The size of the simplex defines the resolution of the picture. The metric inside a D-simplex is assumed to be flat. Thus, we do not see any curvature d.o.f. inside σ.

We can glue together two D-simplices σ_1 and σ_2 through their boundaries so that they meet at a $(D-1)$-simplex. If the side lengths at the intersection $\sigma_1 \cap \sigma_2$ agree, than the two discrete metrics can be merged to a flat metric on $\sigma_1 \cup \sigma_2$.

More than two D-simplices glued together do not necessarily have a flat metric anymore. In fact, in a cluster of D-simplices the metric is flat anywhere except for $(D-2)$-simplices where there is distributional curvature. A $(D-2)$-simplex is also called *hinge h* given that it 'hinges' together multiple D-simplices. Then, a vector parallel transported on a closed loop around a hinge h does not necessarily point in the same direction. It can come back rotated by a deficit angle

$$\delta_h = 2\pi - \sum_{\sigma > h} \Theta_h^\sigma, \tag{2.58}$$

where Θ_h^σ is the dihedral angle at the corner of σ which hinges on h (see Figure 2.1). Summarizing, our manifold is approximated by a piecewise linear flat metric. The edge lengths completely determine the geometric properties of the simplicial space. The deficit angle $\delta_h(l_{ij})$ takes the role of the curvature.

The Regge Calculus formulation of discrete gravity, describes the dynamics of a simplicial discretization in terms of 4-dimensional building blocks. The dynamical variables are the edge lengths l_{ij}. The action that describes the dynamics of the discrete geometry is the Regge action

$$S_{\text{Regge}}[l_{ij}] = \frac{1}{16\pi G} \sum_h A_h \delta_h. \tag{2.59}$$

Its variation with respect to the edge lengths produces the analog of Einstein's equations. As it was shown by Regge, the contribution of the variation of the deficit angles δ_h for all h vanishes so that we can write the equations of motion as

$$\sum_h \frac{\partial A_h(l_{ij})}{\partial l_{ij}} \delta_h = 0. \tag{2.60}$$

A handy introduction on Regge calculus with a discussion on its continuum limit i.e., the limit of infinite refinement of the lattice, can be found in [50].

In Chapter 5, we will explicitly prove the convergence of the Regge equations of motion to the Einsteins solutions, in the specific case of a discrete model describing a isotropic and homogeneous universe whose equations of motion nicely converge to Friedmann ones at first order.

2.2.2   Dual discretization: 2-complexes and graphs

In the usual formulation of the quantum theory that we are going to introduce in the next chapter, rather than the simplicial discretization presented above one uses its dual representation in terms of 2-complexes and graphs.

A *2-complex* $\mathcal{K}$ is a collection of *vertices, edges* and *faces* glued together so to carry some of the combinatorial information of the original discretization Δ. To construct it, we associate a vertex $v \subset \mathcal{K}$ to each D-simplex $\sigma \subset \Delta$. Then an edge $e \subset \mathcal{K}$ is associated to every $(D-1)$-simplex so that any time two D-simplices meet into a $(D-1)$-simplex, then two vertices are connected by an edge. Finally, a face is dual to a $(D-2)$-simplex (i.e., an hinge) so that every time that a hinge is shared by a certain number of $(D-1)$-simplices, then an equivalent number of edges define the boundary of a face $f \subset \mathcal{K}$. One might find useful the 2d and 3d examples depicted in Figure 2.2.
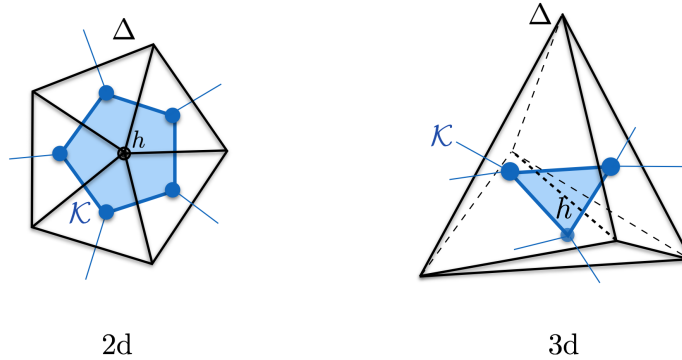
Figure 2.2: On the left, a 2d discretization Δ (in black) in terms of five triangles. The dual 2-complex $\mathcal{K}$ (in blue) is made of vertices, edges and faces. For each triangle in Δ we have a dual vertex in $\mathcal{K}$. Any time two triangles meet on a common side, then the two dual vertices are connected through an edge (dual to the side). The closure of the five bulk edges defines the face dual to the hinge h in the bulk (a point). On the right, a 3d discretization Δ consists of three tetrahedra glued together. Then the dual 2-complex $\mathcal{K}$ has three vertices connected via their common edges. The closure of the three central edges defines the face dual to the hinge h in the bulk (i.e., the dashed common side of the three tetrahedra.

A manifolds $\mathcal{M}$ with boundary $\partial\mathcal{M}$ is triangulated in such a way that if the bulk region is approximated through a simplicial discretization Δ in terms of n-simplices, then its boundary is described by a discretization $\partial\Delta$ in terms of $(D-1)$-simplices. Or, in the dual language, if a 2-complex $\mathcal{K}$ forms a skeleton for the bulk geometry, then the bones of the boundary are determined by a graph $\Gamma_{\mathcal{K}}$.
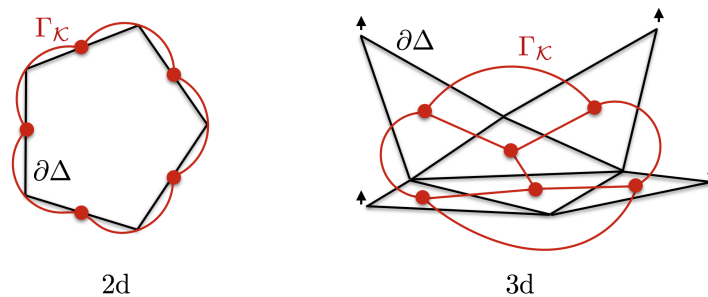
Figure 2.3: On the left, a 1d boundary discretization $\partial\Delta$ (in black) in terms of five sides. The dual graph $\Gamma_{\mathcal{K}}$ (in red) is made of a node for each side, and links connecting them, dual to points (i.e., the corners linking two sides). On the right, for a cleaner representation we have slightly unfolded the 2d boundary $\partial\Delta$ of the 3d cluster Δ in Figure 2.2. Pulling up the arrows and connecting them at the top one recreates the drawing. The boundary consists of six triangles glued together. Then the dual graph $\Gamma_{\mathcal{K}}$ has six nodes connected via links. Each node is 3-valent reflecting the fact that a triangle is bounded by three sides.

In general, a *graph* is a reticulum made of *nodes n* connected by *links ℓ*. For example, since the graph $\Gamma_{\mathcal{K}}$ is dual to $\partial\Delta$, then its nodes n are associated to $(D-1)$-simplices and its links ℓ are dual to $(D-2)$-simplices.

In Figure 2.3 we show the same 2d and 3d objects depicted in Figure 2.2, but now we respectively remove their bulk geometry and just show their boundary $\partial\Delta$ and the associated dual graph $\Gamma_{\mathcal{K}}$.

It is also possible to define a boundary graph Γ_v around each vertex v dual to a D-simplex σ. This is done by assigning a node n_a to each $(D-1)$-simplex $\partial\sigma_a$ in the boundary of σ and connecting the nodes via links ℓ_{ab} any time $\partial\sigma_a$ and $\partial\sigma_b$ meet at a hinge $h_{ab} = \partial\sigma_a \cap \partial\sigma_b$. In Figure 2.4 a 3d example is shown and the resulting graph Γ_v is drawn in red. In order to avoid confusion we will always draw a discretization Δ in black, a 2-complex $\mathcal{K}$ in blue and a graph Γ in red.
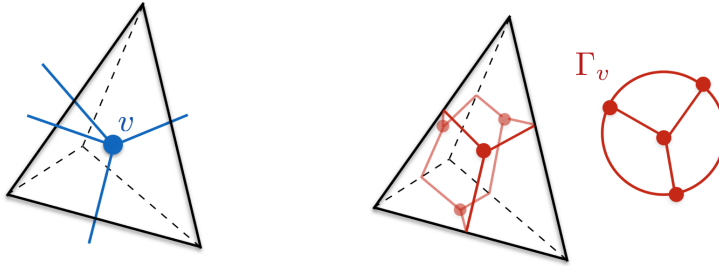
Figure 2.4: On the left a vertex $v \in \mathcal{K}$ dual to a tetrahedron σ. On the right the boundary graph Γ_v around v.

An orientation can be defined on Γ by specifying target t_ℓ and source s_ℓ nodes for each link ℓ. This will then be represented by arrows on the links.

All these concepts have a natural extension to discretizations in terms of general polytopes. In this work we will often work with non-simplicial discretizations.

2.2.3   Partial ordering of graphs

We have defined a graph Γ starting from a discretization Δ of a manifold $\mathcal{M}$. Here we will instead give a more abstract definition of graph from which a geometric interpretation will eventually emerge. In fact, these are two complementary views of the general picture. Let us take a compact 3-dimensional surface Σ. A path on Σ is an equivalence class of oriented curves $\gamma : [0, 1] \to \Sigma$ with no self intersection and piecewise analytic. A graph Γ is defined as a set of paths such that two curves intersect at most in their respective end points e.g.,
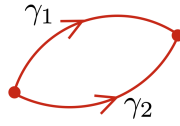
In the notation of the previous section, such intersection is called a node n while a path is another way of defining a link ℓ.

Among graphs there exists a partial ordering so that one can say that $\Gamma \leq \Gamma'$ if and only if all nodes n in Γ are also nodes n' in Γ' and all links ℓ in Γ can be constructed from links ℓ' in Γ' by inverting the orientation, removing links or concatenating several links together. These operations define a *coarse graining* of Γ' into Γ. Then if we call N the number of nodes and L the number of links in Γ one has that Γ' is such that $N \leq N'$ and $L \leq L'$. Similarly, upon partial ordering, one can always obtain Γ' from Γ by a finite sequence of moves. Take for example Γ to be the graph in the figure above. There exists three types of moves defining the *refinement* of a graph. One can add a link e.g.,
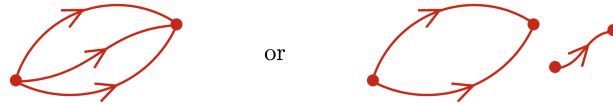
or subdivide a link inserting a node e.g.,

or invert the orientation of a link e.g.,
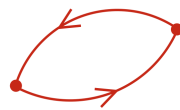
2.3 Discrete Geometric Variables

At the beginning of this chapter we have looked at different formulations of GR, each defined by a characteristic set of dynamical variables entrusted with the task of describing the evolution of spacetime. Here we show how it is possible to distribute these variables on the skeleton structures that we have just defined.

2.3.1   Distribution of BF variables on a 2-complex

Early in this chapter we have introduced the topological BF theory described by the action (2.20) and we have seen how it is related to GR. Now, we want to define BF theory on a triangulation Δ of a manifold $\mathcal{M}$. The idea is to distribute the variables B and ω on the 2-complex $\mathcal{K}$ dual to Δ.

Let us work in the general case of n-dim spacetime and local gauge group G. Then both the B-field and the connection ω have values in the Lie algebra $\mathfrak{g}$. Since the B-field is a $(D-2)$-form, it fits a smearing procedure which distribute it on the $(D-2)$-cells of Δ which are dual to the faces $f \subset \mathcal{K}$. Then we define

$$B_f = \int_{f^*} B \in \mathfrak{g}. \tag{2.61}$$

The connection ω is instead a 1-form that can be naturally 'smeared' along edges $e \subset \mathcal{K}$. It defines the *holonomy*

$$h_e[\omega] = \mathcal{P} \int_e \exp\left(-\omega\right) \in G. \tag{2.62}$$

An action for the discrete BF variables can be written in the form

$$S_{\mathrm{BF}}^{\mathcal{K}}[h_e, B_f] \equiv \sum_f \mathrm{Tr}(B_f \cdot H_f), \tag{2.63}$$

where

$$H_f = H_f[\{h_{e \subset f}\}] = h_{e_1}, \cdots, h_{e_R}, \tag{2.64}$$

denotes the holonomy around a face $f \subset \mathcal{K}$.
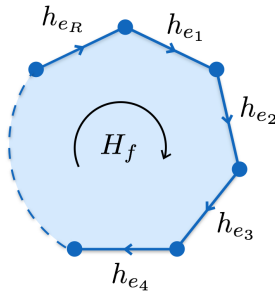
Figure 2.5: The holonomy H_f associated to a face f is the product of the holonomies of its boundary edges.

The action (2.63) is indeed a discrete version of (2.20) written in the new variables. The integral has been substituted by a sum over faces f, which in any dimension are dual to hinges $h \subset \Delta$ i.e., the $(D-2)$-cells where curvature

is distributed. Since the holonomy of the connection around closed loops is a measure of curvature, the matrix H_f resembles a discrete version of the smooth curvature F. The inner product $\langle B, F \rangle$ is written in the new variables as the inner product $\langle B_f, H_f \rangle = \mathrm{Tr}(B_f \cdot H_f)$ for matrices [9].

Example: Discrete 3d gravity

We have already mentioned that continuous BF-theory is equivalent to GR in 3d. Then, let us compare it with discrete BF-theory in 3d by looking at their equations of motion. The gauge group is $G = \mathrm{SU}(2)$ and the generators of the algebra are J_i for $i = 1, 2, 3$ (see Appendix A for details). Then we can write the discrete fields as

$$
\begin{aligned}
h_e &= \exp(X_i^e J^i), \\
B_f &= b_i^f J^i, \\
H_f &= a_0^f \mathbb{1} + a_i^f J^i, \quad \text{with} \quad (a_0^f)^2 + \sum_i (a_i^f)^2 = 1.
\end{aligned}
\tag{2.65}
$$

In these components the action (2.63) takes the form $S_{\mathrm{BF}}^{\mathcal{K}} = \sum_f a_i^f (b^f)^i$. Deriving it with respect to the components b_i^f of the B^f-field we get the first equation of motion

$$
\frac{\delta S_{\mathrm{BF}}^{\mathcal{K}}}{\delta b_i^f} = 0 \quad \Rightarrow \quad a_i^f = 0 \quad \Rightarrow \quad H_f = \pm \mathbb{1}.
\tag{2.66}
$$

The positive solution corresponds to the continuous equation of motion (2.21) i.e., vanishing of curvature. Deriving the action (2.63) with respect to the components X_i^e of h_e and imposing the first equation of motion (2.66) we get instead

$$
\frac{\delta S_{\mathrm{BF}}^{\mathcal{K}}}{\delta X_i^e} = 0 \quad \Rightarrow \sum_{f \supset e} \mathrm{Tr}(b_j^f J^j J^i H^f) = 0 \quad \Rightarrow \quad \sum_{f \supset e} b_i^f = 0,
\tag{2.67}
$$

for all the components $i = 1, 2, 3$. This corresponds to the equation of motion (2.22). In fact, by the divergence theorem, we can write

$$
\int_\sigma \mathrm{d}B = \int_{\partial\sigma} B,
\tag{2.68}
$$

where σ is a 2d surface and $\partial\sigma$ is its 1d boundary. On a simplicial discretization the integral over σ becomes a sum over triangles and the integral over $\partial\sigma$ is

---

[9]The dot product in (2.63) is well defined for matrix groups. We work in the fundamental representation of the group G so that the matrices $B_f \in \mathfrak{g}$ and $H_f \in G$ have the same dimension.

a sum over the sides of a triangle. On a 2-complex the last term corresponds exactly to (2.67) i.e.,

$$\sum_{f \supset e} B^f = 0. \tag{2.69}$$

Discrete BF theory on the boundary

As we have seen in section 2.2.2, a discretization Δ with boundary $\partial\Delta$ can be described on a 2-complex $\mathcal{K}$ inducing a graph $\Gamma_{\mathcal{K}}$ dual to the boundary. The induction is obtained by noticing for each face $f \subset \mathcal{K}$ there is a corresponding link $\ell \subset \Gamma_{\mathcal{K}}$ so that the discrete $B_f \in \mathfrak{g}$ variable becomes $B_\ell \in \mathfrak{g}$ while on the same link we can smear the boundary holonomy $h_\ell \in G$.

In the next chapter we are interested in defining the 4d Euclidean theory. Then the we get at each link of the boundary graph a set of phase space variables

$$(h_\ell, B_\ell), \tag{2.70}$$

where $h_\ell \in \text{Spin}(4) \simeq \text{SU}(2) \times \text{SU}(2)$ is a group element and $B_\ell \in \mathfrak{spin}(4) \simeq \mathfrak{su}(2) \oplus \mathfrak{su}(2)$ is an algebra element. These become operators in the quantum theory. In order to define the model we must however impose some restriction at the quantum level so that, at least in the classical limit, the simplicity constraints (2.30) are satisfied and the BF topological theory reduces to GR.

Discrete simplicity constraints

In 4-dimensions the imposition of the simplicity constraints (2.26) is a fundamental requirement to recover GR. Thus, in the discrete setting that we are defining, it is important to formulate them as constraints on the discrete variables. In a 4d simplicial discretization each component $(\mu\nu)$ of the smooth field $B_{\mu\nu}^{IJ}$ is associated to a triangles $t \subset \Delta$ or equivalently to a face $f \subset \mathcal{K}$, as given in (2.61). While the smooth constraint was defined in every spacetime point, here we define it at every 4-simplex and it takes the form of a constraint on the 10 faces adjacent to v.

From (2.26) we can directly define the following set

- for each face $f \subset v$ we have the *triangle* or *diagonal simplicity constraint*

$$\epsilon_{IJKL} B_f^{IJ} B_f^{KL} \overset{!}{=} 0, \tag{2.71}$$

  which says that B_f is a simple bivector i.e., of the form $u \wedge v$ defining a geometrical plane (Appendix A).

- for all $f, f' \subset v$ sharing a common edge e there is a *tetrahedron* or *cross simplicity constraint*

$$\epsilon_{IJKL} B_f^{IJ} B_{f'}^{KL} \overset{!}{=} 0, \tag{2.72}$$

saying that out of the four vectors defined by B_f^{IJ} and $B_{f'}^{KL}$ only three are independent and span a 3d space.

- for any $f, \bar{f} \subset v$ such that they are attached only through v there is a *4-simplex* or *volume simplicity constraint* $\epsilon_{IJKL} B_f^{IJ} B_{\bar{f}}^{KL} \stackrel{!}{=} \pm 12V$,

where V has the interpretation of the 4-volume of the 4-simplex [30]. These constraints are quadratic in the B-field, however in [40] it was shown that the first two can be written as *linear simplicity constraints*

$$C_f^I = n_J \left(* B_f^{IJ} - \frac{1}{\gamma} B_f^{IJ} \right) \stackrel{!}{=} 0, \tag{2.73}$$

upon imposition of the closure constraint

$$\sum_{f \supset e} B_f^{IJ} = 0, \tag{2.74}$$

where the sum is over triangles of the same boundary tetrahedron. Furthermore these conditions are sufficient to guarantee also the validity of the volume simplicity constraint in the case of a simplicial discretization.

The $\mathfrak{spin}(4) = \mathfrak{su}(2) \oplus \mathfrak{su}(2)$ elements B_f^{IJ} can be decomposed in terms of the generators of rotations L_f^i and boosts K_f^i of the two respective $\mathfrak{su}(2)$ subalgebras. In terms of the bivector B_f^{IJ} they read $K_f^i = B_f^{i0}$ and $L_f^i = \frac{1}{2} \epsilon_{jk}^i B_f^{jk}$. Then one has the constraint

$$D_f^i = L_f^i - \frac{1}{\gamma} K_f^i \stackrel{!}{=} 0, \tag{2.75}$$

which is the discrete version of the condition (2.30) defined on the boundary of a manifold.

The quantization of discrete BF theory is the starting point of the covariant approach to LQG. Here, the quantum states are defined on the boundary of the manifold and therefore, at least in the classical limit, they should satisfy the condition (2.75). The dynamics of the states is encoded in the transition probabilities among the states and is defined in terms of a sum over bulk geometries. There exists different models developed in the covariant approach and governed by such path integral dynamics. They are also called *Spin Foam Models*, and they mainly differ about how the classical constraints (2.75) are implemented at the quantum level. This is the topic of Chapter 4.

2.3.2 Distribution of Ashtekar variables on a graph

In the Hamiltonian formalism we have sliced spacetime into 3d spatial hypersurfaces Σ_t with an orthogonal time axis. On Σ_t we have studied the Ashtekar

variables (A_a^i, E_i^a) which are a set of canonically conjugated variables. Now, we want to distribute them on oriented graphs Γ_{Σ_t} which are dual to Σ_t. Let us write the Ashtekar connection as

$$A(x) = A_a^i(x) J_i \mathrm{d}x^a, \qquad (2.76)$$

where J_i are the generators of the $\mathfrak{su}(2)$ Lie algebra. This is a 1-form, thus we can go over holonomies by integrating it along paths $\gamma \subset \Sigma_t$, or we should say along links $\ell \subset \Gamma_{\Sigma_t}$. We get

$$h_\ell[A] = \mathcal{P} \exp\left(-\int_\ell A\right) \in \mathrm{SU}(2). \qquad (2.77)$$

This object measures the discrepancy of the geometric data undergoing parallel transport. The holonomy satisfies the following nice properties:

- it is invariant under reparametrization of the curve i.e., upon $\phi : [0,1] \to [0,1]$ with $\phi[0] = 0$ one has $h_{\ell \circ \phi}[A] = h_\ell[A]$.

- it satisfies the concatenation rule: given two concatenated curves ℓ_1 and ℓ_2, one has $h_{\ell_1 \circ \ell_2}[A] = h_{\ell_1}[A] \cdot h_{\ell_2}[A]$.

- it satisfies the inversion relation $h_{\ell^{-1}}[A] = h_\ell[A]^{-1}$.

- it has a particularly likable behavior under the gauge transformations generated by the Gauss constraint (2.56) i.e.,

$$h_\ell'[A] \to g_{t_\ell} \cdot h_\ell[A] \cdot g_{s_\ell}^{-1}, \qquad (2.78)$$

  being t_ℓ and s_ℓ the target and source nodes of the link.

- is invariant under diffeomorphisms ϕ generated by the second constraint in (2.54) i.e., $h_\ell[\phi(A)] = h_{\phi(\ell)}[A]$

Also the densitized triad can be distributed on a space skeleton. Let us first notice that from the densitized triad (2.45) we can define a 2-form

$$E_i \equiv \epsilon_{abc} E_i^a \mathrm{d}x^b \mathrm{d}x^c, \qquad (2.79)$$

that can be naturally smeared on 2d surfaces $S \subset \Sigma_t$ as

$$E_i(S) \equiv \int_S \epsilon_{abc} E_i^a \mathrm{d}x^b \mathrm{d}x^c = \int_S n_a E_i^a \mathrm{d}^2\sigma, \qquad (2.80)$$

where σ_1, σ_2 are some local coordinates on the surface S and $n_a = \epsilon_{abc} \frac{\partial x^b}{\partial \sigma_1} \frac{\partial x^c}{\partial \sigma_2}$ is a normal vector. The quantity $E_i(S)$ represents the *flux* of the densitized triad across a surface $S \subset \Sigma_t$, which we recall being dual to a link $\ell \subset \Gamma_{\Sigma_t}$).

Notice that, for each link $\ell \subset \Gamma_{\Sigma_t}$ the area (2.50) of the dual surface $S_\ell = \ell^*$ can be written in terms of the 2-form (2.79) and takes the neat form

$$\alpha(S_\ell) = \int_{S_\ell} \sqrt{E^i E_i}. \tag{2.81}$$

The holonomy (2.77) and the flux (2.80) form a pair of canonically conjugate variables on ℓ

$$(h_\ell[A], E_i(S_\ell)). \tag{2.82}$$

In the quantum theory they become operators defining the so-called *holonomy-flux algebra*.

It is finally time to work out a quantization for the classical theories reviewed above. In the next chapter we will present the canonical and covariant formulations of Loop quantum gravity and explain why and how they rely on the discrete structures just introduced.

Chapter 3

Quantum Theories of Gravity

In this chapter we give a general introduction on the quantization of gravity as given in Loop Quantum Gravity (LQG). Starting from the Hamiltonian formulation of GR we apply the Dirac quantization procedure which defines the Canonical formulation of LQG [47, 31]. We then work out a set of Covariant formulations of LQG which define the so called Spin Foam Models [51, 30].

3.1   Canonical formulation: Loop Quantum Gravity

The canonical approach to LQG starts from the Hamiltonian formulation of GR as given in the Ashtekar variables, and proceeds to the quantization by following the Dirac program [52]. According to it, one would like to promote the Ashtekar phase space variables to quantum operators and to build a kinematical Hilbert space $\mathcal{H}_{kin}$ consisting of a set of functionals of the connection $\psi[A]$ which are square integrable with respect to a suitable (gauge invariant and diffeomorphism invariant) measure on the space $\mathcal{U}$ of all SU(2) connections. On these wave functionals the Ashtekar connection $A \in \mathcal{U}$ would act as a multiplicative operator while the densitized triad would be a derivative operator $E = -i\frac{\delta}{\delta A}$. The constraints (2.54) and (2.56) would then be promoted to quantum operators on $\mathcal{H}_{kin}$, and imposed at the quantum level to define the physical Hilbert space of the theory $\mathcal{H}_{phys}$ [53]. Eventually one would like to define a complete set of observables for the quantum theory. However, working with configuration variables on $\mathcal{U}$ comes with some problems e.g., defining an invariant measure on the Hilbert space. The way out adopted by LQG consist of switching to the holonomies as the basic variables or, rather, quantum operators.

3.1.1   The space of generalized connections

The key observation here is that it would be possible to uniquely reconstruct each element $A \in \mathcal{U}$ knowing the holonomy $h_\ell[A]$ (given by (2.77)) for all the paths ℓ in Σ. The strategy is then to promote the holonomies to quantum operators and then simplify the problem of constructing the kinematical Hilbert space by considering holonomies along a finite set of curves i.e., building the theory on finite-size graphs Γ where the *partial Hilbert space* $\mathcal{H}_\Gamma$ have a well defined measure μ_Γ. The kinematical Hilbert space $\mathcal{H}_{kin}$ would then be defined as the projective limit of $\mathcal{H}_\Gamma$ for infinite refinements $\Gamma \to \infty$ [1].

Let us define the *partial configuration space* as $\mathcal{U}_\Gamma = \mathrm{SU}(2)^{L \subset \Gamma}$ being L the number of links in Γ. Then given two oriented graphs such that $\Gamma \leq \Gamma'$, there exists a projection map $\pi_{\Gamma'\Gamma} : \mathcal{U}_{\Gamma'} \to \mathcal{U}_\Gamma$ defined by

$$\pi_{\Gamma'\Gamma}(\{h_{\ell'}\})_\ell = \overleftarrow{\prod_{\ell' \subset \ell}} h_{\ell'}^{[\ell,\ell']}, \tag{3.1}$$

where the arrow represent the order of the product from the right to the left, as befits parallel transports, while $[\ell, \ell'] = \pm 1$ is the relative orientation of ℓ and ℓ'. The projector $\pi_{\Gamma'\Gamma}$ formalizes the coarse graining procedure $\Gamma' \to \Gamma$ and determines how the fine degrees of freedom in $\mathcal{U}_{\Gamma'}$ combine and reduce to the coarse degrees of freedom on $\mathcal{U}_\Gamma$. In particular it defines the operations

- addition: $\pi_{\Gamma'\Gamma}(h_1 \cdots h_{L+1}) = (h_1 \cdots h_L)$

- subdivision: $\pi_{\Gamma'\Gamma}(\cdots, h_i, h_j, \cdots) = (\cdots, h_i \cdot h_j, \cdots)$

- inversion: $\pi_{\Gamma'\Gamma}(\cdots, h_i, \cdots) = (\cdots, h_i^{-1}, \cdots)$

which, according to the definitions given in the previous chapter, are necessary to move in the partial ordered set of graphs.

For $\Gamma \leq \Gamma' \leq \Gamma''$ the projector (3.1) satisfies the condition

$$\pi_{\Gamma'\Gamma}\pi_{\Gamma''\Gamma'} = \pi_{\Gamma''\Gamma}. \tag{3.2}$$

Using $\pi_{\Gamma'\Gamma}$ we can glue together all the finite-dimensional spaces $\mathcal{U}_\Gamma$ to form the projective limit

$$\overline{\mathcal{U}} = \lim_{\overleftarrow{\Gamma}} \mathcal{U}_\Gamma \equiv \left\{ \{a_\Gamma\}_\Gamma \mid a_\Gamma \in \mathcal{U}_\Gamma, \ \pi_{\Gamma'\Gamma}a_{\Gamma'} = a_\Gamma \ \forall \ \Gamma \leq \Gamma' \right\}. \tag{3.3}$$

The space $\overline{\mathcal{U}}$ is called the space of *generalized connections* and contains all the 'quantum' continuum SU(2) connections $\{a_\Gamma\}_\Gamma$. In other words, a generalized

---

[1]See for example [54] for a short review on the definition of projective limit and its application in LQG.

connection is equivalent to an assignment of $h_\ell \in \mathrm{SU}(2)$ to any path $\ell \subset \Sigma$. Strictly speaking, this space is a distributional extension of $\mathcal{U}$, containing elements which do not come from a connection. Now, the holonomy itself becomes the fundamental variable. Let us notice that the limit in (3.3) is not an analytic one. Rather, a continuum generalized connection is given by the collection of all its partial representatives a_Γ.

We can also define the new projector $\Pi_\Gamma : \overline{\mathcal{U}} \to \mathcal{U}_\Gamma$ such that

$$\Pi_\Gamma(\{a_\Gamma\}_\Gamma) \equiv a_\Gamma, \tag{3.4}$$

and satisfying the rule $\pi_{\Gamma'\Gamma}\Pi_{\Gamma'} = \Pi_\Gamma$.

3.1.2 Partial Hilbert spaces

The challenge now is to proceed in such a way that partial Hilbert spaces built on different graphs are consistently related to each other and consequently there exists a way to reach the continuum limit i.e., the limit of infinite refinement $\Gamma \to \infty$.

The resolutive step is to require the Hilbert space $\mathcal{H}_\Gamma$ to be built of *cylindrical functions* of generalized connections. A function $f : \overline{\mathcal{U}} \to \mathbb{C}$ is cylindrical over a graph Γ if there exists $f_\Gamma : \mathcal{U}_\Gamma \to \mathbb{C}$ such that

$$f(\{a_\Gamma\}_\Gamma) = f_\Gamma(a_\Gamma), \tag{3.5}$$

which is equivalent to say $f = f_\Gamma \Pi_\Gamma$. One can easily check that, if f is cylindrical over Γ, then it is also cylindrical over all Γ' with $\Gamma \leq \Gamma'$ and the following relation holds $f_{\Gamma'} = f_\Gamma \pi_{\Gamma'\Gamma}$. Most notably, the set Cyl of cylindrical functions over a partial ordered set of graphs forms a vector space. In fact, given $f \in \mathrm{Cyl}_\Gamma$ cylindrical over Γ and $f' \in \mathrm{Cyl}_{\Gamma'}$ cylindrical over Γ', then both f and f' are cylindrical on $\Gamma'' \geq \Gamma, \Gamma'$. The same is true for their sum $f + f' \in \mathrm{Cyl}_{\Gamma''}$. [2]

---

[2] A perfect example of cylindrical function is the Wilson loop. This operator is in fact resilient to the operations defining the partially ordered set which were introduced in the previous chapter. Take for example a graph Γ consisting of a single closed loop ℓ. The associated Wilson loop $W_\ell[A] \in \mathrm{Cyl}_\Gamma$ is defined as

$$W_\ell[A] = \mathrm{Tr}(h_\ell[A]). \tag{3.6}$$

On a graph Γ' obtained by a subdivision of the loop into $\ell = \ell_1 \circ \ell_2$ the Wilson loop becomes

$$W_{\ell=\ell_1\circ\ell_2}[A] = \mathrm{Tr}(h_{\ell_1}[A] \cdot h_{\ell_2}[A]), \tag{3.7}$$

and is a function in $\mathrm{Cyl}_{\Gamma'}$. It can be also be defined as a cylindrical function on a graph Γ'' built from Γ' by adding a link ℓ_3, provided that the contribution of the new holonomy $h_{\ell_3}[A]$ is trivial i.e., it carries no curvature. Indeed, the physics that this operator describes it is supposed to be the same, independently of how much we refine the graph. Notice also that, thanks to the cyclicity of the trace, the Wilson loop is invariant under gauge transformations $g \in \mathrm{SU}(2)$. Cylindrical functions satisfying this invariance will be of fundamental importance when defining a basis of the Hilbert space.

The partial Hilbert space $\mathcal{H}_\Gamma$ consists of functions $\psi_{\Gamma,f} : \mathcal{U}_\Gamma \to \mathbb{C}$ which are cylindrical over Γ and defined by

$$\psi_{\Gamma,f}[A] \equiv f_\Gamma(a_\Gamma) = f_\Gamma(h_{\ell_1}[A], \cdots, h_{\ell_L}[A]) \in \text{Cyl}_\Gamma. \tag{3.8}$$

Since these are functions of L elements of SU(2) we can use the Haar measure $\mathrm{d}\mu_H$ to define the inner product

$$\langle \psi_{\Gamma,f} | \psi_{\Gamma,f'} \rangle = \int_{\text{SU}(2)^L} \mathrm{d}\mu_H^{\otimes L} \overline{f_\Gamma(h_{\ell_1}[A], \cdots, h_{\ell_L}[A])} f'_\Gamma(h_{\ell_1}[A], \cdots, h_{\ell_L}[A]). \tag{3.9}$$

Summarizing we finally have

$$\mathcal{H}_\Gamma = L^2(\mathcal{U}_\Gamma, \mathrm{d}\mu_\Gamma), \tag{3.10}$$

having defined $\mathrm{d}\mu_\Gamma \equiv \mathrm{d}\mu_H^{\otimes L}$.

The measure $\mathrm{d}\mu_\Gamma$ satisfies the so-called *cylindrical consistency condition for the measure*

$$(\pi_{\Gamma'\Gamma})_* \mathrm{d}\mu_\Gamma = \mathrm{d}\mu_{\Gamma'}. \tag{3.11}$$

In other words it can be consistently pushed forward into finer graphs in a partial ordered set via the projector $\pi_{\Gamma'\Gamma}$. The collection of measures $\{\mu_\Gamma\}_\Gamma$ comes from a unique [3] measure on $\overline{\mathcal{U}}$ which is called the Ashtekar-Lewandowski measure $\mathrm{d}\mu_{AL}$ [57].

3.1.3 Kinematical embedding maps

In order to relate Hilbert spaces on different graphs Γ and Γ' with $\Gamma \leq \Gamma'$ we define the *embedding maps*

$$\iota_{\Gamma\Gamma'} : \mathcal{H}_\Gamma \to \mathcal{H}_{\Gamma'}, \tag{3.12}$$

such that

$$(\iota_{\Gamma\Gamma'}\psi_\Gamma)(a_{\Gamma'}) \equiv \psi_\Gamma(\pi_{\Gamma'\Gamma}(a_{\Gamma'})). \tag{3.13}$$

For $\Gamma \leq \Gamma' \leq \Gamma''$ the embedding maps satisfy the consistency condition [4]

$$\iota_{\Gamma'\Gamma''} \circ \iota_{\Gamma\Gamma'} = \iota_{\Gamma\Gamma''}. \tag{3.14}$$

The nice feature of the embedding maps $\iota_{\Gamma\Gamma'}$ is that they are isometries i.e., they preserve the Hilbert space inner product (3.9). To prove this statement one needs to study only the three cases of Γ' obtained from Γ via the operations of addition, subdivision and inversion. This is not shown explicitly here for compactness.

---

[3] See LOST theorem [55, 56].

[4] This is the usual construction adopted in LQG, where the embedding maps are defined at the kinematical level with respect to the Ashtekar-Lewandowski measure $\mathrm{d}\mu_{AL}$. However it has been argued, with good reasons, that such embedding maps should be defined at the dynamical level [58, 59]. We will come back on this point in Chapter 6.

3.1.4 The kinematical Hilbert space

The kinematical Hilbert space is defined as

$$\mathcal{H}_{kin} \equiv \bigsqcup_{\Gamma \subset \Sigma} \mathcal{H}_\Gamma \Big/ \sim, \tag{3.15}$$

i.e., the disjoint union of the partial Hilbert spaces modulo the equivalence relation $\sim$ which is defined as follows: two states ψ_Γ and $\psi'_{\Gamma'}$ are equivalent if there exists a Γ'' with $\Gamma \leq \Gamma''$ and $\Gamma' \leq \Gamma''$ such that $\iota_{\Gamma\Gamma''}\psi_\Gamma = \iota_{\Gamma'\Gamma''}\psi'_{\Gamma'}$. In other words, two states on different discretizations Γ, Γ' are equivalent if they can be refined to the same state. This notion of inductive limit allows us to embed any discrete state ψ_Γ into the continuum Hilbert space $\mathcal{H}_{kin}$ via an embedding map. So defined, the space (3.15) corresponds to the space of wave functionals of generalized connections

$$\mathcal{H}_{kin} = L^2(\overline{\mathcal{U}}, \mathrm{d}\mu_{AL}), \tag{3.16}$$

with the Ashtekar-Lewandowski measure $\mathrm{d}\mu_{AL}$ i.e., the measure whose projection to any $\mathcal{U}_\Gamma$ yields the corresponding Haar measure $\mathrm{d}\mu_\Gamma \equiv \mathrm{d}\mu_H^{\otimes L}$, being Γ a graph with L links.

3.1.5 Spin Networks

Under the light of the above theoretical framework, here we define the orthonormal basis of gauge invariant functionals for the Hilbert space. Since we are working with functions of SU(2) elements we can use the Peter-Weyl theorem (Appendix A) which says that given a function $f : \mathrm{SU}(2) \to \mathbb{C}$ we can decompose it into unitary representations of SU(2) as

$$f(h) = \sum_{j \in \frac{\mathbb{Z}}{2}} \sum_{mn=-j}^{j} C_{mn}^j D^j(h)^{mn}, \tag{3.17}$$

being C_{mn}^j the coefficients

$$C_{mn}^j = (2j+1) \int_{\mathrm{SU}(2)} \mathrm{d}\mu_H f(h) \overline{D^j(h)_{mn}}, \tag{3.18}$$

and $D_j(h)$ the Wigner-D matrices whose elements form a complete orthonormal set with respect to the Haar measure. Then, a generic cylindrical function (3.8) defined over a graph Γ consisting of N nodes connected by L links, can be written as a sum

$$\psi_\Gamma = \sum_{\substack{j_i, m_i, n_i \\ \forall i=1,\cdots,L}} C_{m_1,\cdots,m_L,n_1,\cdots,n_L}^{j_1,\cdots,j_L} D^{j_1}(h_{\ell_1})^{m_1 n_1}, \cdots \cdot D^{j_L}(h_{\ell_L})^{m_L n_L}. \tag{3.19}$$

Now, we want to impose the Gauss constraint (2.56) on the states of the Hilbert space i.e., we demand that $C_i\psi_{\Gamma,f}[A] \overset{!}{=} 0$ so to define SU(2) gauge invariant states in the kinematical partial Hilbert space $\mathcal{H}_\Gamma$. Since the holonomy transforms with (2.78), the invariance can be imposed as a group average of (3.8) at each node $n \subset \Gamma$

$$\psi_{\Gamma,\mathrm{Inv}} = \int_{\mathrm{SU}(2)^N} \prod_{n=1}^N \mathrm{d}g_n f_\Gamma\Big(g_{s(\ell_1)}h_{\ell_1}g_{t(\ell_1)}^{-1}, \cdots, g_{s(\ell_1)}h_{\ell_L}g_{t(\ell_L)}^{-1}\Big). \qquad (3.20)$$

Similarly, working in the Wigner D-matrices decomposition we can implement the group averaging by placing at each node a *Haar projector*

$$P_{\mathrm{Inv}}^n = \int \mathrm{d}g \prod_{\ell \supset n} D^{j_\ell}(g), \qquad (3.21)$$

where the product is over links meeting at the node n. Let us call V_{j_ℓ} the base space where the representation $D^{j_\ell}(g)$ acts. Then, the projector P_{Inv}^n acts on the tensor product of base spaces to make it invariant i.e.,

$$P_{\mathrm{Inv}}^n : \bigotimes_\ell V_{j_\ell} \longrightarrow \mathrm{Inv}_{\mathrm{SU}(2)} \bigotimes_\ell V_{j_\ell}. \qquad (3.22)$$

The elements of $\mathrm{Inv}_{\mathrm{SU}(2)} \bigotimes_\ell V_{j_\ell}$ are called *intertwiners* $|\iota\rangle$.

Take for example the simple case of a 3-valent node. Each link $\ell \supset n$ carries a representation labeled by a spin j_ℓ, $\ell = 1, 2, 3$. In this case a basis $\bigotimes_\ell V_{j_\ell}$ is the tensor product $|j_1 m_1\rangle \otimes |j_2 m_2\rangle \otimes |j_3 m_3\rangle$ and the invariant space is spanned by a unique intertwiner so that any state is proportional to

$$|\iota\rangle = \sum_{m_1,m_2,m_3} \iota_{m_1 m_2 m_3} |j_1 m_1\rangle \otimes |j_2 m_2\rangle \otimes |j_3 m_3\rangle. \qquad (3.23)$$

In general, if the valence of a node is $L_n > 3$ (i.e., there are L_n links at the node) one has a higher dimensional invariant space spanned by intertwiners which are tensors with L_n indices $m_1, \cdots, m_{L_n}$.

The intertwiner basis can be used to define the Haar projector (3.22) as a resolution of the identity on the invariant subspace

$$P_{\mathrm{Inv}}^n = \mathbb{1}_{\mathrm{Inv}_{\mathrm{SU}(2)} \bigotimes_\ell V_{j_\ell}} = \sum_\iota |\iota\rangle\langle\iota|. \qquad (3.24)$$

Inserting this operator into (3.19) we can express the coefficients

$$C_{m_1,\cdots,m_L,n_1,\cdots,n_L}^{j_1,\cdots,j_L} = C^{j_1,\cdots,j_L}(\iota_1)_{m_1\cdots} \cdots (\iota_N)_{\cdots n_L}, \qquad (3.25)$$

in terms of N intertwiners, one for each node $n \subset \Gamma$. The generic gauge invariant state $\psi_\Gamma \in \mathcal{H}_\Gamma$ can then be written as a linear superposition of states

$$\psi_\Gamma = \sum_{j_\ell} C_{j_\ell} \psi_{\Gamma, j_\ell, \iota_n}, \tag{3.26}$$

where

$$\psi_{\Gamma, j_\ell, \iota_n} = \bigotimes_n \iota_n \bigotimes_\ell D^{j_\ell}(h_\ell), \tag{3.27}$$

is called *spin network* state and provides a basis element for the invariant partial Hilbert space $\mathcal{H}_\Gamma$.

In total generality, a spin network is an oriented graph Γ whose links are associated with irreducible representations of a compact Lie group G (spins j_ℓ for $G = \mathrm{SU}(2)$) and whose nodes are associated with intertwiners ι_n of the link representations adjacent to it.

We omit here the discussion about the implementation of the vector and diffeomorphism constraints, but the reader is referred to the reviews [30, 48].

3.1.6 Schrödinger representation of holonomy-flux algebra

Let us recall from Chapter 2 that the holonomy and the flux are conjugate variables (2.82), and that in the quantum theory they are operators acting on functions $\psi_\Gamma[h_\ell[A]] \in \mathcal{H}_\Gamma$. It is possible to define their action e.g., in the Schroedinger representation. Details on the derivation of the following formulas are found e.g., in [48]. Let us work for simplicity in the fundamental representation where $D_{1/2}(h_\ell) = h_\ell$. In the Schrödinger representation, the holonomy operator $\hat{h}_\gamma[A]$, defined on a path γ, acts on the holonomy along a link ℓ as

$$\hat{h}_\gamma[A] h_\ell[A] = h_\gamma[A] h_\ell[A]. \tag{3.28}$$

The flux $\hat{E}_i(S)$ associated to a surface S acts instead as a derivative operator

$$\hat{E}_i(S) h_\ell[A] = -i\hbar\gamma \int_S \mathrm{d}^2\sigma\, n_a \frac{\delta h_\ell[A]}{\delta A_a^i(x(\sigma))} = \pm\hbar\gamma h_{\ell_1}[A] J_i h_{\ell_2}[A], \tag{3.29}$$

where we are using the notation of formula (2.80), J_i are $\mathrm{SU}(2)$ generators, ℓ_1, ℓ_2 are two new edges defined by the point where the densitized triad (2.45) acts and are such that $\ell = \ell_1 \circ \ell_2$. The sign $\pm$ depends on the orientation of ℓ and S. Equation (3.29) vanishes when the link ℓ is tangential to the surface S or when it does not puncture the surface i.e., $S \cap \ell = 0$. The scalar product of two fluxes acts on the holonomy as

$$\begin{aligned} \hat{E}_i(S)\hat{E}^i(S) h_\ell[A] &= \hbar^2\gamma^2 h_{\ell_1}[A] J^i J_i h_{\ell_2}[A] \\ &= \hbar^2\gamma^2 C^2 h_{\ell_1}[A] h_{\ell_2}[A] = \hbar^2\gamma^2 C^2 h_\ell[A], \end{aligned} \tag{3.30}$$

being $C^2 = J^2$ the Casimir of SU(2). In analogy with the expression above, in a generic representation one finds

$$\hat{E}_i(S)\hat{E}^i(S)D^{j_\ell}(h_\ell) = \hbar^2\gamma^2 j(j+1)D^{j_\ell}(h_\ell). \tag{3.31}$$

Always in [48], the commutation relations among holonomy and flux are derived.

3.1.7   Discreteness of quantum geometry

As we have seen in (2.81), classically we can define the area of a surface S dual to a link in terms of the flux (defined at the link). Suppose that we want to evaluate the area of a generic 2d surface S. Then a strategy consists in puncturing this surface with N links ℓ_a of a graph, each one dual to a subsurface S_{ℓ_a}. All together, these dual subsurfaces cover the total surface and then provide a triangulation for $S \simeq \cup_a S_{\ell_a}$. According to (2.81), the approximated surface has area

$$\alpha_N(S) = \sum_{a=1}^{N} \sqrt{E_i(S_{\ell_a})E^i(S_{\ell_a})}. \tag{3.32}$$

The area of S is then defined as the infinite refinement limit

$$\alpha(S) = \lim_{N\to\infty} \alpha_N(S). \tag{3.33}$$

In the quantum theory, the area becomes an operator $\hat{\alpha}(S)$, defined by simply upgrading the flux to a quantum operator $\hat{E}_i(S)$. According to (3.31), its action on a state $\psi_\Gamma[h_\ell[A]] \in \mathcal{H}_\Gamma$ is given by

$$\hat{\alpha}(S)\psi_\Gamma = \lim_{N\to\infty} \sum_{a=1}^{N} \sqrt{\hat{E}_i(S_{\ell_a})\hat{E}^i(S_{\ell_a})}\psi_\Gamma = \sum_{p\in S\cup\Gamma} \hbar\sqrt{\gamma^2 j_p(j_p+1)}\psi_\Gamma, \tag{3.34}$$

where in the last term the sum is over punctures p made by the graph Γ on the surface S. Notice that the finite size of the graph is the reason why the limit disappears. In other words, fixing a graph corresponds to fixing the accuracy at which we can look at the physics of a system.

From formula (3.34) we see that spin networks are eigenstates of the area operator. However, the most striking observation is that formula (3.34) offers a genuine prediction about the eigenvalues of the area operator. Namely, the spectrum is discrete and, restoring the Newton's constant, the area can only exist in quanta proportional to the squared Plank length $\hbar G$. A similar result, with some further complication, holds for the spectrum of the volume operator [60, 61]. When we talk about *discreteness* of quantum spacetime in LQG, we

do not refer to the fact that the theory is built on a discretization (or rather on the dual graph). Instead, we refer to the discreteness of the eigenvalues of geometric operators. These results do not depend in fact on the fineness of the base graph Γ or, in other words, there will always be a minimal area element proportional to the Plank length squared.

3.2 Covariant formulation: Spin foams

The quantum theory defined in the covariant formulation consists of two main ingredients. The first is the kinematic defined by a boundary Hilbert space describing states of quantum geometry. The Hilbert space is built from the discrete BF variables at the boundary (2.70), which in the quantum theory are operators. In the next chapter we will see that in the 4d Euclidean theory they correspond to the spin network states of the canonical theory.

The second ingredient is the dynamics, formulated as a path integral over states of geometry. Then, the transition probability between two quantum geometries is given by a partition function. We can built it on a 2-complex $\mathcal{K}$ in terms of the discrete action (2.20) describing the dynamics of the smeared BF variables (2.62) and (2.61). One then writes

$$Z_{BF}^{\mathcal{K}} = \int \mathrm{d}h_e \int \mathrm{d}B_f e^{i\sum_f \mathrm{Tr}(B_f \cdot H_f)}, \tag{3.35}$$

where there is an integration with respect to the Haar measure $\mathrm{d}h_e$ for each of the E edges $e \subset \mathcal{K}$, and an integration in terms of the Lebesgue measure $\mathrm{d}B_f$ for each of the F faces $f \subset \mathcal{K}$. Integrating with respect to the latter, we get [5]

$$Z_{BF}^{\mathcal{K}} = \int \mathrm{d}h_e \prod_f \left(\delta(H_f) + \delta(-H_f) \right). \tag{3.37}$$

According to Peter-Weyl theorem, given a compact group G, we can decompose the delta function $\delta(g)$ with $g \in G$, into a sum of irreducible representations $\rho(g)$ of dimension d_ρ. Explicitly,

$$\delta(g) = \sum_\rho d_\rho \chi(g), \tag{3.38}$$

being

$$\chi(g) = \mathrm{Tr}(\rho(g)), \tag{3.39}$$

---

[5]In fact, writing the holonomy (2.64) as $H_f = \mathbb{1}\cos\theta + i(\hat{n} \cdot \vec{\sigma})\sin\theta$ and $B_f = i(\vec{b} \cdot \vec{\sigma})$ we find

$$\int \mathrm{d}B_f e^{i\mathrm{Tr}(B_f \cdot H_f)} \sim \int \mathrm{d}B_f e^{-i(\hat{n} \cdot \vec{b})\sin\theta}, \tag{3.36}$$

which vanishes apart in the case $\sin\theta = 0$ i.e., $H_f = \pm\mathbb{1}$ which corresponds to $\int \mathrm{d}B_f = \infty$.

the *character* of the irreducible representation $\rho(g)$.

In what follows we consider just the first delta function in (3.37) and proceed to the evaluation of the integral [6]. Then flatness is enforced in the form of trivial parallel transport around each face i.e., $H_f = \mathbb{1}$. The partition function becomes

$$
\begin{aligned}
Z_{BF}^{\mathcal{K}} &= \int \mathrm{d}h_e \prod_f \sum_\rho d_\rho \chi_j(H_f) \\
&= \sum_{\rho_f} \int \mathrm{d}h_e \prod_f d_{\rho_f} \mathrm{Tr}\big(\rho_f(h_{e_1} \cdots h_{e_R})\big),
\end{aligned}
\tag{3.40}
$$

where ρ_f is a representation acting on group elements defined on the face f. The holonomy H_f is expanded using the same notation as in Figure 2.5. We can also expand the representation of the product of holonomies in (3.40) as the product of the representations

$$
\rho_f(h_{e_1} \cdots h_{e_R}) = \rho_f(h_{e_1}) \cdots \rho_f(h_{e_R}),
\tag{3.41}
$$

In a D-dimensional simplicial discretization, for each edge $e \subset \mathcal{K}$ there are always D faces $f_1, \cdots, f_D \subset \mathcal{K}$ meeting [7], each coming with an independent representation $\rho_1, \cdots, \rho_D$. Therefore h_e appears precisely in D different traces in (3.40). Then, for each edge e, we can isolate integrals of the form

$$
P_{\mathrm{Inv}}^e = \int \mathrm{d}h_e \rho_1(h_e) \otimes \cdots \otimes \rho_D(h_e),
\tag{3.42}
$$

where for each $i = 1, \cdots, D$ there is an independent representation matrix ρ_i. Let us call

$$
V_e = V_{\rho_1} \otimes \cdots \otimes V_{\rho_D},
\tag{3.43}
$$

the tensor product of vector spaces on the faces where the respective representations act as

$$
h_e \triangleright (\mathbf{v}_1 \otimes \cdots \otimes \mathbf{v}_D) \equiv \rho_1(h_e)\mathbf{v}_1 \otimes \cdots \otimes \rho_D(h_e)\mathbf{v}_D,
\tag{3.44}
$$

for vectors $\mathbf{v}_i \in V_{\rho_i}$. The operator defined in (3.42) satisfies $P_{\mathrm{Inv}}^e = (P_{\mathrm{Inv}}^e)^2$ and projects V, into its subspace invariant under group transformations i.e.,

$$
P_{\mathrm{Inv}}^e : V_e \longrightarrow \mathrm{Inv}_G(V_e).
\tag{3.45}
$$

---

[6]In fact, the second delta function in often ignored in the literature since one expects geometric fluctuations to happen around the flat metric on which the first delta is peaked. Nonetheless, this point would require a deeper analysis.

[7]In fact, an edge e is dual to a $(D-1)$-simplex which is bounded by D hinges ($(D-2)$-simplices), each of them dual to a face f.

Then for every edge e the projector P^e_{Inv} can be written as resolution of the identity on the invariant subspace. This is spanned by an orthonormal basis of so-called *intertwiners* i.e., invariant tensors $\iota_e \in \text{Inv}_G(V_e)$. Explicitly, we write

$$P^e_{\text{Inv}} = \mathbb{1}_{\text{Inv}_G(V_e)} = \sum_{\iota_e} \iota_e \otimes \iota_e^\dagger = \sum_{\iota_e} |\iota_e\rangle\langle\iota_e|, \qquad (3.46)$$

where in the last term we introduce the classical bra-ket notation.

We can think at the $|\iota_e\rangle$ and $\langle\iota_e|$ in (3.46) as placed at the opposite ends of the edge e as in Figure 3.1. Then, they are respectively inherited by the two extremal vertices v_1, v_2, where a mechanism of contraction have place among the intertwiners coming from the other edges.
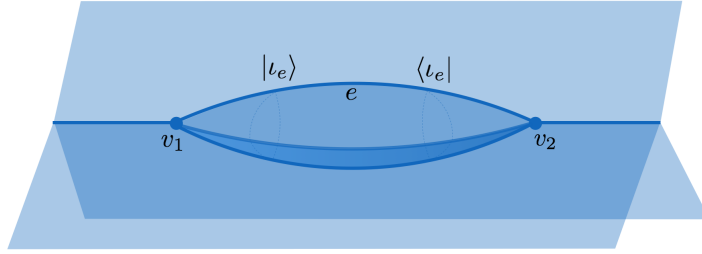
Figure 3.1: Two vertices v_1, v_2 connected through edges. For each edge e there is a resolution of the identity (3.46).

Recall in fact that the intertwiner $|\iota_e\rangle$ is an element in $\text{Inv}_G(V_{\rho_1} \otimes \cdots \otimes V_{\rho_D})$ and, as such, it carries D free indices $m_1, \cdots, m_D$, associated to the D faces that meet at e. Similarly, to $\langle\iota_e|$ are entrusted the indices $n_1, \cdots, n_D$. These are the same indices of the representation matrix elements $(\rho_i)^{m_i}_{n_i}$ appearing in (3.42).

Summarizing, each edge 'entering' into (or 'exiting' from) a vertex, carries D indices corresponding to the D faces of which it is the common juncture. Then, a contraction among all the indices is performed at the vertex. This must take into account the fact that at a vertex $v \subset \mathcal{K}$ there are $D + 1$ edges meeting. We can refer to the 3d example in Figure (3.2).

In other words, there are $D(D + 1)$ indices to be contracted in pairs. The pairs are chosen according to the 2-complex structure i.e., two indices coming from two distinct edges e_1 and e_2 are contracted if and only if they are associated to the unique face $f \supset e_1, e_2$ bounded by both the edges. Eventually, there is one contraction for each of the $D(D + 1)/2$ faces in the vertex.

Let us call $\mathcal{A}_v$ the operator realizing this contraction. We write it as

$$\mathcal{A}_v \equiv \text{tr}\left(\bigotimes_{e \to v} |\iota_e\rangle \bigotimes_{e \leftarrow v} \langle\iota_e| \right), \qquad (3.47)$$
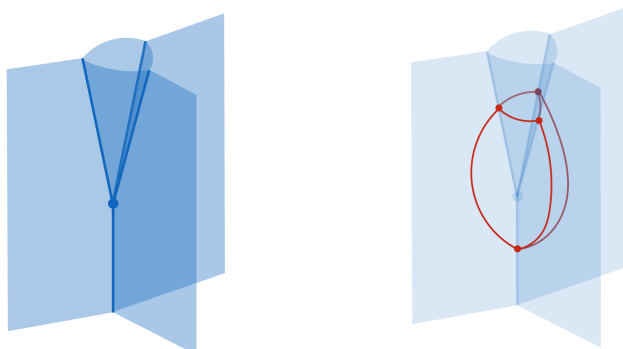
Figure 3.2: On the left: the 2-complex $\mathcal{K}$ dual to a tetrahedron. There are $D+1 = 4$ edges meeting at the vertex, each edge has $D = 3$ faces attached. There are in total $D(D+1)/2 = 6$ faces touching the vertex. On the right: the boundary graph Γ_v around the vertex.

where the trace represents the full contraction among the intertwiners associated to the $D + 1$ edges e connecting to the vertex v (ingoing $\rightarrow$ or outgoing $\leftarrow$). The operator (3.47) is called *vertex amplitude* and will play a fundamental role.

Now, recall from the previous chapter (see also Figure 3.2) that each edge connecting with v can be put in one to one correspondence with a node $n \subset \Gamma_v$ in the boundary graph Γ_v around v. Similarly, every face adjacent to v can be thought in terms of links $\ell \subset \Gamma_v$. Then the group theoretic data can be transfered from the two complex to the boundary graph as $\iota_e \rightarrow \iota_n$ and $\rho_f \rightarrow \rho_\ell$. In other words, the set of all the intertwiners $\{\iota_e\}_v$ and all representations $\{\rho_f\}_v$ converging into a vertex structure v, define a *vertex spin network* state $\psi_{\Gamma_v, \rho_\ell, \iota_n}$ (3.27) in the Hilbert space $\mathcal{H}_{\Gamma_v}$. In this notation, for each vertex we can write the vertex amplitude as a functional

$$\mathcal{A}_{\Gamma_v} : \mathcal{H}_{\Gamma_v} \longrightarrow \mathbb{C}. \tag{3.48}$$

Putting all together, we can write the partition function (3.40) as

$$Z_{BF}^{\mathcal{K}} = \sum_{\rho_f, \iota_e} \prod_f d_{\rho_f} \prod_v \mathcal{A}_v(\{\rho_f\}_v, \{\iota_e\}_v). \tag{3.49}$$

Let us notice here that, unlike in lattice gauge theory, a 2-complex $\mathcal{K}$ does not carry any geometric information a priori (a part for the combinatorial). Rather, its geometry is given by representation-theoretic data (spins and intertwiners) distributed among the edges and faces. Then, once fixed the geometry of the boundary (by assigning a fixed value to the boundary spins and intertwiners), the sum over all bulk data which appears in (3.49) realizes a discrete version of the integral over all metrics. In this way the dynamics is given in terms of transition amplitudes between boundary states.

3.2.1 Path integral of SU(2) BF theory in 3d

We start from the simple case of 3d BF theory. Let us refer, for simplicity, to the example in Figure 3.3 showing in a dual fashion a piece of manifold discretized in terms of tetrahedra and a boundary geometry made of triangles. The associated partition function $Z_{BF}^{\mathcal{K}}$ is built on the 2-complex $\mathcal{K}$ and can be interpreted as giving the transition amplitude among the boundary states built on graphs $\Gamma_{\mathcal{K},A}$ and $\Gamma_{\mathcal{K},B}$.

For each edge $e \subset \mathcal{K}$ there are always three faces $f_1, f_2, f_3 \subset \mathcal{K}$ meeting, each coming with an independent representation ρ_1, ρ_2, ρ_3.
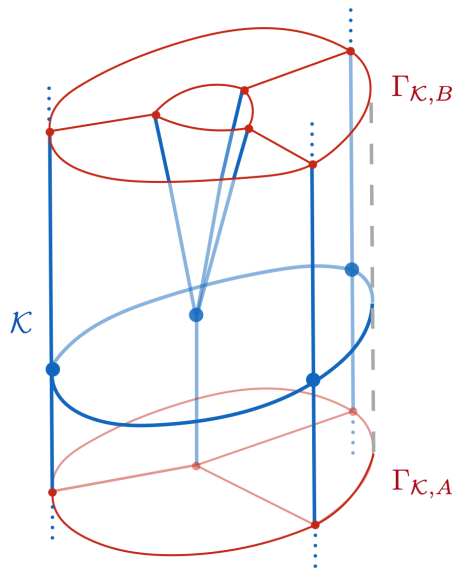
Figure 3.3: The 2-complex $\mathcal{K}$ dual to a 3d simplicial discretization and built between two graphs $\Gamma_{\mathcal{K},A}$ and $\Gamma_{\mathcal{K},B}$ dual to boundary triangulations. All the vertices are 4-valent and dual to tetrahedra. The faces are not colored for clarity, however in Figure 3.2 one can see, for example, the faces around the central vertex. All the nodes are 3-valent and dual to triangles. The graph $\Gamma_{\mathcal{K},A}$ is dual to the 2d boundary of a tetrahedron. The reader is invited to an exercise of visualization of the 2d discretization dual to $\Gamma_{\mathcal{K},B}$.

As we have seen in the previous chapter, 3d BF theory is equivalent to 3d gravity provided that we choose the local gauge group to be $G = \mathrm{SU}(2)$ [8]. In this setting, all the irreducible representations are labeled by a half-integer spin j, have finite dimension $d_\rho = 2j + 1$ and correspond to the *Wigner-D matrices* i.e., $\rho_i(g) = D^{j_i}(g)$. Thus, for a generic element $g \in \mathrm{SU}(2)$ we can

---

[8]Refer to Appendix A for details on the group structure and its representations.

write (3.42) as

$$P_{\text{Inv}}^e = \int_{\text{SU}(2)} dh_e D^{j_1}(h_e) \otimes D^{j_2}(h_e) \otimes D^{j_3}(h_e), \qquad (3.50)$$

or in explicit indices notation

$$(P_{\text{Inv}}^e)^{m_1 m_2 m_3}_{n_1 n_2 n_3} = \int_{\text{SU}(2)} dh_e D^{j_1}(h_e)^{m_1}_{n_1} D^{j_2}(h_e)^{m_2}_{n_2} D^{j_3}(h_e)^{m_3}_{n_3}. \qquad (3.51)$$

Due to the left/right invariance of the Haar measure, this integral is invariant under a separate group action acting respectively on the indices m_i and n_i with $i = 1, 2, 3$. The only invariant object with three indices m_1, m_2, m_3 in the SU(2) representation is the *Wigner 3j-symbol*,

$$\iota^{m_1 m_2 m_3} = \begin{pmatrix} j_1 & j_2 & j_3 \\ m_1 & m_2 & m_3 \end{pmatrix}. \qquad (3.52)$$

Then, equation (3.51) can be written in the form (3.46) as

$$(P_{\text{Inv}}^e)^{m_1 m_2 m_3}_{n_1 n_2 n_3} = \iota_e^{m_1 m_2 m_3} (\iota_e^\dagger)_{n_1 n_2 n_3}. \qquad (3.53)$$

At each vertex $v \subset \mathcal{K}$ there are four edges meeting, which echoes the four faces bounding a tetrahedron. Therefore, at each vertex there are four fully contracted intertwiners defining a so-called *Wigner 6j-symbol* (see Appendix A)

$$\{6j\}_v = \begin{Bmatrix} j_1 & j_2 & j_3 \\ j_4 & j_5 & j_6 \end{Bmatrix}. \qquad (3.54)$$

where the spins j_a, $a = 1, 2, 3, 4, 5, 6$ are associated to the six faces f_a touching $v \subset f_a$. This is reminiscent of the fact that a tetrahedron has six sides. The object (3.54) defines, up to a sign [62], the vertex amplitude for the SU(2) BF theory in three dimensions.

Notice that in the derivation above we relied on the convention of Figure 2.5, where the face is positive (clockwise) oriented and in accordance with the orientation of the boundary edges. However, in an oriented 2-complex it is easy to find opposite orientations of f and some boundary edge $e' \subset f$, in which case the holonomy H_f will be defined in terms of the inverse $h_e'^{-1}$ of the holonomy on e'. Also, we have not mentioned the choice of starting vertices which defines the holonomy around a face. Nonetheless, the partition function depends on the character (3.39) of H_f which is invariant with respect to this choice. Eventually, from the above analysis and taking into account the correct signs we obtain the formula

$$Z_{BF}^{\mathcal{K}} = \sum_{j_f} \prod_f (-1)^{2j_f} (2j_f + 1) \prod_v (-1)^{\sum_{a=1}^6 j_a} \{6j\}_v. \qquad (3.55)$$

The sum is over all bulk spins and, to each of these spin configurations, it assigns a weight which is a real number.

If we had taken into account the other delta function in (3.37) the result would have been the same but with the sum ranging over integer spins $j_f \in \mathbb{N}$.

This model is also called the Ponzano-Regge model. Remarkably, Ponzano and Regge discovered that the $6j$-symbol contains the Regge action in its asymptotic behavior. For a detailed reference see [62].

3.2.2 Path integral of $\mathrm{SU}(2)$ BF theory in 4d

Let us extend the analysis above to the case of a path integral for discrete BF-theory in 4d with gauge group $G = \mathrm{SU}(2)$.

To help the visualization we refer to Figure 3.4 where a 4d simplicial discretization is depicted via the dual 2-complex $\mathcal{K}$ and two selected geometrical states with support on the graphs $\Gamma_{\mathcal{K},A}$ and $\Gamma_{\mathcal{K},B}$.
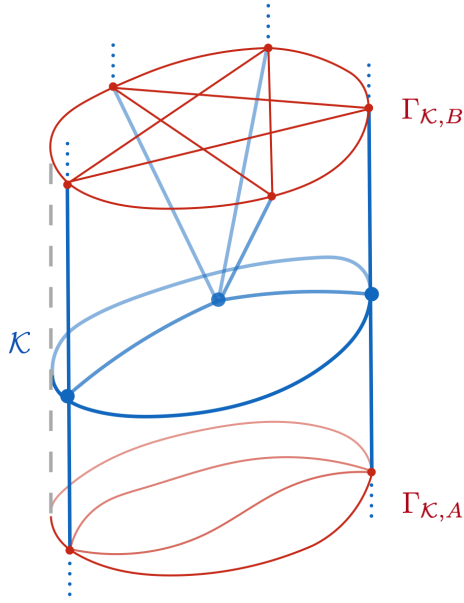
Figure 3.4: The 2-complex $\mathcal{K}$ is dual to a simplicial discretization in terms of three 4-simplices. Each vertex is 5-valent given that a 4-simplex is bounded by 5-tetrahedra. The graphs $\Gamma_{\mathcal{K},A}$ and $\Gamma_{\mathcal{K},B}$ are dual to 3d discretizations. All the nodes are 4-valent and dual to tetrahedra. Then the graph $\Gamma_{\mathcal{K},A}$ is a 3d object made by gluing two tetrahedra face by face. The graph $\Gamma_{\mathcal{K},B}$ is dual to the 3d boundary of a 4-simplex.

For each edge e there are four faces f_1, f_2, f_3, f_4 coming with relative representations $\rho_1, \rho_2, \rho_3, \rho_4$. Now, in 4d the invariant vector space

$$\mathrm{Inv}_G(V_e) = \mathrm{Inv}_G(V_{\rho_1} \otimes V_{\rho_2} \otimes V_{\rho_3} \otimes V_{\rho_4}), \tag{3.56}$$

has dimension grater than one. Then, according to (3.46) we can express the projector P_{Inv}^e in terms of invariant vectors in V_e i.e., using a basis of independent intertwiners $|\iota_e\rangle$.

For every vertex $v \subset \mathcal{K}$ there are five edges, given that a 4-simplex is bounded by five tetrahedra (see Figure 3.4). Then at each vertex a contraction pattern among intertwiners with free indices has place. In analogy with the 3d case, here we can think each intertwiner coming with four indices m_i, $i = 1, 2, 3, 4$. The result of the contraction is a vertex amplitude $\mathcal{A}_v(\{j_f\}, \{\iota_e\})$ which, up to a sign, corresponds to a *15j-symbol* $\{15j\}_v$, so-called in virtue of the fact that each vertex recouples 15 quantum numbers, the ten spins j_f and the five intertwiners ι_e. Explicitly,

$$Z_{BF}^{\mathcal{K}} = \sum_{j_f, \iota_e} \prod_f (2j_f + 1) \prod_v \{15j\}_v. \tag{3.57}$$

3.2.3 The coherent states representation

The 15 quantum numbers defining the vertex amplitude (3.57) are not enough to characterize the classical geometry of the five tetrahedra in the boundary of a 4-simplex. Indeed, a classical tetrahedron in three dimensions is specified by its six lengths or, equivalently, by the area of its four faces (+4 d.o.f.), the relative normal unit vectors ($+4 \cdot 2 = +8$ d.o.f.), a closure relation of its boundary (-3 d.o.f.), and an invariance under rotations (-3 d.o.f.), for a total of six degrees of freedom. In the standard basis however, each tetrahedron is only specified by five degrees of freedom, four spins with the interpretation of face areas, and a 'standard' intertwiner carrying a single degree of freedom which can be interpreted as a 3d dihedral angle among two of its boundary triangles. This means that, in the quantum regime, the remaining degree of freedom (e.g., a second 3d dihedral angle) is totally spread. Then, in order to give a geometric interpretation to the intertwiners at the vertex boundary, it would be convenient to dispose of invariant quantum states $|\iota_e\rangle$ depending on the right amount of quantum numbers, such that they have a direct geometric interpretation in terms of areas and angles minimally spread around their classical values and becoming sharp after taking the classical limit.

A major advancement in the formulation of spin foam models arrived with the adoption of a over-complete basis for the irreducible representations used to define the intertwiners [63]. This springs out from a classical tool of quantum mechanics i.e., with the introduction of *coherent states*.

In this language the invariant basis is given by the so-called *Livine-Speziale coherent intertwiners* obtained by tensoring together coherent states. These new objects allow for a clean semiclassical limit where the intertwiners at the edges of the 2-complex acquire a nice geometric interpretation in terms of 3d

polyhedra.

The $SU(2)$ coherent states

Given the standard eigenstate basis $|j, m\rangle$ of the angular momentum (see Appendix A), the maximal weight vector with respect to the $\hat{e}_3$ direction is $|j, \hat{e}_3\rangle \equiv |j, j\rangle$ for any spin j. This state is an eigenvector of the angular momentum $J_3 = \frac{i}{2}\sigma_3$ such that $J_3|j, j\rangle = j|j, j\rangle$. On such state the dispersion of the angular momentum J_3 is minimized and the uncertainty relations are saturated i.e.,

$$\Delta J_3 = 0 \qquad \text{and} \qquad \Delta J_1 \Delta J_2 = \frac{1}{2}|\langle jj|J_3|jj\rangle|, \qquad (3.58)$$

being

$$\Delta J_i = \sqrt{\langle jj|J_i^2|jj\rangle - (\langle jj|J_i|jj\rangle)^2}. \qquad (3.59)$$

Also, the dispersion of the angular momentum in the x (or y) direction with respect to the total angular momentum, vanishes in the limit $j \to \infty$ e.g.,

$$\frac{\Delta J_1}{\sqrt{\langle jj|J^2|jj\rangle}} = \frac{\sqrt{\frac{j}{2}}}{\sqrt{(j(j+1))}} \to 0. \qquad (3.60)$$

In other words, the state $|jj\rangle$ becomes sharp in the $\hat{e}_3$ direction in the large-j limit. This limit provides indeed the notion of *semiclassical limit* in the context of spin foams. We will come back to this in the next chapter.

A state fulfilling the properties above described is called a *coherent state* [64]. Let us take a group element $g_{\vec{n}} \in SU(2)$ and the unit vector $\vec{n} = g_{\vec{n}} \triangleright \hat{e}_3$ [9] defining a direction on the two-sphere S^2. Starting from the maximal weight vector one finds an infinite set of $SU(2)$ coherent states

$$|j, \vec{n}\rangle = |j, g_{\vec{n}} \triangleright \hat{e}_3\rangle = g_{\vec{n}} \triangleright |j, \hat{e}_3\rangle, \qquad (3.61)$$

for which the angular momentum is minimally spread around $\vec{n}$. Notice that such states are defined up to a $U(1)$ phase, corresponding to a rotation about the $\vec{n}$-direction. Varying $\vec{n}$ one finds an over-complete set spanning the vector space V_j.

The coherent states (3.61) can be written in the canonical basis of eigenstates of J_3 as

$$|j, \vec{n}\rangle = \sum_m C_m(\vec{n})|j, m\rangle, \qquad \text{with} \qquad C_m(\vec{n}) = D^j(g_{\vec{n}})_{mj}, \qquad (3.62)$$

---

[9]We use the symbol $g \triangleright$ to mean the action of the group element g through the appropriate representation e.g., $g \triangleright \vec{v} = \rho(g)\vec{v}$ with $\rho : SU(2) \to SO(3)$.

being $D^j(g)_{mj}$ a Wigner D-matrix element. Using the fact that the basis $|j, m\rangle$ provides a resolution of the identity and that the Wigner D-matrices form an orthonormal set with respect to the Haar measure on SU(2) one can show that the coherent states $|j, \vec{n}\rangle$ form an orthogonal basis such that

$$\mathbb{1}_j = d_j \int_{S^2} \mathrm{d}^2 n |j, \vec{n}\rangle\langle j, \vec{n}|, \tag{3.63}$$

where the integration is with respect to the invariant measure on the two-sphere (see for example [30]). Another key property of coherent states is the following

$$|j, \vec{n}\rangle = |1/2, \vec{n}\rangle \otimes \cdots \otimes |1/2, \vec{n}\rangle \equiv |1/2, \vec{n}\rangle^{\otimes 2j} \equiv |\vec{n}\rangle^{\otimes 2j}. \tag{3.64}$$

Coherent intertwiners

Let us consider a set of F coherent states $|j_i, \vec{n}_i\rangle$ such that they satisfy the *closure condition*[10]

$$\sum_i j_i \vec{n}_i = 0. \tag{3.65}$$

The basic idea is to associate such states to F faces of area j_i and outward-pointing normals $\vec{n}_i$. A coherent polyhedron is constructed by tensoring them together and imposing the invariance under rotations by SU(2)-group averaging. The associated SU(2) *coherent intertwiner* reads

$$|\iota\rangle = \int_{\mathrm{SU}(2)} \mathrm{d}g\ g \triangleright \bigotimes_i |j_i, \vec{n}_i\rangle. \tag{3.66}$$

and spans the space $\mathrm{Inv}_{\mathrm{SU}(2)} \bigotimes_i V_{j_i}$ as the vectors $\vec{n}_i$ vary [65]. The SU(2) integration guarantees the invariance under the group action. A coherent intertwiner then becomes a sharp polyhedron in the large-j limit.

The resolution of the identity (3.63) can be extended to the invariant subspace $\mathrm{Inv}_{\mathrm{SU}(2)} \bigotimes_i V_{j_i}$ where it is written in the coherent intertwiners basis as

$$\mathbb{1}_{\mathrm{Inv}_{\mathrm{SU}(2)} \bigotimes_i V_{j_i}} = \int \Big(\prod_{i=1}^F d_{j_i} \mathrm{d}^2 n_i \Big) |\iota\rangle\langle\iota|$$

$$= \int \Big(\prod_{i=1}^F d_{j_i} \mathrm{d}^2 n_i \Big) \int \mathrm{d}g\ g \triangleright \bigotimes_i |j_i, \vec{n}_i\rangle \int \mathrm{d}g' \bigotimes_i \langle j_i, \vec{n}_i| \triangleleft (g')^{-1}. \tag{3.67}$$

---

[10]A theorem by Minkowski states that if the j_i and $\vec{n}_i$ satisfy the closure condition, then there exists a convex polyhedron, unique up to translation, with face normals $\vec{n}_i$ and face areas j_i.

This expression can then be used in the place of (3.46) to project onto the invariant subspace, at each edge $e \subset \mathcal{K}$. Then we see that the coherent state representation endows each edge e with two group integrations and a bunch of spins j_i and unit vector $\vec{n}_i$ for each face attached to e. This data is evenly split in two and inherited by the extremal vertices $v_1, v_2 \supset e$. In other words the second and the third integrals of (3.67) are respectively entering the contractions in v_1 and v_2. The first integral in (3.67) is a normalization factor.

Notice that the closure condition (3.65) is a crucial requirement for the semiclassical interpretation of the coherent states. This condition is not satisfied by all the states entering the partition function $Z_{BF}^{\mathcal{K}}$. However, as it was shown in [63], the quantum correlations are dominated by the semiclassical states in the large spin limit. Furthermore in [65] it was shown that, by slightly changing the integration measure, one can restrict the integration to the states which satisfy (3.65) exactly.

The coherent tetrahedron

In the 4d analysis which led us to the partition function (3.57), we adopt a simplicial discretization in terms of 4-simplices, tetrahedra and triangles. Therefore, the basic object that we need to define to implement the coherent state representation, is an intertwiner with four magnetic indices, also called a *coherent tetrahedron* [66]. On each edge e we have a base space $V_e = V_{j_1} \otimes V_{j_2} \otimes V_{j_3} \otimes V_{j_4}$ acted upon by the tensor product of SU(2) representations $D^{j_1} \otimes D^{j_2} \otimes D^{j_3} \otimes D^{j_4}$ (one for each face $f_1, f_2, f_3, f_4 \supset e$ attached to the edge). Let us take a coherent state basis for V_e i.e.,

$$|j_1 \vec{n_1}\rangle \otimes |j_2 \vec{n_2}\rangle \otimes |j_3 \vec{n_3}\rangle \otimes |j_4 \vec{n_4}\rangle, \qquad (3.68)$$

such that $\sum_{i=1}^{4} j_i \vec{n}_i = 0$. This can be thought as a tetrahedron with boundary areas j_1, j_2, j_3, j_4 and normals $\vec{n}_1, \vec{n}_2, \vec{n}_3, \vec{n}_4$. The projection of (3.68) onto the subspace invariant under the action of SU(2) is achieved by group averaging

$$|\iota_e\rangle = \int_{SU(2)} dh_e \left(D^{j_1}(h_e)|j_1\vec{n_1}\rangle \otimes D^{j_2}(h_e)|j_2\vec{n_2}\rangle \otimes D^{j_3}(h_e)|j_3\vec{n_3}\rangle \otimes D^{j_4}(h_e)|j_4\vec{n_4}\rangle \right)$$

$$= \int_{SU(2)} dh_e \; h_e \triangleright \bigotimes_{f_e=1}^{4} |j_{f_e}, \vec{n}_{f_e}\rangle, \qquad (3.69)$$

where by f_e we denote the face $f \supset e$. This is the analogue of (3.66) and can be interpreted as a coherent tetrahedron invariant under $SO(3)$ rotations.

The resolution of the identity (3.67) becomes

$$
\mathbb{1}_{\mathrm{Inv}_{\mathrm{SU}(2)}(V_e)} = \int \Big(\prod_{f_e=1}^{4} d_{j_{f_e}} \mathrm{d}^2 n_{f_e} \Big) \times
$$

$$
\times \int \mathrm{d}h_e \bigotimes_{f_e} D^{j_{f_e}}(h_e) |j_{f_e}, \vec{n}_{f_e}\rangle \int \mathrm{d}h'_e \bigotimes_{f_e} \langle j_{f_e}, \vec{n}_{f_e}| (D^{j_{f_e}}(h'_e))^\dagger.
$$

$$(3.70)$$

The two integrals in the second row are respectively sent to the two extremal vertices $v_1, v_2 \subset e$ to get contracted with the data coming from the other edges. At each vertex, dual to a 4-simplex, there are five edges meeting, dual to its five boundary tetrahedra. Therefore, the data inherited by a vertex v from a single edge can be used to describe a boundary tetrahedron with face areas j_i and normals $\vec{n}_i$ with $i = 1, 2, 3, 4$. The group integration implements the invariance of such tetrahedron under 3d rotations. The data at each intertwiner become sharp in the semiclassical limit.

Coherent state representation of 4d BF amplitudes

Contracting all the boundary data entering into the 4-simplex vertex from the five edges and relative faces, we obtain the expression of the vertex amplitude (3.48). In order to get a neat expression let us use the labeling $a = 1, 2, 3, 4, 5$ for the five tetrahedra bounding the vertex v (see Figure 3.5). The contraction
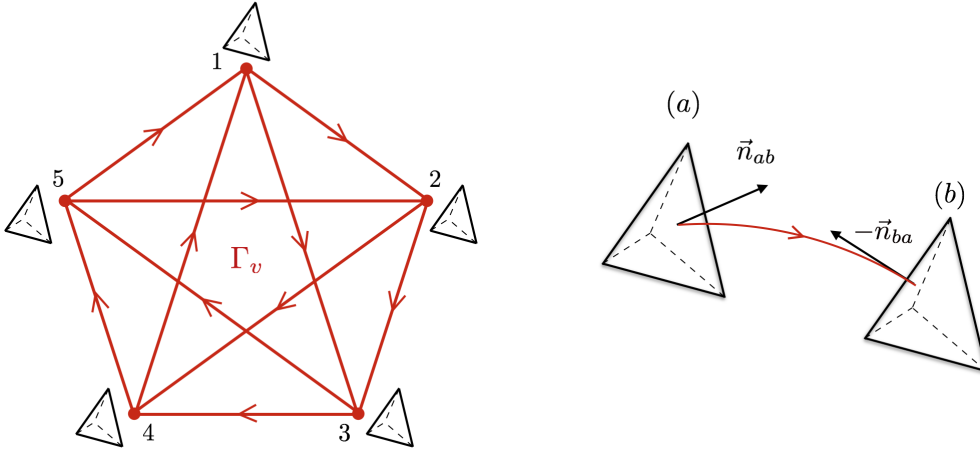
Figure 3.5: On the left: the vertex boundary graph and its nodes dual to tetrahedra a. On the right the labeling of two tetrahedra a and b sharing a triangle (ab) but having independent normal vectors.

happens at each triangle (ab) of area $j_{ab} = j_{ba}$ where the two tetrahedra a and b meet. From a local perspective at a, the normal vector to the boundary triangle (ab) is $\vec{n}_{ab}$, while from the perspective of b the normal vector is $\vec{n}_{ba}$ [11]. The two vectors $\vec{n}_{ab}$ and $\vec{n}_{ba}$ are a priori independent. The vertex amplitude performs such contraction so that one gets

$$\mathcal{A}_v = \int_{\mathrm{SU(2)^5}} \mathrm{d}h_a \prod_{(ab)} \langle j_{ab}, \vec{n}_{ab} | D^{j_{ab}}(h_a)^\dagger D^{j_{ab}}(h_b) | j_{ba}. \vec{n}_{ba} \rangle. \qquad (3.71)$$

Using the coherent state property (3.64) one can write the amplitude as

$$\mathcal{A}_v = \int_{\mathrm{SU(2)^5}} \mathrm{d}h_a e^{S[h_a]}, \qquad (3.72)$$

where we defined

$$S[h_a] = \sum_{(ab)} 2j_{ab} \ln \langle \vec{n}_{ab} | h_a^{-1} h_b | \vec{n}_{ab} \rangle. \qquad (3.73)$$

Finally, we can write the partition function as

$$Z_{BF}^{\mathcal{K}}(\mathrm{SU(2)}) = \sum_{j_f} \prod_f d_{j_f} \prod_e \left(\int \left(\prod_{f_e=1}^4 d_{j_{f_e}} \mathrm{d}^2 n_{f_e} \right) \right) \prod_v \mathcal{A}_v(\{\rho_f\}_v, \{\iota_e\}_v). \qquad (3.74)$$

---

[11] We adopt the convention for which the normal vector points in the same direction as the oriented link i.e., for outgoing links the normal vector in outward-pointing and vice versa.

Chapter 4

The Euclidean EPRL-FK model

Let us recap what we have seen so far. According to section 3.2, the first step to build a spin foam model is to define a path integral for discrete BF theory on a 2-complex $\mathcal{K}$, leading to a partition function $Z_{BF}^{\mathcal{K}}$ of the type (3.49), which is interpreted as a sum over quantum states. A 'path' in this sense corresponds to an assignment of spins j_f to every face $f \subset \mathcal{K}$ and intertwiners ι_e for each edge $e \subset \mathcal{K}$. The most important element in $Z_{BF}^{\mathcal{K}}$ is the so-called vertex amplitude $\mathcal{A}_v$ which is built, at each vertex $v \subset \mathcal{K}$, through the contraction of the data $(\{\rho_f\}_v, \{\iota_e\}_v)$ entering from the edges $e \supset v$ (see (3.47)). This data is in one to one correspondence with the data $(\{\rho_\ell\}_v, \{\iota_n\}_v)$ stored on the boundary graph Γ_v built at each vertex with nodes $n \in \Gamma_v$ and links $\ell \in \Gamma_v$ respectively associated to edges and faces or equivalently, if we are in 4d, to tetrahedra and triangles (see (3.48)).

Thanks to the use of coherent states studied in 3.2.3, we were able to represent the 4d partition function (3.74) and the vertex amplitude (3.71) for the gauge group SU(2) in a form which allows a nice geometric interpretation of the intertwiners at the edges (or at the nodes) as 'quantum tetrahedra'.

4.1   Construction of the Euclidean EPRL-FK model

Let us now extend the analysis of the previous chapter to the case of a path integral for discrete BF-theory in 4d with gauge group $G = \mathrm{SU}(2) \times \mathrm{SU}(2)$. This analysis connects us to Euclidean gravity in 4d. In fact, for Riemannian signature, the local gauge group is $\mathrm{Spin}(4) \simeq \mathrm{SU}(2) \times \mathrm{SU}(2)$.

From the path integral of 4d discrete BF-theory, with this choice of gauge group, one can define a 4d spin foam model by imposing the simplicity constraints (2.75) at the quantum level. The correct implementation of the constraints is a non trivial operation, and different ways of imposing them characterize distinct spin foam models. In this chapter we define the 4d Euclidean EPRL-FK spin foam model [39, 40], which will be used throughout this work.

In fact, it has a pivotal role in the state of the art works of the spin foam community.

4.1.1   The group Spin(4)

Let us give some brief information about the structure group that we are using. The group Spin(4) is isomorphic to $SU(2) \times SU(2)$ and its Lie algebra decomposes into $\mathfrak{spin}(4) \simeq \mathfrak{su}(2) \oplus \mathfrak{su}(2)$ (see (A.25)). The unitary representations $\rho_{(j^+,j^-)}$ of the group are then labeled by two half-integers (j^+, j^-) where $\pm$ indicates the membership to one of the two SU(2)-subalgebras. These representations act on the base space $V_{(j^+,j^-)}$.

The algebra $\mathfrak{spin}(4)$ can be described, for example, in terms of the six SU(2)-generators $J_{i,\pm}$ satisfying the standard angular momentum algebra

$$[J_{i,\pm}, J_{j,\pm}] = i\epsilon_{ijk} J_{k,\pm}. \tag{4.1}$$

A basis in the vector space $V_{(j^+,j^-)}$ is then given by vectors $|j^+ \ j^- \ m^+ \ m^-\rangle$ which are eigenstates of the two Casimirs $C_1 = J_+^2 + J_-^2$, $C_2 = J_+^2 - J_-^2$ and of the two angular momenta operators $J_{3,\pm}$ (see Appendix A). A Spin(4) representation can be decomposed into a direct sum of SU(2)-representations

$$\rho_{(j^+,j^-)} = \rho_{j^-} \otimes \rho_{j^+} = \bigoplus_{j=|j^+-j^-|}^{j^++j^-} \rho_j, \tag{4.2}$$

acting on the base space

$$V_{(j^+,j^-)} = V_{j^+} \otimes V_{j^+} = \bigoplus_{j=|j^+-j^-|}^{j^++j^-} V_j. \tag{4.3}$$

The algebra (4.1) can be equivalently characterized by the generators of rotations L_i and boosts K_i, $i = 1, 2, 3$. The full characterization can be found in (A.25), in Appendix A. The Casimirs in terms of the new generators are $C_1 = L^2 + K^2$ and $C_2 = \vec{K} \cdot \vec{L}$. The choice of this specific SU(2) subgroup of Spin(4) is made at each edge of the 2-complex. Notice that this choice is the analogue of the time gauge used to define the two vectors (2.29). Then the linear simplicity constraints (2.75) can be expressed in terms of the generators L_i and K_i.

4.1.2   Implementation of simplicity constraints

Following the analysis in 3.2.2, at each face $f \subset \mathcal{K}$ there is a representation ρ_f acting on a base space V_f respectively of the form (4.2) and (4.3). The

EPRL-FK model is defined by imposing the linear simplicity constraints D^i_f, given by (2.75), à la Gupta-Bleuler i.e., by selecting from the base space V_f at each face only the states $|\psi\rangle \in V_f$ for which the matrix elements $\langle\psi|D^i_f|\phi\rangle = 0$ vanish[1]. In a Spin(4) basis $|\psi\rangle = |j^+ \ j^- \ j \ m\rangle$, the matrix elements of the constraints read

$$
\begin{aligned}
\langle j^+ \ j^- \ j \ n|D^f_3|j^+ \ j^- \ j \ m\rangle &= \delta_{n,m}m(1 - \frac{\gamma_j}{\gamma}), \\
\langle j^+ \ j^- \ j \ n|D^f_\pm|j^+ \ j^- \ j \ m\rangle &= \delta_{n\pm1,n}\sqrt{(j \pm m + 1)(j \mp m)}(1 - \frac{\gamma_j}{\gamma}),
\end{aligned}
\tag{4.4}
$$

where we used the definition (2.75) and the relations (A.26) in Appendix A. The constraints (4.4) are then satisfied if

$$
\gamma_j = \frac{j^+(j^+ + 1) - j^-(j^- + 1)}{j(j + 1)} = \gamma.
\tag{4.5}
$$

This equation admits different solutions for $\gamma < 1, \gamma = 1$ and $\gamma > 1$.

In the rest of this work we focus on the first case $\gamma < 1$ [2], for which the solution of (4.5) is

$$
j^\pm = \frac{|1 \pm \gamma|}{2}j,
\tag{4.6}
$$

which corresponds to select the maximum weight component $j = j^+ + j^-$ of the expansion (4.3) for each vector space $V_f = V_{(j^+_f, j^-_f)}$. Notice that, according to (4.6), the Barbero-Immirzi parameter γ is restricted so to be compatible with the half-integer-nature of $j \in \frac{\mathbb{N}}{2}$ and $j^\pm \in \frac{\mathbb{N}}{2}$. This is a feature of the Euclidean model which is not present in the Lorentzian [68].

4.1.3 Boosted coherent intertwiners

In the previous chapter we have introduced the coherent state representation for defining the partition function and in particular the vertex amplitude.

---

[1]This 'weak' imposition of the constraints is in contrast with a 'strong' imposition of the form $D^i_f|\psi\rangle = 0$ which, as argued in [39], produces an unwanted elimination of physical degrees of freedom. This is due to the fact that the constraints are second class i.e., they do not commute and then the constraint algebra is not closed [30]. The strong imposition of the constraint was indeed proposed in the Barrett-Crane model [67] which for many years had a leading role in Spin foam models. As of today, this role is taken by the EPLR-FK model that we are reviewing.

[2]The case for $\gamma > 1$ is only marginally more complicated, and we do not expect one were to find qualitatively different results in that case. Nonetheless, this is something to be checked eventually. In the case $\gamma = 1$ the constraint algebra closes and the constraints (2.75) can be imposed 'strongly' (see footnote in the previous page). In such case they reduce to the condition of setting all the j_+-spins to zero in the state sum and the partition function reduces to that of SU(2) BF theory, which is not a good model for quantum gravity [30].

The prototype of SU(2) coherent intertwiner $|\iota\rangle \in \mathrm{Inv}_{\mathrm{SU}(2)} \bigotimes_i V_{j_i}$ described in (3.66), can be lifted to a Spin(4) coherent intertwiner $|\Phi\iota\rangle \in \mathrm{Inv}_{\mathrm{Spin}(4)} \bigotimes_i V_{(j_i^+, j_i^-)}$ by a *boosting* procedure which sends

$$\Phi : \mathrm{Inv}_{\mathrm{SU}(2)} \bigotimes_i V_{j_i} \longrightarrow \mathrm{Inv}_{\mathrm{Spin}(4)} \bigotimes_i V_{(j_i^+, j_i^-)}.$$

In particular the *boosting map* Φ consists in the joint action of a map $\beta_{j_i}^\gamma$ for each spin j_i such that

$$\beta_{j_i}^\gamma : V_{j_i} \longrightarrow V_{(j_i^+, j_i^-)}, \tag{4.7}$$

and a projector P

$$P : \bigotimes_i V_{(j_i^+, j_i^-)} \longrightarrow \mathrm{Inv}_{\mathrm{Spin}(4)} \bigotimes_i V_{(j_i^+, j_i^-)}.$$

In the rest of the paper we will focus on the specific case of Barbero-Immirzi parameter $\gamma < 1$. In this case the spins $j_i^\pm$ are related to γ and j_i via the relation (4.6) and the map (4.7) is defined by embedding the space V_j isometrically into the highest weight space of the Clebsh-Gordan decomposition (4.3), namely $V_{j^+ + j^-}$. Thus, If at each edge there are F faces attached we can write

$$\Phi = P \circ \left(\beta_{j_1}^\gamma \otimes \cdots \otimes \beta_{j_F}^\gamma \right),$$

and the *boosted coherent intertwiner* factorizes in terms of SU(2) coherent intertwiners $|\iota^\pm\rangle$ as

$$|\Phi\iota\rangle = |\iota^+\rangle \otimes |\iota^-\rangle = \int \mathrm{d}g^+ \ g^+ \triangleright \bigotimes_i |j_i^+, \vec{n}_i\rangle \ \otimes \int \mathrm{d}g^- \ g^- \triangleright \bigotimes_i |j_i^-, \vec{n}_i\rangle. \tag{4.8}$$

We also refer to $|\Phi\iota\rangle$ as Spin(4) coherent intertwiner and we are going to use it to build the transition amplitudes in our spin foam model.

Finally, let us write the resolution of the identity for the boosted coherent intertwiners in the form

$$\begin{aligned}
\mathbb{1}_{\mathrm{Inv}_{\mathrm{Spin}(4)} \bigotimes_i V_{(j_i^+, j_i^-)}} &= \sum_{\Phi\iota} \frac{1}{\|\Phi\iota\|^2} |\Phi\iota\rangle\langle\Phi\iota| \\
&= \sum_{\iota^\pm} \frac{1}{\|\iota^+\|^2 \|\iota^-\|^2} (|\iota^+\rangle\langle\iota^+|) \otimes (|\iota^-\rangle\langle\iota^-|).
\end{aligned} \tag{4.9}$$

This is the analogue of (3.67) where we have substituted the integration over the 2-sphere with a sum normalized by the squared norm of the coherent intertwiner $\|\Phi\iota\|^2 = \langle\Phi\iota|\Phi\iota\rangle$.

4.1.4 The EPRL-FK partition function

A resolution of the identity of the form (4.9) is inserted at each edge $e \subset \mathcal{K}$. The 'bra' and 'ket' parts are respectively sent to the two vertices at the opposite ends of the edge. Then, the vertex amplitudes contracts the five boosted coherent intertwiners coming from the edges with the information of spins and intertwiners. In analogy with (3.47), it is defined as the trace of the boosted coherent intertwiners

$$\mathcal{A}_v \equiv \mathrm{tr}\left(\bigotimes_{e \to v} |\Phi \iota_e\rangle \bigotimes_{e \leftarrow v} \langle \Phi \iota_e| \right), \tag{4.10}$$

where we recall that the boosting map Φ is required to enforces the simplicity constraints (2.75) at the quantum level and to lift the SU(2) coherent intertwiners to elements of $V_{j^+ + j^-}$ invariant under Spin(4) transformations. Thanks to the factorization (4.8) for $\gamma < 1$, also the vertex amplitude factorizes as

$$\mathcal{A}_v(\{j_f\}_v, \{\iota_e\}_v) := \mathcal{A}_v^+(\{j_f^+\}_v, \{\iota_e^+\}_v) \cdot \mathcal{A}_v^-(\{j_f^-\}_v, \{\iota_e^-\}_v), \tag{4.11}$$

where $\mathcal{A}_v^\pm$ have the SU(2) form (3.72).

Eventually, we can write the partition function for the 4d Euclidean EPRL-FK model with Barbero-Immirzi parameter $\gamma < 1$ as

$$Z_{BF}^{\mathcal{K}} = \sum_{j_f^\pm, \iota_e^\pm} \prod_f \mathcal{A}_f \prod_e \mathcal{A}_e \prod_v \mathcal{A}_v, . \tag{4.12}$$

where $\mathcal{A}_f$, $\mathcal{A}_e$ and $\mathcal{A}_v$ are respectively the *face-*,*edge-* and *vertex-amplitudes* associated to each element of the 2-complex. Explicitly,

$$\mathcal{A}_f = [(2j^+ + 1)(2j^- + 1)]^\alpha, \tag{4.13}$$

$$\mathcal{A}_e \equiv \frac{1}{\|\iota^+\|^2 \|\iota^-\|^2}, \tag{4.14}$$

$$\mathcal{A}_v = \mathcal{A}_v^+ \mathcal{A}_v^-, \quad \mathcal{A}_v^\pm = \int_{\mathrm{SU}(2)^5} \mathrm{d}h_a^\pm e^{S_\pm}, \quad S_\pm = \sum_{(ab)} 2j_{ab}^\pm \ln\langle \vec{n}_{ab}^\pm|(h_a^\pm)^{-1} h_b^\pm|\vec{n}_{ab}^\pm\rangle \tag{4.15}$$

In other words, for $\gamma < 1$ one obtains a full factorization of the $\pm$ labels and the EPRL-FK partition function becomes the 'square' of the SU(2) partition function (3.74).

The choice of the face amplitude is not unique and influences the convergence of the state sum [69, 70]. We choose the definition (4.13) depending on a parameter α. For $\alpha = 1$ one gets the standard definition $d_{j_f^+} d_{j_f^-}$. The parameter α will play the role of a coupling constant, in that it is a free parameter in the path integral measure.

It is important to mention that there exists a generalization of spin foam model to arbitrary polyhedral discretization [71]. Therefore, a part for details in the implementation of the simplicity constraints [72], the validity of the formulas obtained up to this point can be extended to discretizations different from the simplicial one.

4.2 Semiclassical limit

The semiclassical limit of a spin foam model is defined through the large spin limit of the amplitudes written in the coherent state representation. The asymptotic limit is taken by rescaling by a parameter λ each spin simultaneously,

$$j \rightarrow \lambda j \tag{4.16}$$

and then taking the limit $\lambda \rightarrow \infty$.

Notice that each factor $\pm$ of the vertex amplitude (4.15) corresponds to an oscillatory integral and the phase of the oscillation, given by the function $S_{\pm}$, allows for complex values. The asymptotic limit of these kind of integrals is performed through a so-called *extended stationary phase approximation*. Let us briefly explain how this method works and give an algorithm to use in the upcoming calculations.

4.2.1 The extended stationary phase approximation

The *extended* stationary phase method provides a tool to compute the asymptotic approximation of oscillatory integrals whose phases are smooth complex valued functions S defined over a closed D-dimensional manifold X and such that $\text{Re}S \leq 0$. Let us consider the following scalar function

$$f(\lambda) = \int_X \mathrm{d}x \ a(x) \ e^{\lambda S(x)}, \tag{4.17}$$

being λ a positive real parameter and $a(x)$ a smooth complex test function. In the extended stationary phase approximation the asymptotic limit $\lambda \rightarrow \infty$ is dominated by the points x_0 such that $\partial_x S|_{x_0} = 0$ and $\text{Re}S(x_0) = 0$. These are the stationary and critical points. The leading term in the large-λ expansion of (4.17) is given by

$$f(\lambda) \sim \sum_{x_0} \left[a(x_0) \left(\frac{2\pi}{\lambda} \right)^{n/2} \frac{e^{\lambda S(x_0)}}{\sqrt{\det(-H)}} \right]. \tag{4.18}$$

The $n \times n$ Hessian matrix H is given by the second-order partial derivative of S and encodes the informations about the stationary points, which are assumed

to be isolated and non-degenerate i.e., $\det H \neq 0$.

Summarizing, in order to compute the asymptotic limit of an oscillatory integral:

- we find the critical and stationary points, i.e. those satisfying $\mathrm{Re} S = 0$ and $dS = 0$.

- we compute the Hessian of S in these points and calculate its determinant

- we use equation (4.18) to find the leading term of the large-λ limit

Using this method, it was shown in [73] that the asymptotic limit of the Euclidean EPRL-FK vertex amplitude (4.15) for $\gamma < 1$[3] contains the Regge action (2.59) as [4]

$$\mathcal{A}_v \to \frac{e^{i\lambda S_R}}{-D} + \frac{e^{-i\lambda S_R}}{-D^*} + 2\frac{\cos(\lambda\gamma S_R)}{\sqrt{DD^*}}, \tag{4.19}$$

where D is the determinant of the Hessian of $S_\pm$. We then see that the amplitude contains both the exponential of the Regge action and its sign-reversed part (commonly referred to as the cosine problem), as well as other, non-geometric terms (colloquially called weird terms)

$$W = \frac{e^{i\lambda S_R}}{-D}. \tag{4.20}$$

In this work, we are going to perform this calculation explicitly in two situations: in the next section we apply the stationary phase method to the case of a vertex amplitude deformed at the quantum level to include a cosmological constant term. There, we will show that in the semiclassical limit the deformation has the sole effect of adding the right cosmological constant term in the Regge action, and it does so without altering the determinant function D of the undeformed setting. Then, in the next Chapter we are going to apply the same approximation in the case of a path integral state sum reduced to certain symmetric configurations, so that a finite number of spin variables are required to describe the partition function. The advantage of this setting is that, differently from the most general case, the determinant D appearing in (5.45) will become an explicit function of the spins. Relying on the results from the deformed amplitude, we can also couple a cosmological constant term to the

---

[3]The calculation in the reference is also performed for the case $\gamma > 1$. Furthermore, in [68] the calculation is performed also in the Lorentzian setting.

[4]Here there are some caveats e.g., on the number of solutions of the critical point equation. We return on the subject in the next chapters.

Regge action of the reduced model, without further changes of the asymptotic formulas. Both calculations are an original work of the author and collaborators, published in[41, 42]. These will provide the required ingredients that in Chapter 6 allows us to study the renormalization properties of our reduced spin foam model.

4.3   Spin foams with cosmological constant

There are several ways to include a non-zero cosmological constant into spin foam models e.g. using Chern-Simons theory [74]. The most technically clean one is probably a deformation of the underlying group SU(2) to a quantum group $SU(2)_q$, with $q = e^{\frac{2\pi i}{k+2}}$ a root of unity, where $\Lambda = 6\pi/(\ell_P^2 k)$. [75, 76, 77, 78]. One of the earliest deformations of the model, however, was still on the level of classical groups, by deforming $\mathcal{A}_\Gamma$, keeping $\mathcal{H}_\Gamma$ unchanged. The definition was given by Han [76], for the case of a 4-simplex, and a partial analysis of the asymptotic regime was given, which demonstrated the emergence of the Regge action plus a cosmological constant term.

While this deformation of the EPRL-FK model shows no obvious connection to the later definitions with quantum groups, it is a useful tool for calculations. In particular, in recent calculations concerning the RG flow of the EPRL-FK model (see [79, 42, 80]), it turned out to be desirable to have a running cosmological constant. The boundary graphs are more complicated in that case, so a generalization of Han's deformation to more complicated graphs is needed. Also, the analysis should include the explicit treatment of the Hessian matrix in the asymptotic analysis of the deformed model. This is what is going to be undertaken in this chapter.

4.3.1   Deformation of the EPRL-FK model

Given the definition of the vertex amplitude $\mathcal{A}_{\Gamma_v}$, the deformation is given in terms of a parameter $\omega \in \mathbb{R}$. It is constructed as follows: The graph Γ_v needs to be projected down to the 2d plane, where it can be depicted with *crossings*. See for example Figure 4.1 representing in a 'minimally braided' form the boundary graph of a 4-simplex, which has a unique crossing. We anticipate that the result does not depend on how we project the graph on the 2d plane. For each crossing C in the graph between two links ℓ, ℓ' with spins $k_\ell, k_{\ell'}$, define the crossing operator

$$R_C := e^{i\omega\sigma(C)V_C}, \tag{4.21}$$
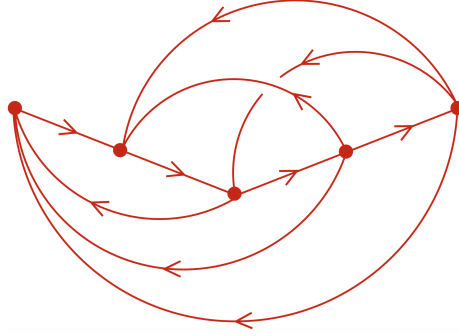
Figure 4.1: The graph dual to the boundary of a 4-simplex. Instead of the standard pentacle-shape of Figure (3.5), we represent it by minimizing the number of crossings.

$$\sigma = -1 \qquad\qquad \sigma = +1$$
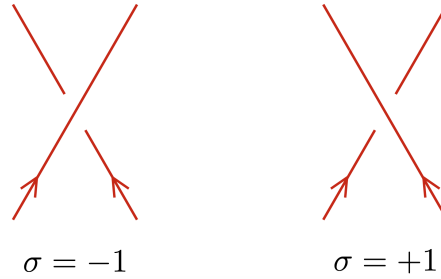
Figure 4.2: The two types of crossings C get assigned different numbers $\sigma(C) = \pm 1$.

were $\omega \in \mathbb{R}$ is the deformation parameter, $\sigma(C) = \pm 1$ is the type of crossing (over- or under-crossing, see Figure 4.2), and with

$$V_C := \sum_{\epsilon = \pm} \frac{\epsilon 4}{(1 \, \epsilon \, \gamma)^2} \sum_{I=1}^{3} D_{(j_\ell^\epsilon)}(X_I^\epsilon) \otimes D_{(j_{\ell'}^\epsilon)}(X_I^\epsilon), \qquad (4.22)$$

where the X_I^+ (X_I^-) are an orthonormal basis of the self-dual (anti-self-dual) $\mathfrak{su}(2)$.

The operator R_C acts as endomorphism on the base spaces $V_{(j_\ell^+, j_\ell^-)} \otimes V_{(j_{\ell'}^+, j_{\ell'}^-)}$ (4.3). By tensoring $\otimes_C R_C$ with the identity operator for all links in Γ_v which do not appear in a crossing, we obtain an endomorphism on $\mathcal{H}^5$. The deformed

---

[5]Technically, by this definition, the graph has to be such that each link in the graph Γ is part of at most one crossing. This is of course not the most general case, but our definition can be straightforwardly extended to a graph with arbitrarily many crossings per link, by trivially subdividing that link with 2-valent vertices, onto which one places the unique (by Schur's lemma) normalized intertwiner.

vertex amplitude $\mathcal{A}_{\Gamma_v}^\omega$ is then defined as

$$\mathcal{A}_{\Gamma_v}^\omega \ := \ \mathrm{tr}\left(\bigotimes_N \iota_N^\pm \left(\mathbb{1} \otimes \bigotimes_C R_C\right)\right). \tag{4.23}$$

Note that while R_C depends on the choice of orthonormal basis, the amplitude $\mathcal{A}_{\Gamma_v}^\omega$ does not, due to the gauge-invariance of each boosted Livine-Speziale intertwiner.

4.4   Large-j asymptotics of the deformed amplitude

In the case of $\gamma < 1$, the undeformed amplitude $\mathcal{A}_{\Gamma_v} = \mathcal{A}_{\Gamma_v}^+ \mathcal{A}_{\Gamma_v}^-$ factorizes over the two sectors (selfdual and anti-selfdual). Since the respective generators $[X_I^+, X_J^-] = 0$ commute, so do the $R_C = R_C^+ R_C^-$, of course. Hence, also the deformed amplitude factorizes:

$$\mathcal{A}_{\Gamma_v}^\omega \ = \ \mathcal{A}_{\Gamma_v}^{\omega,+} \mathcal{A}_{\Gamma_v}^{\omega,-}. \tag{4.24}$$

First we note that, due to the factorization property, it is enough to look at only the +-part. To simplify notation, in what follows we omit the vector symbol on the variables $\vec{n}_{ab} \to n_{ab}$ and we abbreviate $j_\ell^+ \to j$, $j_{\ell'}^+ \to j'$, $D_{J_\ell^+}(X_I^\pm) \to X_I$, $g_a^+ \to g_a$, etc..

In particular, we have that the (undeformed) +-amplitude (4.15) is given by

$$\mathcal{A}_{\Gamma_v}^+ \ = \ \int_{\mathrm{SU}(2)^{N_{\Gamma_v}}} dg_a \prod_{b\to a} \langle j_{ab}, n_{ab}|\, (g_a)^{-1} g_b\, |j_{ab}, n_{ba}\rangle,$$

where the product ranges over all links, where in the formula b is the starting point (source) of the link, and a is the end point (target).

Now assume that there is a crossing between the link $b \to a$ and $b' \to a'$. Then, in the deformed amplitude, the two corresponding factors in the product (4.25) are replaced by

$$\langle \Psi |\, \exp\left(\frac{4i\omega\sigma(C)}{(1+\gamma)^2} \sum_{I=1}^3 X_I \otimes X_I\right)\, |\Phi\rangle \tag{4.25}$$

with

$$\begin{aligned}
\langle \Psi | &= \langle j_{ab}, n_{ab}|(g_a)^{-1} \otimes \langle j_{a'b'}, n_{a'b'}|(g_{a'})^{-1}, \\
|\Phi\rangle &= g_b\, |j_{ab}, n_{ba}\rangle \otimes g_{b'}\, |j_{a'b'}, n_{b'a'}\rangle.
\end{aligned}$$

The expression (4.25) can be expanded to

$$\sum_{n=0}^{\infty} \frac{1}{n!} \left(\frac{4i\omega}{(1+\gamma)^2} \right)^n \sum_{I_1, I_2, \ldots, I_n = 1}^{3} \langle j_{ab}, n_{ab} | (g_a)^{-1} X_{I_1} X_{I_2} \cdots X_{I_n} g_b | j_{ab}, n_{ba} \rangle$$

$$\times \langle j_{a'b'}, n_{a'b'} | (g_{a'})^{-1} X_{I_1} X_{I_2} \cdots X_{I_n} g_{b'} | j_{a'b'}, n_{b'a'} \rangle. \tag{4.26}$$

To consider the stationary phase of an individual term, we use the resolution of identity

$$(2j+1) \int_{S^2} d^2 n \, |j, n\rangle\langle j, n| \; = \; \mathbb{1}_{V_j}, \tag{4.27}$$

$n-1$ times, and write

$$\langle j_{ab}, n_{ab} | (g_a)^{-1} X_{I_1} X_{I_2} \cdots X_{I_n} g_b | j_{ab}, n_{ba} \rangle =$$

$$= \; (2j+1)^{n-1} \int_{(S^2)^{n-1}} d^2 n_i \, \langle j, n_{ab} | (g_a)^{-1} X_{I_1} | j, n_1 \rangle$$

$$\times \langle j, n_1 | X_{I_2} | j, n_2 \rangle \cdots \langle j, n_{n-1} | X_{I_{n-1}} g_b | j, n_{ba} \rangle.$$

The X_I are the generators of the $\mathfrak{su}(2)$ Lie algebra $[X_I, X_J] = i\epsilon_{IJK} X_K$, which is why, in the spin-$\frac{1}{2}$-representation, we have $X_I = \sigma_I/2$ in terms of the Pauli matrices σ_I. We have therefore

$$\langle j, n | X_I | j, n' \rangle \; = \; j \langle n | \sigma_I | n' \rangle \, \langle n | n' \rangle^{2j-1}, \tag{4.28}$$

where $|n\rangle := |\frac{1}{2}, n\rangle$. [6] With this, we can write

$$\langle j_{ab}, n_{ab} | (g_a)^{-1} X_{I_1} X_{I_2} \cdots X_{I_n} g_b | j_{ab}, n_{ba} \rangle = \tag{4.29}$$

$$= \int_{(S^2)^{n-1}} d^2 n_i \, a(n_i, g_a, g_b) \, e^{S(n_i, g_a, g_b)}, \tag{4.30}$$

with

$$a(n_i, g_a, g_b) \; = \; (2j+1)^{n-1} j^n \frac{\langle n_{ab} | (g_a)^{-1} \sigma_{I_1} | n_1 \rangle}{\langle n_{ab} | (g_a)^{-1} | n_1 \rangle} \frac{\langle n_1 | \sigma_{I_2} | n_2 \rangle}{\langle n_1 | n_2 \rangle} \cdots \frac{\langle n_{n-1} | \sigma_{I_n} g_b | n_{ba} \rangle}{\langle n_{n-1} | g_b | n_{ba} \rangle},$$

$$S(n_i, g_a, g_b) \; = \; 2j \Big(\ln\langle n_{ab} | (g_a)^{-1} | n_1 \rangle + \ln\langle n_1 | n_2 \rangle + \cdots + \ln\langle n_{n-1} | g_b | n_{ba} \rangle \Big).$$

---

[6] One can show (4.28) easily by using $X_I = -i \frac{d}{dt}\big|_{t=0} e^{itX_I}$ and the product rule.

This is now in a form where one can perform the (extended) stationary phase approximation, applying the algorithm given in section 4.2.1. Note that this is for one term in the sum (4.26) only, and the variables are all the g_a, and, for every crossing, n_i and n'_i with $i = 1, \ldots, n - 1$ (the n'_i vectors come from the term similar to (4.29), with the dashed nodes a', b'). First, we note that the criticality condition $\mathrm{Re} S = 0$ (where we consider the whole action for $\mathcal{A}_\Gamma^\omega$ now), is equivalent to

$$g_a n_{ab} \;=\; g_b n_{ba}, \tag{4.31}$$

and

$$n_i = g_b n_{ba}, \qquad n'_i = g_{b'} n_{b'a'} \; \forall i. \tag{4.32}$$

One should note that the criticality equations (4.31) for the group elements g_a are precisely the ones for the *undeformed* amplitude [73]. The criticality equations for the unit vectors n_i, n'_i (remember that, per crossing, there are $2(n-1)$ unit vectors), are such that, on each edge which participates in some crossing, all vectors have to be equal, and coincide with the two normal vectors $g_a n_{ab} = g_b n_{ba}$. This shows that, using the same gauge symmetry as in the undeformed case, setting one $g_a = \mathbb{1}$, all critical points are isolated, when they are also isolated in the undeformed case.[7]

The stationary points are equally easily identified, and they are, as in the undeformed case, the closure condition for each node, and $n_i = g_b n_{ba}$, $n'_i = g_{b'} n_{b'a'}$ for all i.

In particular, this means that, after gauge-fixing, the critical and stationary points of the deformed and the undeformed amplitude are in one-to-one correspondence. Furthermore, it is easy to see that the value of the respective actions, evaluated at corresponding critical stationary points, coincide.

4.4.1   The Hessian matrix

To make the notation easier, we assume that there is only one crossing. The general case with many crossings can be treated similarly, though. We also assume that there is at least one critical, stationary point $g_a^{(c)}$ for the undeformed (gauge-fixed) amplitude. Before we continue, we perform a coordinate transformation on the g_a, n_i, n'_i variables, via

$$g_a \to g_a, \qquad n_i \to g_b n_i, \qquad n'_i \to g_{b'} n'_i. \tag{4.33}$$

---

[7]This is, indeed, the generic case, e.g in the case of the n_{ab} forming a Regge boundary geometry at the 4-simplex [73], in all cases of the hypercuboid [81], or the hyperfrustum, if $\alpha \in (\pi/4, 3\pi/4)$ (see next chapter and reference [42]).

Since $SU(2)$ acts via rotations on S^2, the Jacobi matrix for this transformations is equal to unity. The action after the coordinate transformation is then given by

$$
\begin{aligned}
S(g_a, n_i, n'_i) &= \sum_{cd \neq ab, a'b'} 2j_{cd} \ln \langle n_{cd} | (g_c)^{-1} g_d | n_{dc} \rangle \\
&+ 2j_{ab} \Big(\ln \langle n_{ab} | (g_a)^{-1} g_b | n_1 \rangle + \ln \langle n_1 | n_2 \rangle + \cdots + \ln \langle n_{n-1} | n_{ba} \rangle \Big) \quad (4.34) \\
&+ 2j_{a'b'} \Big(\ln \langle n_{a'b'} | (g_{a'})^{-1} g_{b'} | n'_1 \rangle + \ln \langle n'_1 | n'_2 \rangle + \cdots + \ln \langle n'_{n-1} | n_{b'a'} \rangle \Big).
\end{aligned}
$$

Note that the first two lines in (4.34) are the same as in the undeformed case, while the remaining two come from the deformation due to the crossing. We compute the Hessian matrix for the deformed amplitude, at the critical stationary point

$$
g_a = g_a^{(c)}, \qquad n_i = n_{ba}, \qquad n'_i = n_{b'a'}. \qquad (4.35)
$$

In particular, we introduce coordinates around this point via $g_a = e^{ix_a^I \sigma_I} g_a^{(c)}$ and

$$
n_i = g_{n_{ba}} \begin{pmatrix} \sin \theta_i \\ \sin \phi_i \, \cos \theta_i \\ \cos \phi_i \, \cos \theta_i \end{pmatrix}, \qquad n'_i = g_{n_{b'a'}} \begin{pmatrix} \sin \chi_i \\ \sin \xi_i \, \cos \chi_i \\ \cos \xi_i \, \cos \chi_i \end{pmatrix},
$$

where the angles take values in $\phi_i, \xi_i \in (-\pi, \pi)$ and $\theta_i, \chi_i \in (-\frac{\pi}{2}, \frac{\pi}{2})$. The critical and stationary point is assumed at $x_I^a = 0, \phi_i = \xi_i = \theta_i = \chi_i = 0$. The vectors $|n_i\rangle$ are then given by

$$
\begin{aligned}
|n_i\rangle &= g_{n_{ba}} \exp \left(i \frac{\phi_i}{2} \sigma_1 \right) \exp \left(-i \frac{\theta_i}{2} \sigma_2 \right) |e_z\rangle \\
&= g_{n_{ba}} \left[\left(\cos \frac{\phi_i}{2} \cos \frac{\theta_i}{2} + i \sin \frac{\phi_i}{2} \sin \frac{\theta_i}{2} \right) | \uparrow \rangle \right. \\
&\qquad \left. + \left(\cos \frac{\phi_i}{2} \sin \frac{\theta_i}{2} + i \sin \frac{\phi_i}{2} \cos \frac{\theta_i}{2} \right) | \downarrow \rangle \right],
\end{aligned}
$$

where $|e_z\rangle = | \uparrow \rangle$ is the highest weight vector in the spin $\frac{1}{2}$-representation. A similar formula holds for $|n'_i\rangle$. This leads to

$$
\frac{\partial}{\partial \phi_i} \langle n_i | n_{i+1} \rangle_{|\text{crit, stat}} = 0, \qquad (4.36)
$$

and similar relations for the other angles. Also,

$$\langle n_i | n_{i+1} \rangle_{|\text{crit, stat}} = 1. \tag{4.37}$$

Therefore, for all second derivatives which have at least one derivative w.r.t. one of the angles, the logarithm can be left out, e.g.:

$$\frac{\partial^2}{\partial \phi_i \partial \phi_{i+1}} \ln \langle n_i | n_{i+1} \rangle_{|\text{crit, stat}} = \frac{\partial^2}{\partial \phi_i \partial \phi_{i+1}} \langle n_i | n_{i+1} \rangle_{|\text{crit, stat}},$$

and similar relations for all other varying types of angles. Thus we get, at the stationary and critical points:

$$\frac{\partial^2 S}{\partial \phi_i^2} = \frac{\partial^2 S}{\partial \theta_i^2} = -j_{ab}, \tag{4.38}$$

$$\frac{\partial^2 S}{\partial \xi_i^2} = \frac{\partial^2 S}{\partial \chi_i^2} = -j_{a'b'}.$$

Also, we get

$$\frac{\partial^2 S}{\partial \theta_i \partial \theta_{i+1}} = \frac{\partial^2 S}{\partial \phi_i \partial \phi_{i+1}} = \frac{j_{ab}}{2}, \qquad \frac{\partial^2 S}{\partial \phi_i \partial \theta_i} = 0,$$

$$\frac{\partial^2 S}{\partial \phi_i \partial \theta_{i+1}} = i\frac{j_{ab}}{2}, \qquad \frac{\partial^2 S}{\partial \phi_{i+1} \partial \theta_i} = -i\frac{j_{ab}}{2}. \tag{4.39}$$

All other mixed ϕ, θ angle derivatives are zero. For ξ, χ angles similar relations hold. Furthermore, we have

$$\langle n_{ab} | (g_a)^{-1} g_b | n_1 \rangle_{|\text{crit, stat}} = e^{i\psi}. \tag{4.40}$$

Using this and $g_a g_{n_{ab}} = g_b g_{n_{ba}} e^{-i\psi \sigma_3}$, we get on the critical and stationary point that

$$\frac{\partial^2 S}{\partial x_b^I \partial \phi_1} = 2j_{ab} \frac{\partial^2}{\partial x_b^I \partial \phi_1} \ln \langle n_{ab} | (g_a)^{-1} e^{ix_b^J \sigma_J} g_b g_{n_{ba}} e^{i\phi_1 \sigma_1 / 2} e^{-i\theta_1 \sigma_2 / 2} | \uparrow \rangle$$

$$= 2j_{ab} e^{-i\psi} \frac{\partial^2}{\partial x_b^I \partial \phi_1} \langle n_{ab} | (g_a)^{-1} e^{ix_b^I \sigma_I} g_b g_{n_{ba}} e^{i\phi_1 \sigma_1 / 2} e^{-i\theta_1 \sigma_2 / 2} | \uparrow \rangle \tag{4.41}$$

$$= j_{ab} \left(iV_2^I - V_1^I \right),$$

where in the end we have taken all angles $\phi_i = \theta_i = 0$. Also, V_J^I is the I-th component of the image of the J-th unit vector under the rotation $G := (g_b g_{n_{ba}})^{-1}$, i.e.

$$G\sigma_J G^{-1} = V_J^I \sigma_I. \tag{4.42}$$

Furthermore, we have

$$\frac{\partial^2 S}{\partial x_b^I \partial \phi_1} \;=\; -\frac{\partial^2 S}{\partial x_a^I \partial \phi_1}, \tag{4.43}$$

and

$$\frac{\partial^2 S}{\partial x_b^I \partial \theta_1} \;=\; j_{ab}\left(iV_1^I + V_2^I\right) \tag{4.44}$$

$$\;=\; -\frac{\partial^2 S}{\partial x_a^I \partial \theta_1} \;=\; \frac{1}{i}\frac{\partial^2 S}{\partial x_b^I \partial \phi_1}.$$

Also, there are, again, equivalent relations for the ξ_1 and χ_1 angles, where $a \to a'$, $b \to b'$. Finally, it is not hard to see that the matrix of second derivatives of x_a^I

$$\tilde{H}_{IJ}^{cd} \;:=\; \frac{\partial^2 S}{\partial x_c^I \partial x_d^J}, \tag{4.45}$$

at the critical and stationary point coincides precisely with the matrix in the undeformed case - even if $(cd) = (ab)$ or $(a'b')$. The determinants of the Hessian matrix H of the whole integral evaluates to

$$\det(H) \;=\; (j_{ab}j_{a'b'})^{2(n-1)}\det(\tilde{H}). \tag{4.46}$$

This is shown in Appendix B.

From the analysis, it is clear that that the case of more than one crossing is treated in complete analogy, since each link is allowed to partake in at most one crossing. Therefore, the Hessian matrix for the case of more than one crossing can simply be computed by an induction over the number of crossings C, and reduced to

$$\det(H) \;=\; \det(\tilde{H})\prod_C (j_{ab}j_{a'b'})^{2(n-1)}. \tag{4.47}$$

4.4.2   Putting everything together

We now replace $j_{cd} \to \lambda j_{cd}$, and consider the asymptotic expression for $\lambda \to \infty$. Using the normalized measure on S^2 in ϕ, θ-coordinates (4.36), we get

$$dn_i \;=\; \frac{1}{4\pi}d\phi_i d\theta_i \,\cos\theta_i, \;\; dn_i' \;=\; \frac{1}{4\pi}d\xi_i d\chi_i \,\cos\chi_i. \tag{4.48}$$

Denote by $\mathcal{B}$ the large-j-expression for the undeformed +-amplitude (4.25), and by $\mathcal{B}^\omega$ its deformation. Then, because the critical and stationary points

are in one-to-one correspondence, and the Hessian matrix $\det(\tilde{H})$ for the un-deformed case can be pulled out of the sum, we have $\mathcal{B}^\omega = \mathcal{B}\mathcal{C}$ with

$$
\begin{aligned}
\mathcal{C} &= \sum_{n=0}^{\infty} \frac{1}{n!} \left(\frac{4i\omega\sigma(C)}{(1+\gamma)^2} \right)^n \left(\frac{1}{4\pi} \right)^{2(n-1)} \left(\frac{2\pi}{\lambda} \right)^{2(n-1)} \\
&\quad \times \sum_{I_1,I_2,\ldots,I_n=1}^{3} 4^{n-1} \frac{(\lambda j_{ab})^{2n-1}(\lambda j_{a'b'})^{2n-1}}{\sqrt{(j_{ab}j_{a'b'})^{2(n-1)}}} \\
&\quad \times \prod_{i=1}^{n} (\tilde{n}_{ba})^{I_i} \, (\tilde{n}_{b'a'})^{I_i} \\
&= \sum_{n=0}^{\infty} \frac{\lambda^{2n}}{n!} (j_{ab}j_{a'b'})^n \left(\frac{4i\omega}{(1+\gamma)^2} \right)^n \left(\sum_{I=1}^{3} (\tilde{n}_{ba})^I \, (\tilde{n}_{b'a'})^I \right)^n \\
&= e^{i\omega\lambda^2\sigma(C)\vec{X}_{ab}\cdot\vec{Y}_{a'b'}},
\end{aligned}
\tag{4.49}
$$

with the vectors $\tilde{n}_{ab} = g_a n_{ab}$, and

$$
\vec{X}_{ab} = k_{ab}\,\tilde{n}_{ab}, \quad \vec{Y}_{a'b'} = k_{a'b'}\,\tilde{n}_{a'b'},
\tag{4.50}
$$

with $\frac{1+\gamma}{2}k_{cd} = j_{ab}^+ = j_{ab}$. This stays finite if, additionally to scaling j_{cd} up by λ, one scales the deformation parameter as $\omega \to \omega\lambda^{-2}$ at the same time.

This is the computation of the $+$-part, i.e. $\mathcal{C}^+$. It is noteworthy that $\mathcal{C}^-$ is the same expression, just with a minus sign in the exponential, i.e. $\mathcal{C}^- = (\mathcal{C}^+)^{-1}$.

Expression (4.49) is for one crossing. The case of many crossings is straightforward, since we demanded that each edge is part of at most one crossing. For many crossings, one gets

$$
\mathcal{C} = e^{i\omega \sum_C \sigma(C)\vec{X}_{ab}\cdot\vec{Y}_{a'b'}}
\tag{4.51}
$$

4.4.3   Relation to the cosmological constant

We now relate our final result (4.49) to the cosmological constant. For this, we assume an amplitude in which there are two distinct solutions to the stationary phase equations (4.31).[8] We denote these as $g_a^{(i)}$, with $i = 1, 2$.

We denote the asymptotic expression for the undeformed amplitude by

$$
\mathcal{A}_{\Gamma_v}^\pm \longrightarrow \mathcal{B}_{(1)}^\pm + \mathcal{B}_{(2)}^\pm,
\tag{4.52}
$$

---

[8]This seems to be the case whenever the boundary data allows for a unique, non-degenerate 4-geometry [81, 82, 42].

and from this and (4.49) one gets that

$$\mathcal{A}_{\Gamma_v}^{\omega} \longrightarrow \left(\mathcal{B}_{(1)}^+\mathcal{C}_{(1)}^+ + \mathcal{B}_{(2)}^+\mathcal{C}_{(2)}^+\right)\left(\mathcal{B}_{(1)}^-\mathcal{C}_{(1)}^- + \mathcal{B}_{(2)}^-\mathcal{C}_{(2)}^-\right)$$

$$= \mathcal{B}_{(1)}^+\mathcal{B}_{(1)}^- + \mathcal{B}_{(2)}^+\mathcal{B}_{(2)}^- \tag{4.53}$$

$$+ \mathcal{B}_{(1)}^+\mathcal{B}_{(2)}^- \, \mathcal{C}_{(1)}^+\mathcal{C}_{(2)}^- + \mathcal{B}_{(2)}^+\mathcal{B}_{(1)}^- \, \mathcal{C}_{(2)}^+\mathcal{C}_{(1)}^-.$$

The terms $\mathcal{B}_{(1)}^+\mathcal{B}_{(1)}^-$ and $\mathcal{B}_{(2)}^+\mathcal{B}_{(2)}^-$ evaluated on the same solution, have been called "weird terms", and one can see that they remain unchanged under the deformation of the model. The mixed terms however do get changed, and one has

$$\mathcal{C}_{(1)}^+\mathcal{C}_{(2)}^- = \left(\mathcal{C}_{(2)}^+\mathcal{C}_{(1)}^-\right)^{-1}$$

$$= \exp\left(i\omega\sum_C \sigma(C)\left(\vec{X}_{ab}^{(1)} \cdot \vec{Y}_{a'b'}^{(1)} - \vec{X}_{ab}^{(2)} \cdot \vec{Y}_{a'b'}^{(2)}\right)\right)$$

$$= \exp\left(12i\omega\sum_C \sigma(C) \, *(B_{ab} \wedge B_{a'b'})\right). \tag{4.54}$$

Here $*$ denotes the Hodge dual, $B_{ab} = (\vec{X}_{ab}^{(1)}, \vec{X}_{ab}^{(2)})$ and $B_{a'b'} = (\vec{Y}_{ab}^{(1)}, \vec{Y}_{ab}^{(2)})$ are the bivectors in $\mathbb{R}^4 \wedge \mathbb{R}^4 \simeq \mathfrak{so}(4) \simeq \mathbb{R}^3 \oplus \mathbb{R}^3$ associated to the edges (ab) and $(a'b')$, which are constructed from the two distinct solutions $g_a^{(i)}$. See Appendix A for details.

In the case of a 4-simplex, the expression in (4.54) has been shown to be proportional to the 4-volume of such a simplex, given by the boundary data [76]. In the case of a hypercuboid, a similar calculation can be carried out. With the notation from [72] and the conventions in Appendix A, one finds

$$\sum_C \sigma(C) \, *(B_{ab} \wedge B_{a'b'}) = \frac{j_1j_6 + j_2j_5 + j_3j_4}{3}, \tag{4.55}$$

which coincides with $V_{\text{hypercuboid}}$ if the geometricity conditions $j_1j_6 = j_2j_5 = j_3j_4$ are satisfied. See [72] for a closer discussion of this point, and the relation to the volume simplicity constraints within the EPRL-FK model.

In the next chapter we study a new geometry, whose main building block is a so-called hyperfrustum. In that case, the critical and stationary equations are solved, and the solution can be shown to be

$$\sum_C \sigma(C) \, *(B_{ab} \wedge B_{a'b'}) = V_{\text{frustum}}, \tag{4.56}$$

where V_frustum is the 4-volume of the hyperfrustum (see Chapter 5 and Appendix C or [42]).

One can show, indeed, that for convex 4-dimensional polyhedra P one has in general that [83]

$$V_P = \sum_C \sigma(C) \, * (B_{ab} \wedge B_{a'b'}) \,. \tag{4.57}$$

Thus eventually we have

$$\mathcal{C}^+_{(1)} \mathcal{C}^-_{(2)} = \exp\left(12i\omega V_P\right). \tag{4.58}$$

Summarizing, we can write the deformed amplitude as

$$\mathcal{A}^\omega_{\Gamma_v} \to W + W^* + \frac{2}{|D|} \cos\left(S_\text{Regge} - \Lambda V\right), \tag{4.59}$$

calling W the 'weird terms' in (4.20), This way, the deformation provides, in a straightforward way, a generalization of the EPRL-KKL model to include a non-zero cosmological constant Λ.

There are two points of note in this analysis:

1. There are cases in which the boundary data does not describe a vector geometry (in that there are two critical and stationary points), while not describing a 4d polyhedron. These "non-geometric" configurations have been discussed in [81, 82], and their presence can be attributed to the insufficient implementation of the volume simplicity constraint. The expression V, however, still exists and is non-zero. It is unclear what its geometric interpretation is in that case.

2. The original EPRL-KKL amplitude $\mathcal{A}_{\Gamma_v}$ is defined on a graph Γ_v, but does not depend on its knotting class. As a consequence, the physical inner product therefore also does not [84]. Interestingly, the deformation $\mathcal{A}^\omega_\Gamma$, however, does depend on the knotting of Γ. This is a property it shares with the quantum group deformations of the model. One can conjecture that this would lead to a physical Hilbert space in which graphs with different knotting classes are not equivalent. This could have interesting physical ramifications. [85]

It should also be noted that, while the expression V (4.54) is a knotting invariant in the asymptotic limit, i.e. does not depend on the way in which the graph Γ_v is presented on the plane [72], it is unknown whether the same is true for the quantum amplitude.

Chapter 5

Reduced Spin Foam Model

In general, one major obstacle towards progress, and also from allowing to use the model to make actual, testable, predictions, is the complexity of SFM, and in particular of the EPRL-FK amplitude [1]. A possible strategy to tackle this issue consists in restricting state sum to certain symmetric configurations. On one hand this approach limits the range of physical systems that can be described by the model, on the other hand it greatly simplifies the expressions of the transition amplitudes. Provided that one can restrict the analysis to a subset of states which dominate the path integral, the sum over such domain would tell us something about the continuum limit of spin foams, expectation values and renormalization group flow of the model.

In the canonical framework, a similar line of thinking has been introduced in [88]. In the covariant setting, this approach has recently been investigated in [81] in the context of $4d$ Euclidean EPRL-FK Spin Foam model. Here spacetime is described by a hypercuboidal lattice and the state sum is restricted to coherent intertwiners [63] that in the large-spin limit resemble a cuboidal geometry. Despite the drastic reduction of the degrees of freedom the model presents several interesting features. In particular it has been shown that in the semiclassical limit the parameters of the theory tune the restoration of the diffeomorphism symmetry and provide a classification of the dominant states in the path integral. Under the imposed restrictions, such results open the path to a preliminary analysis of the renormalization properties of spin foams. Recent analysis based on this reduced model have in fact shown numerical evidences of a phase transition in the RG flow [79, 80].

A first clear limitation of such a model is the absence of curvature due to

---

[1]Numerical tools for performing such tasks are under development. For example, in [86] it is provided a C-coded library for the evaluation of the Lorentzian EPRL-FK vertex amplitude. Using these tools, in [87] the transition amplitudes between two spin networks with dipole graphs are evaluated in the Lorentzian framework of the EPRL-FK model with up to two (non-simplicial) vertices.

vanishing dihedral angles between the cuboidal blocks. In this chapter we take
the next step along this path by including an elementary form of curvature.
In particular we focus on a discretization in which spacetime is chopped into
hyperfrusta F_n i.e., the four dimensional generalization of a truncated regular
square pyramid (to which we will in short refer as *frustum*). The state sum
is reduced to coherent intertwiners that in the large-spin limit describe the
geometry of a frustum. The emergent curvature is a function of the angle
variable that defines the slope of the frustum itself. This extension of degrees
of freedom will allow us to go beyond the features of the cuboid model and to
forward some cosmological considerations. [2]

The results presented in this chapter are part of an original work of the
author and collaborators and is published in [42].

5.1   Isotropic and homogeneous reduction

We define the model on a 2-complex $\mathcal{K}$ (as described in section 2.2.2) which
is the dual skeleton of our particular discretization of the manifold. The com-
binatorics of vertices v, edges e and faces f in $\mathcal{K}$ is the same of a hypercubic
lattice in which all the vertices are 8-valent. In particular each vertex v in
$\mathcal{K}$ is dual to a 4d hyperfrustum, and the eight edges meeting at v are dual
to the eight 3d hexahedra (two cubes and six pyramidal frusta) which bound
the hyperfrustum (see figure 5.1). The faces f of the 2-complex are dual to
squares or to regular trapezoids, which in turn form the 2d boundary of cubes
and frusta.

The hyperfrustum geometry arises by equipping every face f with a spin j_f
and every edge e with an intertwiner ι_e. A 2-complex colored by such specific
labeling describes a spacetime configuration in the state sum. Varying the
values of the labels in the bulk while keeping fixed the boundary ones amount
to consider different 'paths' in the path integral. The physical information is
deduced from the transition amplitudes between fixed boundary states which
belong to the kinematical Hilbert space of LQG (see Chapter 3).

---

[2]The reader familiar with spin foam models might be puzzled by our setup, where we claim
to allow for discrete geometries with curvature while using spin foam amplitudes in the large-j-
limit. Indeed, this limit is the context in which the so-called "flatness-problem" was discovered and
discussed in great detail [89, 90]. It states that in this limit, no matter the boundary state of the spin
foam, the bulk geometry is flat and accidental curvature constraints occur. In our case, where we
only study a subset of the full spin foam path integral, the configurations that we permit in principle
allow for curvature, in particular compared to the previously studied cuboid configurations. From
our numerical studies, which we report in this article, we do not observe that this subset of the path
integral is dominated by flat, i.e. cuboid, geometries. Due to the restrictiveness of the path integral
studied here, this finding is by no means a proving that the flatness problem is non-existent, yet it
hints towards its intricacies that we need to understand better
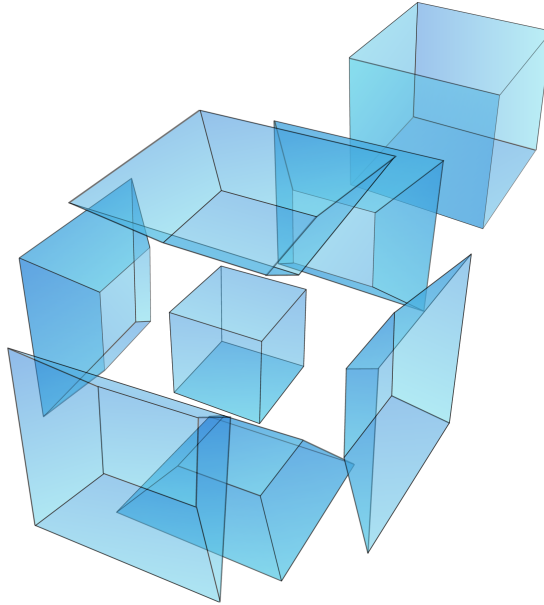
Figure 5.1: The figure shows the 3d boundary of a hyperfrustum, obtained by unfolding it into six equal frusta and two cubes of different size. This is the analogue, one dimension higher, of the unfolding of a 3d pyramidal frustum into four trapezoids and two squares.

The use of the hyperfrustum as the fundamental grain of spacetime is justified by a number of advantages:

- A regular hyperfrustum is defined by using just three spins. Consequently, all the formulas that we obtain depend on a quite restricted set of variables. This feature makes the analysis of the model more easy to manage.

- The geometry of a hyperfrustum allows a simple and intuitive interpretation as a time-evolving homogeneous and isotropic flat space. Therefore we can use it to model the evolution of a Friedmann universe (see the next sections). Varying the values of the spins one obtains hyperfrusta with different shapes representing spacetime with different curvature.

- Taking the flat spacetime limit of an hyperfrustum i.e., choosing the spin variables so that the two boundary cubes have the same size, one degenerates into a hypercuboid. Thus, as a double check on our computations, we can use the results of [81] where the semiclassical limit of a reduced spin foam built on a hypercuboidal geometry is carried out.

- The analysis in this chapter is ultimately a setup to the extension of the renormalization computations performed with hypercuboidal geometries in [79, 80], in that also states with $4d$ curvature are included in the

path integral. In fact, as in the hypercuboid setting, the handiness of the hyperfrustum formulas makes possible the numerical analysis of the dynamics of more complex lattices made of hundreds of vertices. This represents a crucial requirement to access the renormalization sector of a spin foam model given that the RG flow is precisely defined by the comparison of the expectation values of observables on finer and coarser lattices. This is studied in details in Chapter 6.

In our model the spin network associated to the boundary of a vertex consists of eight 6-valent nodes (see figure 5.2), reflecting the fact that a hyperfrustum is bounded by eight hexahedra: two cubes and six regular pyramidal frusta.

Following the prescriptions in Chapter 4, to each node $a = 0, \ldots, 7$ we assign a boosted coherent intertwiner $\Phi \iota_a$ and two SU(2) group elements (g_a^-, g_a^+) which account for the group averaging in (4.8). Each link ab is oriented and is labeled by a spin j_{ab}. All the links are automatically endowed with two other spins j_{ab}^- and j_{ab}^+ which are related to j_{ab} via the Barbero-Immirzi parameter γ as in (4.6). The allowed values for j_{ab} are such that j_{ab}^- and j_{ab}^+ are half integers. For consistency we also require that $j_{ab} = j_{ba}$.
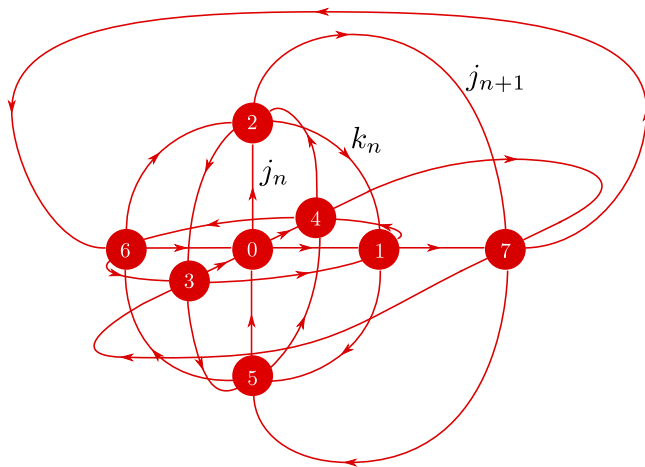
Figure 5.2:   The figure shows the spin network associated to a vertex boundary. This is the dual representation of the 3d boundary in figure 5.1. All the links attached to the node 0 are labeled by the spin j_n, the links attached to node 7 carry a spin j_{n+1} and the remaining ones have spin k_n.

The colored spin network just described admits a dual representation in terms of hexahedra ε_a which are associated to the nodes a (Figure 5.1). We call $\vec{n}_{ab} \in S^2 \subset \mathbb{R}^3$ the normalized outgoing normal to the face $\square_{ab} \subset \varepsilon_a$ in the direction of the neighboring hexahedron ε_b. The area of $\square_{ab}$ is given by the spin j_{ab}. The high degree of symmetry chosen ensures that a boundary state is

defined by using just three independent values of the spins j_{ab}, $\forall a, b, = 0 \ldots 7$. We call such values j_n, j_{n+1}, k_n and they correspond to the top, bottom and side face areas of any one of the boundary pyramidal frusta represented in Figure 5.1. The previous labeling defines the boundary state and the geometry in our lattice up to a phase factor.

5.1.1 A note on the boundary data

Particular attention needs to be paid in defining the initial configuration of the vectors $\vec{n}_{ab}$ at the boundary of a vertex. In fact this choice influences the semiclassical limit of the theory. In order to clarify this point let us start from the definition of the single vertex amplitude. Usually we build it by forming a closed spin network tensoring together the eight intertwiners $\Phi \iota_a$ at the nodes and joining pairwise the free ends of the links according to the combinatorics (see equation (4.10) and figure 5.2). In our case the outcome of this operation depends on the initial choice of the vectors $\vec{n}_{ab}$ which are used to define the coherent intertwiners $\Phi \iota_a$. For example, embedding the vertex boundary depicted in figure 5.1 into a coordinate space and defining the vectors $\vec{n}_{ab}$ accordingly to the oriented axes, one finds out that the asymptotic expression of the vertex amplitude carries a phase factor. Nonetheless, a change of the boundary data can set such phase to zero. However, at the level of one vertex there are no preferred criteria to chose such initial configuration of the vectors $\vec{n}_{ab}$. The situation changes if one takes into account the symmetry of a larger structure $\mathcal{K}$ in which many vertices are glued together to form a regular hypercubic lattice. For the sake of clarity let us refer to the example in figure 5.3 in which the two vertices $v, v' \subset \mathcal{K}$ meet along an oriented common edge.

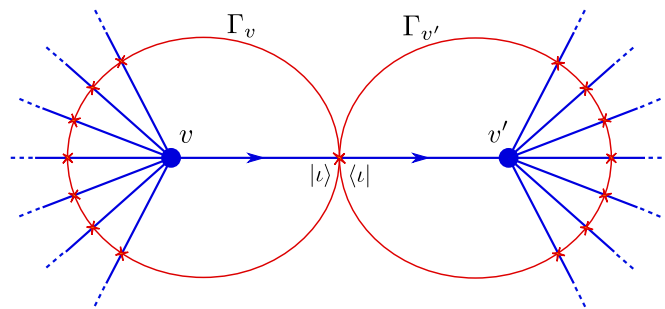Figure 5.3: The figure shows the gluing of two eight-valent vertices v and v' and their respective boundaries graphs Γ_v and $\Gamma_{v'}$ (represented for simplicity as closed lines). In this picture the coherent intertwiners are sitting in the intersections between the boundaries and the edges (straight lines).

Here the circles Γ_v and $\Gamma_{v'}$ surrounding the vertices represent their respec-
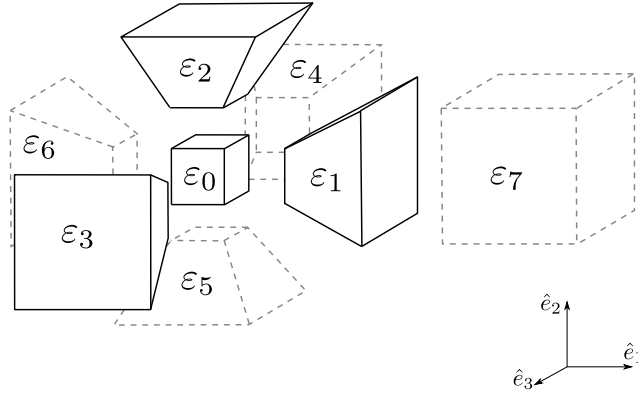
Figure 5.4:   The figure shows a specific configuration of the boundary of a vertex. The hexahedra drawn using continuous lines are oriented by relying on the axes $\hat{e}_1, \hat{e}_2, \hat{e}_3$. The remaining hexahedra are defined from the first by applying the condition (5.1).

tive boundaries. The intertwiners are placed at the marked intersection points to mean that each of them is associated to an edge $e \subset \mathcal{K}$ and is also an element of a vertex boundary. Let us notice that the intertwiner sitting at the shared edge can be 'seen' as an element of Γ_v as well as of $\Gamma_{v'}$. In the bra-ket notation adopted in figure (5.3) it is denoted by $|\iota\rangle$ or by $\langle\iota|$ depending whether the edge is outgoing or ingoing w.r.t. the associated vertex. In a regular lattice the proper gluing of the vertices is such that, given a fixed node $a \subset \Gamma_v$, the associated intertwiner $\Phi\iota_a$ is contracted to the intertwiner $(\Phi\iota'_{7-a})^\dagger$ in $\Gamma_{v'}$. Such (nonlocal) condition must be imposed at all the edges in the lattice. We can however translate this operation in the following (local) constraint on the boundary data of a single vertex

$$(|\vec{n}_{ab}\rangle)^\dagger \equiv \langle-\vec{n}_{(7-a)\ b}|, \qquad \forall a = 4, 5, 6, 7. \qquad (5.1)$$

In the dual representation, the example in figure (5.3) shows two hyperfrusta meeting along a shared hexahedron. Such object lives independently in the boundaries of Γ_v and $\Gamma_{v'}$ and it must be identified as the unique hexahedron shared by the two hyperfrusta. In the general case in which the lattice is regular in all the directions, equation (5.1) ensures the proper identification of the boundary hexahedra shared by neighboring hyperfrusta.

With this purpose in mind we can depict the boundary state starting from representing the first four nodes $0, 1, 2, 3$ as in figure 5.4, and then build the remaining nodes $4, 5, 6, 7$ (dashed lines) respecting the imposition (5.1).

Remarkably, once the lattice symmetry is taken into account by imposing (5.1) at the local level, the asymptotic expression of the single vertex amplitude shows no dependence on the choice of phase for the boundary states.

5.1.2 Quantum frustum

The first step towards the definition of the local amplitudes is finding the expressions of the coherent intertwiners. The *quantum frustum* is a coherent intertwiner that in the large-spin limit describe the geometry of a regular frustum (see figure 5.5). It depends on three spins j_n, j_{n+1} and k_n corresponding to its face areas and in the symmetric case $j_n = j_{n+1} = k_n = j$ it reduces to a *quantum cube*. Thus, this object furnishes a prototype for the description of all the intertwiners appearing in our model.
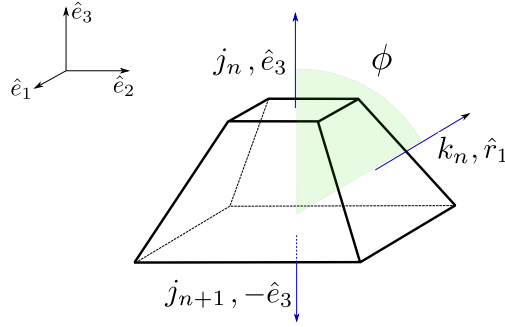
Figure 5.5: The figure shows a *frustum* i.e., a truncated regular square pyramid

Following the instructions given in the Chapter 3, and in particular from (3.66), we can define a quantum frustum as

$$\iota_{j_n,j_{n+1},k_n} = \int \mathrm{d}g \ g \triangleright \left(|j_n, \hat{e}_3\rangle \otimes |j_{n+1}, -\hat{e}_3\rangle \otimes \bigotimes_{l=0}^{3} |k_n, \hat{r}_l\rangle \right), \qquad (5.2)$$

where $\hat{r}_l \equiv e^{-i\frac{\pi}{4}l\sigma_3} e^{-i\frac{\phi}{2}\sigma_2} \triangleright \hat{e}_3$ $(l = 0, 1, 2, 3)$ are the four vectors perpendicular to the side faces of the frustum. It is possible to express the slope angle ϕ of the frustum in terms of the face areas (i.e., the spins) as

$$\cos\phi = \frac{j_{n+1} - j_n}{4k_n}. \qquad (5.3)$$

Using the invariance of the Haar measure to remove one group integration and applying the coherent states property (3.64), the norm of the coherent intertwiner (5.2) can be put in the form

$$\|\iota_{j_n,j_{n+1},k_n}\|^2 = \int_{SU(2)} \mathrm{d}g \ e^{S_e[g]}, \qquad (5.4)$$

with

$$S_e = 2j_n \ln\langle \hat{e}_3|g|\hat{e}_3\rangle + 2j_{n+1} \ln\langle -\hat{e}_3|g| - \hat{e}_3\rangle + 2k_n \sum_{l=0}^{3} \ln\langle \hat{r}_l|g|\hat{r}_l\rangle. \qquad (5.5)$$

In the next section we derive the expression of the edge amplitudes in the large-spin limit starting from the above sample description. In terms of the coherent states also the vertex amplitude takes the simple and compact form (4.15). In particular, for $\gamma < 1$ it factorizes as $\mathcal{A}_v = \mathcal{A}_v^+ \mathcal{A}_v^-$ being

$$\mathcal{A}_v^\pm = \int_{SU(2)^8} \mathrm{d}g_a e^{S_\pm[g_a]}, \tag{5.6}$$

and

$$\begin{aligned} S_\pm[g_a] &= \frac{|1 \pm \gamma|}{2} \sum_{ab \supset a} 2j_{ab} \ln\langle -\vec{n}_{ab}|g_a^{-1}g_b|\vec{n}_{ab}\rangle \\ &\equiv \frac{|1 \pm \gamma|}{2} S_v[g_a], \end{aligned} \tag{5.7}$$

where we are using the general notation introduced at the beginning of this section to feature the boundary data [3].

5.2 Semiclassical Limit

The semiclassical limit of the probability amplitude described by a spin foam model corresponds to the large-spin limit of the partition function (4.12). Let us redefine all the spins $j_i \to \lambda j_i$ so that the asymptotic limit is obtained by sending $\lambda \to \infty$. The limit of the face amplitude is straightforward. From formula (4.13) we obtain

$$\mathcal{A}_f \xrightarrow{\lambda \to \infty} (8\pi \Omega j_n)^{2\alpha}, \tag{5.8}$$

where we have defined the function

$$\Omega \equiv \frac{\sqrt{1 - \gamma^2}}{8\pi}. \tag{5.9}$$

For edge and vertex amplitudes the task is instead not trivial. Notice that the norm of the coherent intertwiner (5.4) and the vertex amplitude (5.6) possess a similar form. To find their large-λ limit we will make use of the *extended* stationary phase approximation presented in section 4.2.1 and already used to carry out the asymptotics of the deformed amplitude in Chapter 4. Now, the high degree of symmetry will allow us to explicitly evaluate the amplitudes, and in particular the determinant of the Hessian, as functions of the spins.

---

[3]The minus sign appearing in the 'bra' part of (5.7) depends on the fact that, from Figure 5.6 we are using the convention (3.65) with all vectors $\vec{n}_i$ pointing outward, which disagrees with the orientation of the links in Figure 5.1. See [73] for details.

5.2.1 The asymptotic norm of the coherent intertwiner

In order to describe the semiclassical behavior of the edge-amplitude $\mathcal{A}_e$ associated to a quantum frustum we study the large-spin limit of the norm of the coherent intertwiner (5.2). As a first step we look for the critical points of the action S_e in (5.5). In our case the manifold carries the structure of a group and the critical points will be $SU(2)$ group elements. The condition $\mathrm{Re}S_e = 0$ that they have to satisfy can be rephrased in the requirement $|e^{\lambda S_e(x_0)}| = 1$. Using the general formula for coherent states

$$|\langle \vec{n}|\vec{m}\rangle| = \left(\frac{1 + \vec{n}\cdot\vec{m}}{2}\right)^{1/2},$$

one finds

$$\left(\frac{1 + \hat{e}_3 \cdot (g \triangleright \hat{e}_3)}{2}\right)^{j_n} \times \left(\frac{1 + (-\hat{e}_3) \cdot (g \triangleright (-\hat{e}_3))}{2}\right)^{j_{n+1}}$$

$$\times \prod_l \left(\frac{1 + \hat{r}_l \cdot (g \triangleright \hat{r}_l)}{2}\right)^{k_n} \overset{!}{=} 1.$$

Since the scalar products in the parentheses have real values in the set $[-1, 1]$, the above condition is satisfied only for $g = \pm\mathbb{1}$. It is easy to check that in these two points the function S_e vanishes. Let us now assign a set of coordinates x^K, $K = 1, 2, 3$ to the $SU(2)$ group elements as follows

$$g \to g_c e^{\frac{i}{2} x^K \sigma_K}, \qquad g_c = \pm\mathbb{1},$$

being σ_K the standard Pauli matrices. In these variables x^K, the Haar measure is normalized as

$$\frac{1}{(4\pi)^2} \int_{\|x\| < \pi} \mathrm{d}^3 x \left(\frac{\sin(\|x\|/2)}{\|x\|/2}\right)^2 = 1. \tag{5.10}$$

This operation allows to perform the partial derivative of the action S_e w.r.t. the group elements. The first derivative of S_e evaluated in $x = 0$ reads

$$\left.\frac{\partial S_e}{\partial x^K}\right|_{x=0} = i\left(j_n \hat{e}_3^{(K)} - j_{n+1}\hat{e}_3^{(K)} + \sum_l k_n \hat{r}_l^{(K)}\right),$$

where we have used the coherent states property $\langle \vec{n}|\sigma_K|\vec{n}\rangle = \vec{n}^{(K)}$ and the expression $\vec{n}^{(K)}$ indicates the K-th component of the vector $\vec{n}$. The above expression is always vanishing since it corresponds to the closure condition. Thus, we deduce that $g_c = \pm\mathbb{1}$ are the critical and stationary points that

dominate the asymptotic limit of the norm of the coherent intertwiner. The components of the Hessian matrix evaluated at the g_c read

$$
\begin{aligned}
H_{KL} &= \left. \frac{\partial^2 S_e}{\partial x^L \partial x^K} \right|_{x=0} \\
&= \frac{j_n + j_{n+1}}{2} \left(\hat{e}_3^{(K)} \hat{e}_3^{(L)} - \delta_{KL} \right) + \sum_{l=0}^{3} \frac{k_n}{2} \left(\hat{r}_l^{(K)} \hat{r}_l^{(L)} - \delta_{KL} \right).
\end{aligned}
$$

From the above matrix elements one can derive the determinant of the Hessian

$$
\det(-H) = \frac{k_n \sin^2 \phi}{2} \left(j_n + j_{n+1} + 2k_n(1 + \cos^2 \phi) \right)^2,
$$

where the slope angle ϕ is given by (5.3).

Now that we have all the ingredients we can use equation (4.18) to find the leading term of the norm of the coherent intertwiner (5.2) in the large-λ expansion. Inserting the result into equation (4.14) we finally obtain the asymptotic limit of the edge amplitude for a quantum frustum

$$
\mathcal{A}_{e,\text{frustum}}^{j_n, j_{n+1}, k_n} \to \frac{\Omega^3 k_n^3}{2(4\pi)^4} (1 + K^2)(1 + K^2 - 2Q)^2, \tag{5.11}
$$

where we have used the functions

$$
Q \equiv 2 + \frac{j_n + j_{n+1}}{2k_n}, \qquad K \equiv \sqrt{-\cos 2\theta}, \qquad \theta \equiv \arccos \frac{1}{\tan \phi}, \tag{5.12}
$$

to guarantee a compact expression. From equation (5.11) we can easily deduce the large-spin limit of the edge amplitude associated to a quantum cube of side area j. By setting $j_n = j_{n+1} = k_n \to j$ we find

$$
\mathcal{A}_{e,\text{cube}}^{j} \longrightarrow \frac{1}{16\pi^4} \left(\frac{\lambda \sqrt{1 - \gamma^2}}{8\pi} \right)^3 j^3. \tag{5.13}
$$

5.2.2 Asymptotics of the vertex-amplitude

The factorization of the vertex amplitude $\mathcal{A}_v$ for $\gamma < 1$ allows us to study its semiclassical limit by focusing on the asymptotic expression of equation (5.6). We will make our considerations ignoring the $\pm$ indices and working with the function S_v defined in (5.7). The invariance of the Haar measure $\mathrm{d}g$ allows to discard one of the eight integrations by fixing one of the critical points g_a. In particular, we choose to fix $g_0 = \mathbb{1}$. The first condition that the critical points have to satisfy is

$$
|e^{\lambda S_v(x_0)}| = 1 \Rightarrow g_a \triangleright \vec{n}_{ab} = -g_b \triangleright \vec{n}_{ba}. \tag{5.14}
$$

In the geometric picture introduced in the previous section, this condition corresponds to glue the eight boundary hexahedra by properly rotating the vectors $\vec{n}_{ab}$ and $\vec{n}_{ba}$ so that in the end they will point in relative opposite directions $\forall a,b$. Modulo the symmetry $g_a \rightarrow -g_a$ of the action S_v the critical points equation (5.14) has two sets of solutions which we list in Table 5.1.

	Σ_1	Σ_2
g_1	$\exp(i\frac{\theta}{2}\sigma_1)$	$\exp(-i\frac{\theta}{2}\sigma_1)$
g_2	$\exp(i\frac{\theta}{2}\sigma_2)$	$\exp(-i\frac{\theta}{2}\sigma_2)$
g_3	$\exp(i\frac{\theta}{2}\sigma_3)$	$\exp(-i\frac{\theta}{2}\sigma_3)$
g_4	$\exp(i\frac{\pi-\theta}{2}\sigma_3)$	$\exp(-i\frac{\pi-\theta}{2}\sigma_3)$
g_5	$\exp(i\frac{\pi-\theta}{2}\sigma_2)$	$\exp(-i\frac{\pi-\theta}{2}\sigma_2)$
g_6	$\exp(i\frac{\pi-\theta}{2}\sigma_1)$	$\exp(-i\frac{\pi-\theta}{2}\sigma_1)$
g_7	$\mathbb{1}$	$\mathbb{1}$

Table 5.1: The two sets of critical points which are solutions of equation (5.14). We will see that the dihedral angles between the boundary hexahedra are functions of the angle θ in the exponentials.

The rotation angle θ can be expressed in terms of the slope angle ϕ of the frustum as

$$\cos\theta = \frac{1}{\tan\phi}. \tag{5.15}$$

The equation (5.15) poses a consistency condition on the allowed values of ϕ i.e.,

$$\frac{\pi}{4} \leq \phi \leq \frac{3\pi}{4}.$$

Using equation (5.3) it is easy to check that the allowed values of the spins in our system are

$$-\frac{1}{\sqrt{2}} \leq \frac{j_{n+1} - j_n}{4k_n} \leq \frac{1}{\sqrt{2}}, \tag{5.16}$$

which correspond to a restriction of the phase space. The action in the two

sets of critical points listed in Table 5.1 reads

$$S_v(\Sigma_1) = +6i(j_n - j_{n+1})\left(\frac{\pi}{2} - \theta\right) + 12ik_n\left(\frac{\pi}{2} - \arccos\left(\cos^2\theta\right)\right),$$

$$S_v(\Sigma_2) = -6i(j_n - j_{n+1})\left(\frac{\pi}{2} - \theta\right) - 12ik_n\left(\frac{\pi}{2} - \arccos\left(\cos^2\theta\right)\right).$$

The Hessian is a 21×21 matrix and is constructed with the second derivatives of the action (5.7). Defining the vectors $\tilde{n}_{ab} \equiv g_a \triangleright \vec{n}_{ab}$, its components evaluated on the critical points are

$$H_{aa,KL} = \left.\frac{\partial^2 S_v}{\partial x_a^L \partial x_a^K}\right|_{x=0} = \sum_{(ab)\supset a} \frac{j_{ab}}{2}\left(-\delta_{KL} + \tilde{n}_{ab}^{(K)}\tilde{n}_{ab}^{(L)}\right),$$

$$H_{ab,KL} = \left.\frac{\partial^2 S_v}{\partial x_b^L \partial x_a^K}\right|_{x=0} = \frac{j_{ab}}{2}\left(\delta_{KL} - i\epsilon_{KLI}\tilde{n}_{ab}^{(I)} - \tilde{n}_{ab}^{(K)}\tilde{n}_{ab}^{(L)}\right).$$

Using a computer algebra program it is possible to calculate the exact expression of the determinant of the Hessian matrix $D \equiv \det H$, which is a homogeneous function of the spins. Finally, computing the leading order (4.18) for both $\mathcal{A}_v^+$ and $\mathcal{A}_v^-$ and taking their product one obtains the leading order of the vertex amplitude $\mathcal{A}_v$ in the large-λ limit

$$\mathcal{A}_v^{j_n,j_{n+1},k_n} \rightarrow \left(\frac{1}{8\pi\Omega}\right)^{21}\left(\frac{e^{\frac{(1+\gamma)}{2}\lambda S_v(\Sigma_1)}}{\sqrt{-D}} + \frac{e^{\frac{(1+\gamma)}{2}\lambda S_v(\Sigma_2)}}{\sqrt{-D^*}}\right)\left(\frac{e^{\frac{(1-\gamma)}{2}\lambda S_v(\Sigma_1)}}{\sqrt{-D}} + \frac{e^{\frac{(1-\gamma)}{2}\lambda S_v(\Sigma_2)}}{\sqrt{-D^*}}\right)$$

$$\rightarrow \left(\frac{1}{8\pi\Omega}\right)^{21}\left(\frac{e^{i\lambda S_R}}{-D} + \frac{e^{-i\lambda S_R}}{-D^*} + 2\frac{\cos(\lambda\gamma S_R)}{\sqrt{DD^*}}\right),$$

(5.17)

where $D = D(j_n, j_{n+1}, k_n)$ the determinant of the Hessian which in terms of the functions defined in (5.12) reads

$$D = \frac{j_n^3 j_{n+1}^3 k_n^{15}}{16} K(K - 3i)^2\left(K - iK^2 + iQ\right)^3\left(1 + K^2 - 2Q\right)^3$$

$$\left(1 + 3K^2 - 2Q - 2iK(Q - 1)\right)^3 (K + i)^6.$$

(5.18)

The function $S_R = S_R(j_n, j_{n+1}, k_n)$ reads

$$S_R = 6(j_n - j_{n+1})\left(\frac{\pi}{2} - \theta\right) + 12k_n\left(\frac{\pi}{2} - \arccos(\cos^2\theta)\right),$$

(5.19)

and is interpreted as the Regge action describing the dynamics of the classical model. Let us observe that it has indeed the form

$$S_R \sim \sum_h A_h \delta_h,$$

being A_h the area of the hinge h (i.e., a 2-dimensional face) to which is associated a spin j_h and $\delta_h = \frac{\pi}{2} - \Theta_h$ the contribution of the analyzed vertex to the deficit angle at the hinge. The 24 dihedral angles $0 < \Theta_{ab} < \pi$ can be computed by performing the scalar product between all the couples $N_a, N_b \in \mathbb{R}^4$ of outward pointing normals to the boundary hexahedra ε_a and ε_b (see Appendix C). We find six dihedral angles $\Theta = \theta$ associated to hexahedra which meet along j_n faces, six dihedral angles $\Theta' = \pi - \theta$ associated to hexahedra meeting along j_{n+1} faces and twelve dihedral angles $\Theta'' = \arccos(\cos^2 \theta)$ corresponding to boundary frusta meeting along k_n faces.

Notice that for the allowed values (5.16) of the spins, the function K is real and has values in the set $[0, 1]$. In particular $K = 1$ corresponds to the flat cuboid case while $K = 0$ corresponds to a degenerate frustum with $\phi = \frac{\pi}{4}, \frac{3\pi}{4}$. The full expression (5.18) of the determinant D is relative to the first set Σ_1 of critical points. The solution for the second set of critical points Σ_2 is simply given by its complex conjugate.

Let us also notice that both the determinant function (5.18) and the Regge action (5.19) are invariant under exchange $j_n \leftrightarrow j_{n+1}$. In the light of the physical interpretation which we propose in the next section, a consequence of this symmetry is that the full transition amplitude does not distinguish locally between space expansions or contractions at the same rate.

Finally, we can absorb the expressions (5.8),(5.11) and (5.13) of $\mathcal{A}_f$ and $\mathcal{A}_e$ in the vertex amplitude (5.17) in order to write the generating functional (4.12) in terms of a dressed vertex amplitude $\hat{\mathcal{A}}_v$. Since every edge e is bounded by two vertices, we split the contribution of the corresponding edge amplitude by assigning to each vertex sitting at the extremes of e the square root of $\mathcal{A}_e$. In the same fashion, since a face is shared by four vertices (corresponding to the fact that four hyperfrusta meet in a 2d trapezoid) we multiply each vertex amplitude with the fourth root of $\mathcal{A}_f$. Summarizing, for a generic vertex v we have

$$\hat{\mathcal{A}}_v \equiv \prod_{f \supset v} \mathcal{A}_f^{1/4} \prod_{e \supset v} \mathcal{A}_e^{1/2} \, \mathcal{A}_v, \tag{5.20}$$

and the generating functional (4.12) takes the compact form

$$Z_\Gamma = \sum_{j_f, \iota_e} \prod_v \hat{\mathcal{A}}_v. \tag{5.21}$$

As we have already mentioned in Chapter 3, the spin foam sum can be written in terms of boundary amplitudes in the following way: For each vertex v and configuration j_f, ι_e, a $SU(2)$-spin network function $\psi_{\Gamma_v, j_f, \iota_e}$ is induced on the corresponding boundary graph $\Gamma(v)$. The boundary amplitude $\mathcal{A}_{\Gamma_v}$ is then an operator on $\mathcal{H}_{\Gamma_v}$, which is defined by

$$\mathcal{A}_{\Gamma_v}(\psi_{\Gamma_v, j_f, \iota_e}) := \hat{\mathcal{A}}_v. \tag{5.22}$$
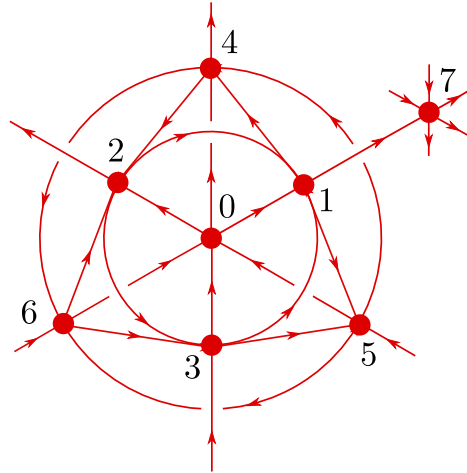
Figure 5.6:   The projection of the boundary graph of a hyperfrustum (see also Figure 5.1). This graph has 8 nodes, 24 links, and 6 crossings. All the outgoing lines meet at node 7.

5.2.3   Coupling to the cosmological constant

Following the instructions of Chapter 4, we can also couple a cosmological constant term to the Frustum model. The spin network around a vertex which is depicted in Figure 5.1 can be flattened with a minimal number of crossings as in 5.6.

Then for each crossing we can assign a quantum operator (4.21) to the vertex amplitude (5.6). Eventually, in the semiclassical limit the right discrete cosmological constant term appears together with the Regge action (5.19). Also, the determinant of the Hessian (5.18) will remain unchanged as we have shown in the general case. The final set of asymptotic deformed amplitudes is explicitly reported in the summary section at the end of this chapter.

This concludes the semiclassical analysis of the EPRL-FK spin foam model in the reduced state sum approximation. Starting from these results, we will study in Chapter 6 the renormalization properties of this model.

In the next section we continue the analysis of the Frustum model, this time at the classical level i.e., by focusing only on the (Regge-type) action (5.19) (and not on the partition function). We will see how the restricted set of geometrical configurations considered carries enough information to reproduce the standard cosmological dynamics of a flat FLRW universe in the limit of fine discretization of the lattice as well as in the small deficit angles limit.

5.3 Discrete Classical Cosmology

The action (5.19) encodes the classical properties of the system under study. It is the generalization of the Regge action (2.59) to the case of hyperfrusta, instead of triangulations, where the areas (instead of edge lengths) are the free variables. Nonetheless, we will refer to (5.19) as "Regge action" in what follows, and show that, in the limit of large lattices, classical cosmology is obtained. To this end, we investigate the dynamics of the spin variables described by the equations of motion, which we are going to derive in the next section. Here we consider a spacetime manifold $\mathcal{M} \sim T^3 \times [0, 1]$ given by the product of the 3-torus and a closed interval. In particular we define homogeneous and locally isotropic states on T^3 and let them evolve. Such states are represented by a Daisy graph (see figure 5.7 on the left) in which the node is dual to a cube and all the links are labeled by the same spin value. A similar construction has been studied in the context of spin foam cosmology where the transition amplitudes between holomorphic coherent states are calculated [91]. The dressed vertex amplitude defined in the previous section can be interpreted as the transition probability between two space-like hypersurfaces Σ_i and Σ_f at different time steps t_i and t_f as it is shown in figure 5.7 on the right. In particular, we regard the two cubes at the boundary of a hyperfrustum as isotropic and homogeneous space-like hypersurfaces. The evolution occurs in the bulk region bounded by the six boundary frusta, which in our setup are time-like hypersurfaces. The characteristic size of space at a fixed time is then
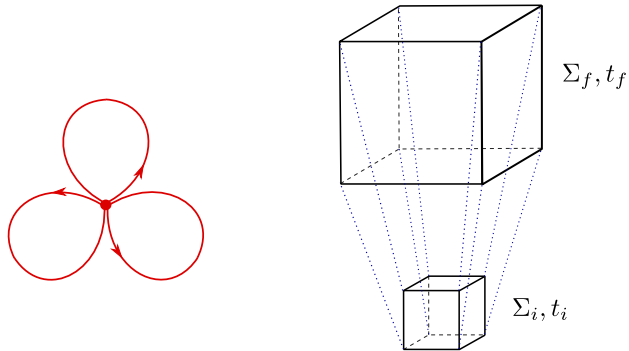
Figure 5.7: The figure on the left shows a Daisy graph which corresponds to the spin network graph associated to a boundary cube. On the right we represent a hyperfrustum as the time evolution of its space-like boundary cubes Σ_i and Σ_f.

encoded by the spin values associated to the cube faces. The peculiar choice of reducing the state sum to hyperfrusta makes possible the variation in size of the boundary cubes at successive time steps. Thus, from an intuitive perspective the model allows a basic concept of expansion and contraction of a
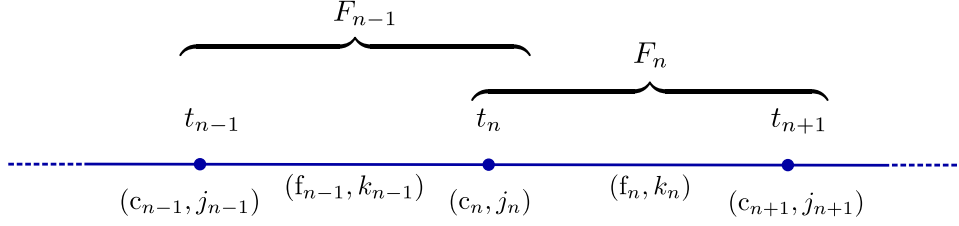
Figure 5.8:   The figure shows a chain obtained by gluing together many hyperfrusta. In particular, the n-th node in the chain represents the 'past' cube c_n in the boundary of the hyperfrustum F_n. The $(n+1)$-th cube c_{n+1} is the 'future' cube in the boundary of F_n. The line connecting these two cubes is associated to the remaining six boundary frusta f_n.

flat space.

5.3.1   Classical Dynamics of the Frustum

In order to describe the classical dynamics of the space slices let us consider the chain in figure 5.8 obtained by gluing together a series of hyperfrusta F_n and representing the time evolution of their boundary cubes c_n having areas j_n. At each step the evolution occurs in the bulk region bounded by the six boundary frusta f_n with bottom faces j_n, top faces j_{n+1} and side faces of area k_n. Let us observe that such construction resembles a so-called CW skeleton (Collins-Williams), which is a discrete structure specifically designed to approximate a FLRW universe in the context of Regge calculus [92, 93] [4]. The Cauchy surfaces of a CW skeleton are discretized by regular polytopes (in our case cubes) and, as in the FLRW approximation, they are identical to each other apart from an overall scaling factor. This analogy allows us to interpret the spin j_n associated to the n-th cube as a discrete surrogate of the scale factor at a fixed time. Therefore, we define the *scale factor* at the n-th step as [5]

$$a_n \equiv \sqrt{j_n}. \tag{5.23}$$

Let us also define the time step of the evolution between the cubes c_n and c_{n+1} to be the distance between their centers or, equivalently, the height H_n of F_n i.e.,

$$t_{n+1} - t_n \equiv H_n.$$

Let θ_n be the dihedral angle between c_n and f_n and let h_n be the height of f_n. From the results of the last section and using arguments of classical geometry

---

[4]A similar construction is investigated in [94] and [95] to model the flat FLRW and the Kasner solutions of general relativity.

[5]The scale factor here is dimensionless. In order to give the right dimensions to a_n one should insert physical fundamental constants such as G Newton. However this operation does not change the results of the present analysis and we will omit these details for the sake of clarity.

one can show that their values in terms of the spins are

$$
\begin{aligned}
\theta_n &= \arccos(\cot \phi_n), \\
h_n &= \frac{2k_n}{\sqrt{j_{n+1}} + \sqrt{j_n}} \sin \phi_n,
\end{aligned}
\tag{5.24}
$$

being ϕ_n the slope angle of the frustum f_n such that (in analogy with (5.3))

$$
\cos \phi_n = \frac{j_{n+1} - j_n}{4k_n}.
$$

In terms of these variables we find the expression for the n-th time step

$$
H_n = h_n \sin \theta_n = \frac{2k_n}{\sqrt{j_{n+1}} + \sqrt{j_n}} \sqrt{1 - \frac{(j_{n+1} - j_n)^2}{8k_n^2}}.
\tag{5.25}
$$

Before proceeding to the explicit computation of the equations of motion, let us find out how the vacuum Friedmann equations look like in the reduced model under study by performing a qualitative analysis. From the above definitions we can compute the discrete time derivative of the scale factor as a function of the spin variables

$$
\dot{a}_n = \frac{a_{n+1} - a_n}{t_{n+1} - t_n} = \frac{2}{\sqrt{\tan^2 \phi_n - 1}}.
$$

Using the first equation in (5.24) it is easy to check that, in terms of the dihedral angle θ_n between c_n and f_n, the expression above reads

$$
\dot{a}_n = 2 \cot \theta_n.
\tag{5.26}
$$

The first vacuum Friedman equation $\dot{a}_n = 0$ would then tell us that locally the classical evolution happens for $\phi_n = \frac{\pi}{2}$ i.e., on a hypercubic lattice in which all the dihedral angles are $\theta_n = \frac{\pi}{2}$. Since at each square in the lattice the contribution to the deficit angle is given by four hypercuboids, then the sum of the angles vanishes at all the hinges, which corresponds to flat space. The second derivative of the scale factor is easily derivable and reads

$$
\ddot{a}_n = -\frac{2}{\sin^2 \theta_n} \left(\frac{\theta_n - \theta_{n+1}}{t_{n+1} - t_n} \right).
\tag{5.27}
$$

Since $1/2 \leq \sin \theta_n \leq 1$ is constrained by the consistency condition (5.16) and is not vanishing, we deduce that the acceleration of the scale factor vanishes only when the dihedral angle does not vary with the time flow i.e., $\theta_n = \theta_{n+1}$. Therefore, at the scale defined by the building blocks, the vacuum Friedman equations $\ddot{a}_n = \dot{a}_n = 0$ are fulfilled only in the case of a flat reduced universe

with vanishing deficit angles at the hinges. Let us note that in general an accelerated expansion (contraction) of the universe would be described by a growth (decrease) of the dihedral angles at successive steps.

The next step in our analysis is the explicit derivation of the equations of motion, that we obtain by deriving the discrete action with respect to the spins i.e., the area variables. In fact we want to verify that the expected results are obtained without imposing the Friedmann equations a priori as we just did.

An important remark: it is known that, given a generic triangulation, difficulties may arise in the context of Regge calculus when considering two-dimensional areas as independent variables instead of the edge lengths [96]. In particular, the information given by the areas of a four dimensional polyhedron is in general not enough to unambiguously reconstruct its geometry. For example, although a 4-simplex has the same number of edge lengths and faces, one can construct two 4-simplices with the same triangular areas but different edge lengths. The situation gets worse in the case of many four-dimensional blocks glued together. Another ambiguity is in the interpretation of the Regge equations where, for instance, the vanishing of the deficit angles (seen as functions of the areas) does not necessarily imply flatness. Various solutions to these issues have been studied in the literature [97, 98, 99], and extensions of the so-called area Regge calculus have been proposed [100]. These concerns, however, are not necessary in the context of our model where the spins are a priori constrained into a rigid symmetric configuration. In fact, the number of spins required to reconstruct the geometry of a regular hyperfrustum is equal to the number of independent edge lengths. Further, this result holds for arbitrary numbers of hyperfrusta glued together. As a consequence, one can freely invert the relationship between length and spin variables without affecting the accuracy of the geometrical description. Finally, as we will see, the equations of motion derived are equal to the standard Regge calculus ones.

We study the classical dynamics of the discrete model in three cases: pure gravity, in presence of a cosmological constant and in the case of dust matter coupling. The following analysis is inspired by a collection of works on cosmological models with Regge calculus [92, 94, 93, 101, 102, 103, 104, 95].

5.3.2   Flat vacuum FLRW universe

Let us refer once again to the chain model in figure 5.8. The full Regge action is given by a sum of terms of the form (5.19) for each hyperfrustum F_n

$$
\begin{aligned}
S_R(\{j_n\}, \{k_n\}) &= \sum_n S_{R,n}(j_n, j_{n+1}, k_n) \\
&= \sum_n \left(\frac{3}{2}(j_n - j_{n+1})\delta_n^{(j)} + 3k_n\delta_n^{(k)} \right),
\end{aligned}
\tag{5.28}
$$

being the deficit angles

$$\delta_n^{(k)} = 2\pi - 4\arccos(\cos^2\theta_n),$$
$$\delta_n^{(j)} = 2\pi - 4\theta_n,$$
(5.29)

and

$$\cos\theta_n = \frac{j_{n+1} - j_n}{\sqrt{16k_n^2 - (j_{n+1} - j_n)^2}}.$$
(5.30)

Deriving the Regge action with respect to the spins k_n and j_n and setting the result equal to zero gives the equations of motion which solve the classical dynamics of the discrete model [6]. A direct calculation shows that the contribution of the derivatives of the dihedral angles sum up to zero. Thus, a posteriori, one does not need to derive the deficit angles in the Regge action in order to obtain the equations of motion. This can be regarded as the analogue of the Schläfli identity [105]. The Regge equations of motion for the spins k_n and j_n are then

$$\frac{\partial S_R}{\partial k_n} = 3\,\delta_n^{(k)} = 0,$$
$$\frac{\partial S_R}{\partial j_n} = \frac{3}{2}\left(\delta_n^{(j)} - \delta_{n-1}^{(j)}\right) = 0.$$
(5.31)

Let us notice that these equations correspond respectively to the vanishing of (5.26) and (5.27). Indeed, the first equation of motion implies the vanishing of the dihedral angle θ_n, while the second equation tells us that the dihedral angle remains constant at successive time steps i.e., $\theta_n = \theta_{n+1}$. Therefore, as it is illustrated in the previous subsection, the equations of motion (5.31) can be interpreted as a discrete version of the vacuum Friedmann equations.

Let m_n be the length of a 'strut' of the n-th frustum (i.e., the diagonal edge of its trapezoidal faces) and l_n the edge length of the n-th cube. One can show that the first equation in (5.31) is equivalent to the one obtained by deriving the Regge action w.r.t. the strut length, apart from an overall non-vanishing factor. Explicitly,

$$\frac{\partial S_R}{\partial m_n} = \frac{\partial k_n}{\partial m_n}\frac{\partial S_R}{\partial k_n} = 0.$$
(5.32)

It has been noted that such equation can be interpreted as the analogue of the Hamiltonian constraint (2.39) of the ADM formalism studied in Chapter

---

[6] Such procedure is regarded as a global variation since the six spins j_n of c_n, as well as the twelve spins k_n of the frusta f_n, are first constrained to form a regular hyperfrustum and then they are all derived at once. A local variation would instead consider each spin separately and impose the constraints at the end. For more details see [93].

2 [93]. In the same way, the equation of motion for the variable l_n is linked to the evolution equation (2.35) of ADM formalism and it can be written as

$$\frac{\partial S_R}{\partial l_n} = \frac{\partial j_n}{\partial l_n}\frac{\partial S_R}{\partial j_n} + \frac{\partial k_n}{\partial l_n}\frac{\partial S_R}{\partial k_n} + \frac{\partial k_{n-1}}{\partial l_n}\frac{\partial S_R}{\partial k_{n-1}} = 0. \qquad (5.33)$$

This coincides with the equation of motion for the spin j_n only when it is evaluated on the solution of the equations of motion for the variables k_n and k_{n-1}. We will still refer to $\partial S_R/\partial k_n = 0$ as the *Hamiltonian constraint* and to $\partial S_R/\partial j_n = 0$ as the *evolution equation*. Such observations will be valid also in the next subsections where we study the Friedmann universe in presence of a cosmological constant and coupled to dust particles.

In order to remove any doubt about the connection between the Regge equations of motion (5.31) and the vacuum Friedmann equations, let us pass to the continuum *time* limit. From the time step formula (5.25) we get

$$k_n^2 = \frac{(\sqrt{j_{n+1}} + \sqrt{j_n})^2}{4}H_n^2 + \frac{(j_{n+1} - j_n)^2}{8}. \qquad (5.34)$$

Substituting this expression into the dihedral angle (5.30), one can write the Regge equations (5.31) in terms of the spins j_n's and the time steps H_n's. Let us now perform the following replacement in the equations of motion

$$\begin{aligned} H_n, H_{n-1} &\rightarrow \mathrm{d}t, \\ j_n &\rightarrow j(t), \\ j_{n+1} &\rightarrow j(t) + j'\mathrm{d}t + \frac{1}{2}j''\mathrm{d}t^2 + \mathcal{O}(\mathrm{d}t^3), \\ j_{n-1} &\rightarrow j(t) - j'\mathrm{d}t + \frac{1}{2}j''\mathrm{d}t^2 + \mathcal{O}(\mathrm{d}t^3), \end{aligned} \qquad (5.35)$$

and find the continuum time limit by sending $\mathrm{d}t \rightarrow 0$. Note that we have imposed that the time step H_n is constant in this limit $\forall n$. This corresponds to a gauge fixing choice and it is justified by the fact that the equations of motion (5.31) do not impose constraints on the allowed values of k_n and H_n. At the leading order in $\mathrm{d}t$ the Regge equations read

$$\begin{aligned} 3\left(2\pi - 4\arccos\frac{j'^2}{16j + j'^2}\right) &= 0, \\ 12\,\frac{1}{\sqrt{j}}\frac{2jj'' - j'^2}{16j + j'^2} &= 0. \end{aligned} \qquad (5.36)$$

Deriving the Hamiltonian constraint (first equation) one can easily check that it is a first integral of the evolution equation (second equation). Let us note

that we are still working in Euclidean signature. To argue a solution which is comparable to the standard Friedmann cosmology we need to perform a Wick rotation $t \to it$. This results in the replacements $j'' \to -j''$ and $j'^2 \to -j'^2$. One can check that the vacuum solutions remain unchanged. However, this step will be fundamental when investigating the coupling to cosmological constant and to dust particles. We stress the fact that the Wick rotation is effective only because we are working on the classical action (5.28). Thus there is no statement of relation between the Euclidean and the Lorentzian EPRL-FK models nor among the semiclassical limit of their amplitudes.

The solutions of the Hamiltonian constraint and the evolution equation are readily derived

$$ j' = 0, \qquad j'' = \frac{j'^2}{2j}. \tag{5.37} $$

In the interpretation given in the previous section in which the scale factor is $a = \sqrt{j}$, the Regge equations correspond to

$$ \begin{aligned} \frac{a'^2}{a^2} &= 0, \\ \frac{a''}{a} &= 0, \end{aligned} \tag{5.38} $$

which are the standard vacuum Friedmann equations for a flat universe.

5.3.3 Flat Λ-FLRW universe

In Chapter 4 we have studied the coupling of a cosmological constant term to the EPRL-FK model via a deformation of the quantum amplitudes. Taking the semiclassical limit of the deformed vertex amplitude one obtains the Regge action $S_R = S_R(\{j_n\}, \{k_n\}, \Lambda)$ in presence of a cosmological constant term $\Lambda > 0$. Explicitly,

$$ S_R = \sum_n \left(\frac{3}{2}(j_n - j_{n+1})\delta_n^{(j)} + 3k_n\delta_n^{(k)} - \Lambda V_n \right), \tag{5.39} $$

being V_n the four dimensional volume of the n-th hyperfrustum. We can express it in terms of the spins as (see Appendix C)

$$ V_n = \frac{k_n(j_n + j_{n+1})}{2} \sqrt{1 - \frac{(j_{n+1} - j_n)^2}{8k_n^2}}. \tag{5.40} $$

Let us notice that in the present notation all the spins, the volume and Λ are dimensionless. In the last section of this chapter we will reintroduce the

dependence on G Newton and with that also the physical dimensions of areas, volumes and cosmological constant. The new Regge equations are

$$
\frac{\partial S_R}{\partial k_n} = 3\,\delta_n^{(k)} - \Lambda\frac{\partial V_n}{\partial k_n} = 0,
$$

$$
\frac{\partial S_R}{\partial j_n} = \frac{3}{2}\left(\delta_n^{(j)} - \delta_{n-1}^{(j)}\right) - \Lambda\left(\frac{\partial V_n}{\partial j_n} + \frac{\partial V_{n-1}}{\partial j_n}\right) = 0.
$$

(5.41)

Performing the continuum time limit as we did in the vacuum case, one can find the Hamiltonian constraint and the evolution equation for a flat Λ-FLRW universe. After a Wick rotation $t \to it$, $j'' \to -j''$, $j'^2 \to -j'^2$ they read

$$
2\pi - 4\arccos\frac{j'^2}{j'^2 - 16j} = \frac{\Lambda}{3}j\sqrt{1 - \frac{j'^2}{8j}},
$$

$$
\frac{2jj'' - j'^2}{j'^2 - 16j} = \frac{\Lambda}{12}j\left(1 - \frac{j'^2}{16j} - \frac{j''}{8}\right).
$$

(5.42)

As in the vacuum case, the Hamiltonian constraint (first equation) is the first integral of the evolution equation (second equation). Thus, we can use it to study the evolution of the model. Notice that the Hamiltonian constraint is only defined for

$$
\frac{j'^2}{8j} \leq 1,
$$

(5.43)

which imposes a condition on the maximal rate of expansion of the space surfaces. Let us define the Wick-rotated dihedral angle associated to the time-like hinges

$$
\Theta_W \equiv \arccos\frac{j'^2}{j'^2 - 16j}.
$$

(5.44)

When evaluated in the range (5.43) this is a function with real values

$$
\frac{\pi}{2} \leq \Theta_W \leq \pi, \qquad -1 \leq \cos\Theta_W \leq 0.
$$

(5.45)

From (5.44) we find

$$
j'^2 = -16j\frac{\cos\Theta_W}{1 - \cos\Theta_W}.
$$

(5.46)

Using the above definitions the Hamiltonian constraint becomes

$$
j^2 = \frac{9}{\Lambda^2}\frac{1 - \cos\Theta_W}{1 + \cos\Theta_W}\left(2\pi - 4\Theta_W\right)^2.
$$

(5.47)

Expressing the volume of the universe as $U = j^{3/2}$ we can find the equation describing its time evolution

$$
\begin{aligned}
\frac{\mathrm{d}U}{\mathrm{d}t} &= \frac{3}{2} j^{\frac{1}{2}} j' = 6j \sqrt{\frac{-\cos\Theta_W}{1 - \cos\Theta_W}} \\
&= -\frac{18}{\Lambda} \sqrt{\frac{-\cos\Theta_W}{1 + \cos\Theta_W}} \, (2\pi - 4\Theta_W).
\end{aligned}
\tag{5.48}
$$

where we have used the equations (5.44) and (5.46). Let us notice that also the square root of equation (5.47) is involved in the above derivation. Since it can assume both positive and negative values, one must carefully select the signs according to the angle range (5.45) in order to get a positive value of j. The volume and its time variation form a set of parametric equations which can be solved using numerical methods.

Note that the use of a rigid hyperfrustum is not well suited to capture the degrees of freedom of a constantly curved spacetime such as in the case of a Friedmann universe in presence of a cosmological constant. Thus, in order to get a better approximation of the Friedmann dynamics one needs to refine the lattice discretization by describing the evolution of a larger number of cubes tessellating each Cauchy surface [7] as in figure (5.9).
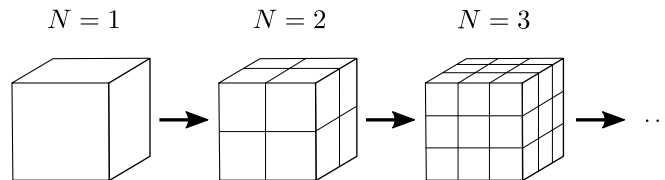
Figure 5.9: The figure shows some coarse graining steps of a 3-Torus.

In the case we want to describe the evolution of N^3 identical cubes, the Hamiltonian constraint does not vary since the number of cubes factorizes in the action (5.39) and the continuum time limit procedure is not affected by the coarse graining. What changes is instead (modulo rescaling) the volume of the universe

$$
U \to N^3 U.
\tag{5.49}
$$

In figure (5.10) we plot the time derivative of the volume (for some positive value of Λ) against the volume of the universe itself for different numbers of cubes tessellating a Cauchy surface. The results are compared to the analytic ones obtained from the Friedmann equations of a flat universe with cosmolog-

---

[7]Actually, one can also consider the use of constantly curved building blocks to discretize spacetime as in [106, 107]
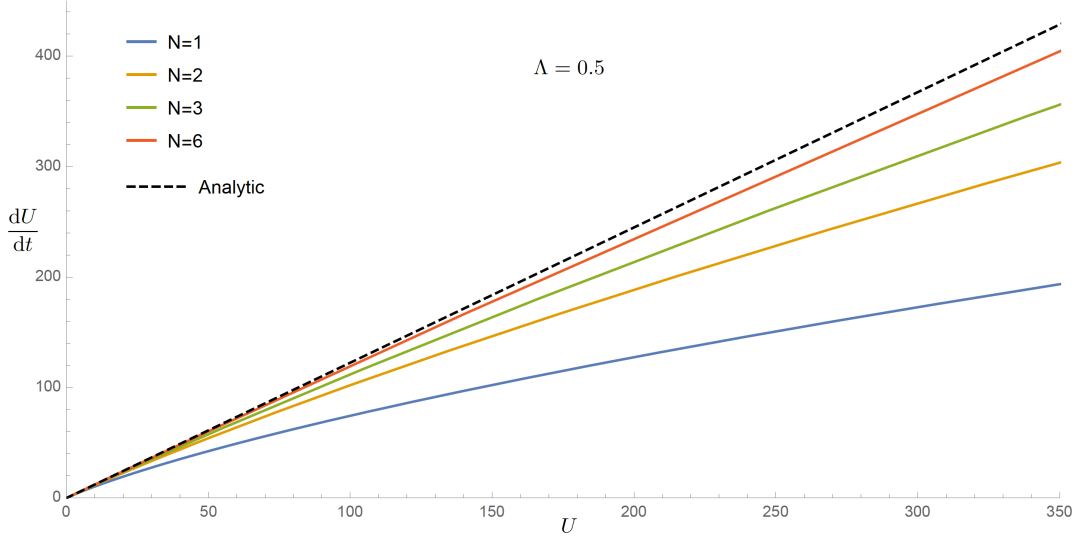
Figure 5.10:   Flat universe with cosmological constant $\Lambda = 0.5$, as approximated by the hyperfrustal evolution with N^3 cubes.

ical constant i.e.,

$$U_{\text{analytic}} = a^3 = e^{\sqrt{3\Lambda}t}, \qquad \frac{dU_{\text{analytic}}}{dt} = \sqrt{3\Lambda}\, e^{\sqrt{3\Lambda}t}. \qquad (5.50)$$

In many models which make use of the CW formalism the Cauchy surfaces analyzed are 3-spheres triangulated by using *regular* tetrahedra. Therefore the universe examined is a closed one. However a 3-sphere can be triangulated by using only 5, 16 or 600 regular tetrahedra (see for example [108]), thus there exists a geometric constraint which prevents from approaching the analytic limit at will. The advantage of the model studied in this article is that a flat 3-torus can be tessellated by an arbitrarily high number of cubes and there is no theoretical limit to the refinement steps that one can take to show the convergence to the analytic results.

Another way to solve the Hamiltonian constraint is by studying the limit in which the deficit angle at the hinges is small, corresponding to a slow (measured in Planck times) expansion or contraction of the universe. In fact, only in this regime the discrete lattice of Regge calculus approximates the continuous smooth manifold of general relativity [49]. In our case such limit is made explicit by the requirement

$$\Theta_W = \frac{\pi}{2} + \eta, \qquad |\eta| \ll 1. \qquad (5.51)$$

Intuitively this condition indicates that the boundary frusta f_n in figure 5.8 present a small deviation from a cuboidal geometry. Substituting the above

expression into equation (5.46) and taking the limit $\eta \to 0$ we find at the leading order of η and j'^2, that

$$\eta = \frac{j'^2}{16j}. \tag{5.52}$$

Let us come back to the Hamiltonian constraint (5.47) and substitute the angle (5.52). We get

$$j^2 = \frac{9}{\Lambda^2}\,(-4\eta)^2 = \frac{9}{\Lambda^2}\,16\left(\frac{j'^2}{16j}\right)^2 \tag{5.53}$$

Finally, from the definition of the scale factor $a = \sqrt{j}$ we obtain the first Friedmann equation for a flat Λ-FLRW universe

$$a'^2 = \frac{\Lambda}{3}a^2. \tag{5.54}$$

The second Friedmann equation is simply given by the time derivative of the first and reads

$$a'' = \frac{\Lambda}{3}a. \tag{5.55}$$

Let us note that this is consistent with the fact that the evolution equation is the derivative of the Hamiltonian constraint in (5.42). In fact, one can check that the second Friedmann equation can also be derived from the evolution equation using the same arguments just presented.

5.3.4 Flat FLRW universe with dust

Let us place a test particle of mass M at the center of each cube c_n in the chain (5.8). Classically, the motion of a point particle in a gravitational field is found by applying the variational principle to the following action

$$S_M = -M \int \mathrm{d}s, \tag{5.56}$$

being $\mathrm{d}s$ the line element. We define the discrete analogue of the line element as the length s_n of the trajectory joining the centers of the cubes c_n and c_{n+1}. In fact the choice of placing the test particle at the center of the cubes guarantees that it is comoving and travels along geodesics [101]. Thus in our case the discrete line element is given by the time step (5.25) i.e., $s_n = H_n$ (remember that we are working in Euclidean signature). More general settings have been studied on a simplicial discretization of a closed universe. For example, in [101] it has been shown that the Hamiltonian constraint depends on the particle position inside the tetrahedra.

In order to describe a universe in which more than one dust particle is present, one can refine the lattice as in 5.9 and distribute N^3 particles, each of mass M/N^3, over the initial cubes, such that one particle sits at the center of each cube. The full action $S_R = S_R(\{j_n\}, \{k_n\}, M)$ becomes

$$S_R = \frac{N^3}{8\pi} \sum_n \left(\frac{3}{2}(j_n - j_{n+1})\delta_n^{(j)} + 3k_n\delta_n^{(k)} \right) - M\sum_n H_n, \qquad (5.57)$$

where we have rehabilitated the factor $1/8\pi$ in front of the Regge action[8] and we are working in Plank units $c = G = 1$. The new Regge equations are

$$\begin{aligned}
\frac{\partial S_R}{\partial k_n} &= \frac{3N^3}{8\pi}\, \delta_n^{(k)} - M\frac{\partial H_n}{\partial k_n} = 0, \\
\frac{\partial S_R}{\partial j_n} &= \frac{3N^3}{16\pi}\left(\delta_n^{(j)} - \delta_{n-1}^{(j)} \right) - M\left(\frac{\partial H_n}{\partial j_n} + \frac{\partial H_{n-1}}{\partial j_n} \right) = 0.
\end{aligned} \qquad (5.58)$$

Performing the continuum time limit and the Wick rotation we get the Hamiltonian constraint and the evolution equation

$$\begin{aligned}
2\pi - 4\arccos\frac{j'^2}{j'^2 - 16j} &= \frac{8\pi M}{3N^3}\frac{1}{\sqrt{j}}\sqrt{1 - \frac{j'^2}{8j}}, \\
\frac{2jj'' - j'^2}{j'^2 - 16j} &= -\frac{\pi M}{3N^3}\frac{1}{\sqrt{j}}\left(1 - \frac{j'^2}{4j} + \frac{j''}{4} \right).
\end{aligned} \qquad (5.59)$$

Once again, it is easy to check that the second equation is the time derivative of the first. Substituting equation (5.46) in the Hamiltonian constraint and applying the Wick rotation one gets

$$\dot{j} = \left(\frac{8\pi M}{3N^3} \right)^2 \frac{1 + \cos\Theta_W}{1 - \cos\Theta_W}\frac{1}{(2\pi - 4\Theta_W)^2}, \qquad (5.60)$$

where the Wick-rotated angle Θ_W is given in (5.44). From the above equation we can write the set of parametric equations describing the volume of the universe and its time variation

$$U = N^3 j^{\frac{3}{2}}, \qquad \frac{dU}{dt} = 6N^3 j\sqrt{\frac{-\cos\Theta_W}{1 - \cos\Theta_W}}. \qquad (5.61)$$

---

[8]In the previous cases the factor $1/8\pi$ does not contribute to the dynamics since it factorizes in the action.
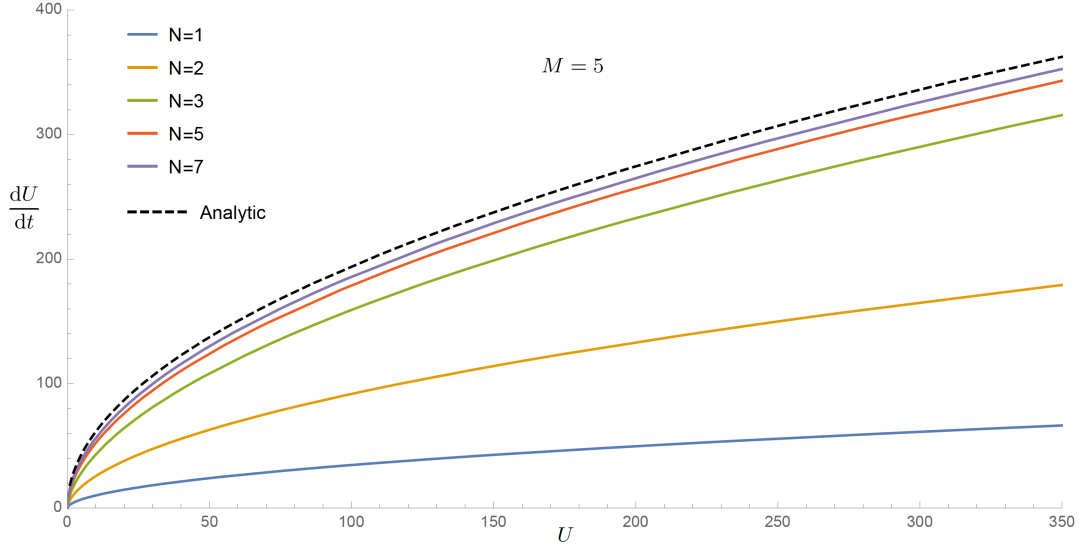
Figure 5.11: Evolution of flat universe filled with dust of mass M, with space approximated by N^3 cubes.

The Friedmann equations describing the evolution of the scale factor $a(t)$ in a flat space and in presence of dust are

$$\frac{\dot{a}^2}{a^2} = \frac{8\pi}{3}\rho,$$
$$\frac{\ddot{a}}{a} = -\frac{4\pi}{3}\rho,$$

being $\rho = M/a^{\frac{3}{2}}$ the density of the universe. Using the same arguments that we applied in the cosmological constant case, one can check that the above equations can in fact be obtained as the small deficit angle limit of the Hamiltonian constraint and the evolution equation. Their solution is

$$a(t) = (6\pi M)^{\frac{1}{3}} t^{\frac{2}{3}}, \tag{5.62}$$

thus the analytic expression for the volume of the universe and its time variation are

$$U_{\text{analytic}} = a^3 = 6\pi M t^2, \qquad \frac{dU_{\text{analytic}}}{dt} = 12\pi M t.$$

For some value of the mass M we can plot the numerical result (5.60),(5.61) to find that the model converges quite rapidly to the analytic curve (see figure 5.11).

5.4   Summary and dimensional analysis

In this summary section the dependence on G Newton of the asymptotic formulas derived in the first sections of this chapter is made explicit. Thus, the physical dimensions of areas, volumes, and cosmological constant are restored. We work in units in which $\hbar = 1$, so $[G] = \ell_{\text{Planck}}^2$ has the dimension of an area. As we have shown in Chapter 4, the deformation of the vertex amplitude depends on an additional parameter ω. In the asymptotic formula this parameter appears in the action in front of the dimensionless volume term (see (4.58)), i.e. the volume expressed in terms of spins. Thus ω is dimensionless and related to the cosmological constant via $\omega \sim \Lambda G$ so that one gets the correct dimension $[\Lambda] = 1/\ell_{\text{Planck}}^2$. The spins variables j are instead related to areas by $A = Gj$. In order to keep in line with the majority of the literature, we will, from now on, substitute $Gj \to j$, and also change the corresponding notations. In other words we are giving the spins a physical dimension of areas i.e., $[j] = \ell_{\text{Planck}}^2$. For example, expressing equation (5.40) in terms of the functions (5.12) we can write the physical 4d volume of a hyperfrustum as

$$V = k_n^2 \, K \, (Q - 2), \tag{5.63}$$

and it has already the right dimensions $[V] = \ell_{\text{Planck}}^4$. Also the Regge action S_R in equation (5.19) is now expressed in terms of areas.

Finally, summing up all the contributions of the hyperfrustum amplitudes (5.8), (5.11) and (5.17) and arranging the determinant of the Hessian (5.18) as $D = |D| \exp(i\varphi)$ we can write the dressed vertex amplitude (5.20) with the correct dimensions as

$$\widehat{\mathcal{A}}_v \sim \frac{(j_n j_{n+1})^{3\alpha - \frac{3}{2}} k_n^{6(\alpha-1)}}{B} \Big(\cos(\frac{S_R}{G} + \varphi) + \cos(\frac{\gamma S_R}{G} - \frac{\Lambda}{G}V) \Big), \tag{5.64}$$

being

$$B = \frac{|D|}{(1 + K^2)^3 \, (1 + K^2 - 2Q)^6}.$$

The partition function (4.12) can be written in the compact form (5.21).

In the next sections we use the fact that in the large spin limit the sum over the spins is well approximated by an integral $\sum_j \to \int \mathrm{d}j$ so that we can numerically integrate observables $\mathcal{O}$ weighted with the dressed vertex amplitude (5.64) and thus evaluate their expectation values

$$\langle \mathcal{O} \rangle = \frac{\int \mathrm{d}j_f \mathcal{O} \prod_v \widehat{\mathcal{A}}_v}{\int \mathrm{d}j_f \prod_v \widehat{\mathcal{A}}_v}. \tag{5.65}$$

Again notice that, strictly speaking, one is actually integrating over areas A rather than spins j. We also recall that the determinant D is a homogeneous

function of the spins, thus the overall integration measure acquires additional powers of G as a factor, which do not play a role in the path integral nor in expectation values of observables. Eventually the state sum will depend on the three parameters α, G and Λ as they appear in (5.64).

Chapter 6

Renormalization of Spin Foam Models

6.1 Background independent renormalization

Renormalization in this work is understood in the Wilsonian sense [109]. A theory with infinitely many degrees of freedom can be formulated in terms of effective theories on only part of those degrees of freedom. This effective theory then depends on the scale, usually by scale-dependent parameters called coupling constants. In perturbative QFT for example, the cut of degrees of freedom introduces an energy scale μ which interpolates between the IR and the UV regimes.

$$\text{IR} \xleftrightarrow{\mu} \text{UV}$$

In lattice gauge theories a scale $g(a)$ is instead defined by the lattice spacing a.
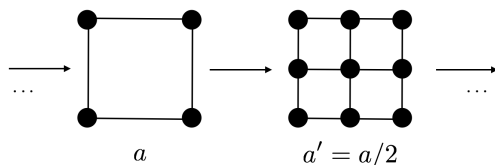
These are all examples of background dependent theories. On the contrary, in the background independent setting of spin foam models, lengths or energy are encoded in the variables, not in any background structure. This prevents the use of e.g. a fixed lattice spacing to characterize the scale, and requires one to generalize the well-established renormalization group methods from e.g. lattice gauge theory. This has been achieved in recent years [110, 111, 112, 58, 59, 38, 113], and has led to a version of the RG flow in which space-time discretization

itself is regarded as scale.[1] Hence the scale is taken to be the 2-complex $\mathcal{K}$ itself, or equivalently the set of graphs $\{\Gamma_i\}$ in the boundary of its vertices.
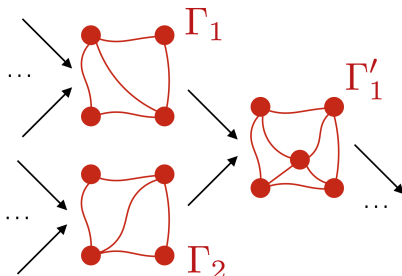
The regularization is understood as restricting the theory to only finitely many holonomies, i.e. those which are associated to $\{\Gamma_i\}$. On a technical level, this makes the RG flow procedure very similar to those employed e.g. in tensor network renormalization [114, 115], see also e.g. [116]. Of course, this begs the question how the results of this article compare to ones obtained in similar approaches, such as quantum Regge calculus, see e.g. [117, 118, 119], or causal dynamical triangulations [120]. We refer to the discussion in [81], although this is still an open question at this point.

In the background independent framework for renormalization we employ, the spin foam sum (4.12), is understood as an effective theory for the available degrees of freedom provided by the 2-complex. It can be seen as the result of integrating out all of the finer degrees of freedom, which are below the lattice resolution. The lattice itself, then, can be regarded as the result of successive coarse graining of a much finer lattice.

The question, then, is how the theories on different lattices, i.e. on different scales, are related. Mathematically, the amplitudes are given in terms of linear maps on the boundary graphs Γ of vertices (5.22). However, several of them together can be made to a linear map onto a larger lattice, with refined boundary graph Γ'. This allows to rewrite the RG flow of bulk lattices into equations for boundary amplitudes. See also [113].

To relate the amplitudes on the original vertex, and the new effective one, one needs an identification of degrees of freedom. This can be realized by a projection of configuration spaces, or injection of boundary Hilbert spaces [2] [3]

---

[1]Note that on a fixed geometry, refinement of the lattice is equivalent to shrinking of lattice length, while in the background independent setting of spin foam models, only the former can be defined, since the lattice spacing is a variable to be summed over in the path integral.

[2]For a definition of the partial Hilbert spaces $\mathcal{H}_\Gamma$ see section 3.1 and the subsection 3.1.2 therein.

[3]Notice that a similar embedding map was defined in (3.12) when we introduced the canonical formalism of LQG. Such an embedding map was acting at the kinematical level and was not tied to a dynamics. However, when refining a theory with a dynamics i.e., involving time evolution, the embedding maps should be able to separate among the mathematical refinement of a state and its

[4]

$$\iota_{\Gamma\Gamma'} : \; \mathcal{H}_\Gamma \longrightarrow \; \mathcal{H}_{\Gamma'}$$
$$\psi_\Gamma \longmapsto \; \psi_{\Gamma'} = \iota_{\Gamma\Gamma'}\psi_\Gamma, \tag{6.1}$$

$$\psi_\Gamma \qquad\qquad \psi_{\Gamma'}$$
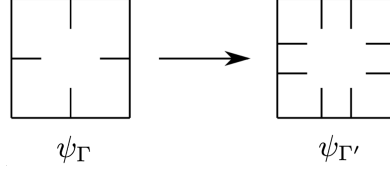
such that $\iota_{\Gamma\Gamma} = \mathrm{Id}$ and $\iota_{\Gamma'\Gamma''} \circ \iota_{\Gamma\Gamma'} = \iota_{\Gamma\Gamma''}$. for $\Gamma \le \Gamma' \le \Gamma''$.

If the state sum (4.12) on the coarse lattice Γ is defined by a total amplitude $\mathcal{A}_\Gamma : \mathcal{H}_\Gamma \longrightarrow \mathbb{C}$, then on the fine boundary Γ' the dynamics is specified by a fine amplitude $\mathcal{A}_{\Gamma'} : \mathcal{H}_{\Gamma'} \to \mathbb{C}$. We make the ansatz for the fine amplitude to be of the EPRL-FK type, i.e. a local expression over the vertices (5.21) which gives a fine amplitude

$$\mathcal{A}_{\Gamma'}(\psi_{\Gamma', j_\ell, \iota_n}) := \sum_{j'_f, \iota'_e} \prod_v \widehat{\mathcal{A}}_v, \tag{6.2}$$

where the sum ranges over all bulk spins and intertwiners j'_f, ι'_e of the fine lattice, while the boundary spins and intertwiners j_ℓ, ι_n ($\forall \ell \subset f$ and $n \subset e$) are kept fixed. Let us notice that the overall boundary geometry is the same in the coarse and in the fine settings i.e., we are basically describing the same physical process but with more or less degrees 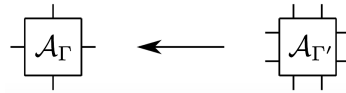of freedom. The amplitude $\mathcal{A}_{\Gamma'}$ contains all information of the fine theory, represented as amplitude on the fine boundary. Then we want to compare the amplitudes $\mathcal{A}_{\Gamma'}(\psi_{\Gamma'})$ and $\mathcal{A}_\Gamma(\psi_\Gamma)$

Here the amplitude operators are represented with outgoing lines to be imagined as plugs which can be inserted in the appropriate sockets (defined by the ingoing lines) in equation (6.1). To do so we relate the fine amplitude to the coarse boundary via the embedding map as

$$\mathcal{A}_{\Gamma'}(\psi_{\Gamma'}) = \mathcal{A}_{\Gamma'}\iota_{\Gamma\Gamma'}(\psi_\Gamma) \equiv \mathcal{A}_\Gamma^{\mathrm{R}}(\psi_\Gamma) \tag{6.3}$$

time evolution. Using a quite cheap example, in Figure 3.3 the graph $\Gamma_{\mathcal{K},\mathrm{B}}$ could be thought as a refinement of $\Gamma_{\mathcal{K},\mathrm{A}}$, while it actually corresponds to its time evolution. Understanding the role of dynamical embedding maps is of pivotal importance. We will come back to this topic in the following.

[4]In what follows we adopt a schematic representation of the equations in order to help the visualization of the general reasoning.

where we have defined the renormalized amplitude $\mathcal{A}_\Gamma^{\mathrm{R}} : \mathcal{H}_\Gamma \to \mathbb{C}$. The renormalization group flow equation is then defined on the amplitudes by requiring

$$\mathcal{A}_\Gamma \overset{!}{=} \mathcal{A}_\Gamma^{\mathrm{R}} \tag{6.4}$$

Notice that, even though these amplitudes describe a transition on the same boundary geometry, they do not necessarily coincide since $\mathcal{A}_\Gamma^{\mathrm{R}}$ is defined from the richer information of the fine graph Γ'. Practically, in order to satisfy (6.4) one has to carefully tune the parameters of the theory defined on the fine lattice. This is the essence of the concept of "running coupling" in the RG flow.

Mathematically, equation (6.4) is the notion of cylindrical consistency, which is required to define the continuum limit.[5] Notably, assume one has solved the RG flow equations along all lattices, i.e. one has a collection of amplitudes $\{\mathcal{A}_\Gamma\}_\Gamma$ which satisfy cylindrical consistency:

$$\mathcal{A}_\Gamma = \mathcal{A}_{\Gamma'} \, \iota_{\Gamma\Gamma'}. \tag{6.5}$$

for all $\Gamma \leq \Gamma'$, i.e. whenever Γ arises as a refinement of Γ'. Then, this is a necessary condition that the continuum amplitude $\mathcal{A}_\infty : \mathcal{H}_\infty \to \mathbb{C}$ can be defined on the continuum Hilbert space

$$\mathcal{H}_\infty := \lim_{\Gamma \to \infty} \mathcal{H}_\Gamma, \tag{6.6}$$

which is the inductive limit of all the $\mathcal{H}_\Gamma$. See [58] for details.

This shows a nice interplay between mathematical concepts and physical intuition. The notion of scale is here played by the choices of lattices, and their relation to one another, which provides a hierarchy among the degrees of freedom. Once again note that, even though in our case the lattices are regular hypercubic ones, there are no lengths or other geometric properties assigned to them. Rather, the sum (6.2) ranges over different geometries *of the same lattice*.

---

[5] This should not be confused with the notion of cylindrical consistency of Chapter 3, employed in the construction of the Ashtekar-Lewandowski vacuum in loop quantum gravity, which is entirely kinematical (see e.g. [121], and the discussions in [111, 58, 38, 113]).

6.1.1 Observables

In this context, using the notation from section 3.1, an observable $\mathcal{O} : \overline{\mathcal{U}} \to \mathbb{C}$ is a continuous function acting on the generalized connections (3.3). In order to be adaptable to a graph structure Γ, we require it to be cylindrical over such graph i.e., we demand the existence of a continuous function $\mathcal{O}_\Gamma : \mathcal{U}_\Gamma \to \mathbb{C}$, which in the projective limit of infinite refinement corresponds to the continuous function $\mathcal{O}$. In other words, using the projector $\Pi_\Gamma : \overline{\mathcal{U}} \to \mathcal{U}_\Gamma$ defined in (3.4), we can write

$$\mathcal{O} = \mathcal{O}_\Gamma \Pi_\Gamma. \tag{6.7}$$

The expectation value of such observable, weighted by some amplitude function $\mathcal{A}_\infty$ (which is also cylindrical over Γ and Γ'), is defined as

$$\langle \mathcal{O} \rangle = \int \mathrm{d}\mu_{AL} \mathcal{O} \mathcal{A}_\infty = \int \mathrm{d}\mu_\Gamma \mathcal{O}_\Gamma \mathcal{A}_\Gamma = \langle \mathcal{O}_\Gamma \rangle_\Gamma, \tag{6.8}$$

where $\mathrm{d}\mu_{AL}$ and $\mathrm{d}\mu_\Gamma$ are respectively the Ashtekar-Lewandowski measure and the partial measure defined in (3.10) and at the end of subsection 3.1.2.

Notice that, whenever $\mathcal{O}$ is cylindrical over Γ, then it is automatically cylindrical over all $\Gamma' \geq \Gamma$, since

$$\mathcal{O} = \mathcal{O}_\Gamma \Pi_\Gamma = (\mathcal{O}_\Gamma \pi_{\Gamma'\Gamma})\Pi_{\Gamma'} = \mathcal{O}_{\Gamma'}\Pi_{\Gamma'}, \tag{6.9}$$

where we used the projector (3.1) and its properties listed in Chapter 3.

The RG flow equation (6.5) can be rephrased as a condition on the expectation values of observables

$$\langle \mathcal{O}_\Gamma \rangle_\Gamma \;=\; \langle \mathcal{O}_{\Gamma'} \rangle_{\Gamma'}. \tag{6.10}$$

6.1.2 On embedding maps

It should be noted that the coarse graining prescription depends on the way in which degrees of freedom are represented, and identified along different scales. In particular, the embedding map $\iota_{\Gamma\Gamma'}$ depends on these choices, which are not unique. For instance, any family of unitary operators U_Γ on $\mathcal{H}_\Gamma$ lead to an equivalent theory with

$$\tilde{\mathcal{A}}_\Gamma \;\; := \;\; \mathcal{A}_\Gamma U_\Gamma,$$
$$\tilde{\iota}_{\Gamma\Gamma'} \;\; := \;\; U_{\Gamma'}^{-1} \iota_{\Gamma\Gamma'} U_\Gamma.$$

However, the freedom one has in this choice is much larger than this. The precise definition of $\iota_{\Gamma\Gamma'}$ can make the actual problem of solving (6.5) harder

or easier. In particular, there are, in general, some choices which can work well – or not so well – in conjunction with certain approximation methods.

In [58], it is argued that the most beneficial way would be to use dynamical embedding maps, which in and of themselves already contain all the information of the dynamics of the theory. The reason for this is that one can interpret the embedding maps $\iota_{\Gamma\Gamma'}$ as ways to identify and add degrees of freedom under refinement. Then (6.5) suggests that refining should be done with respect to the dynamics encoded in the amplitude $\mathcal{A}_\Gamma$, i.e. degrees of freedom should be added in the dynamical vacuum state. This is a highly non-trivial condition on both $\mathcal{A}_\Gamma$ and $\iota_{\Gamma\Gamma'}$. A real-space coarse graining algorithm, called tensor network renormalization [115, 114, 122], aims exactly at implementing such a scheme: the partition function of the system is rewritten as the contraction of a (local) network of tensors, which does not refer to a background and does not require a notion of scale. This network is coarse grained by defining effective coarse degrees of freedom from fine ones and ordering them by dynamical relevance. Thus these variable transformations, given by the dynamics, are the inverse of embedding maps. To keep this algorithm numerically feasible, one usually has to truncate the maximum number of degrees of freedom kept in each iteration. In quantum gravity, this algorithm has been successfully applied to 2D analogue spin foam models for finite [116, 123] and quantum groups [124, 125, 126] and 3D lattice gauge theories [127, 126]. One of its main advantages is the applicability to oscillating amplitudes and fermionic systems [128]. However a main disadvantage is the exponential growth in numerical cost with growing number of degrees of freedom, which has prohibited a direct application to 4D spin foam models.

When using the physical embedding maps, the continuum Hilbert space is equivalent to the physical Hilbert space, in which time translation becomes trivial, i.e. scattering matrix elements are simply computed taking the inner product between in- and out-states.

Since we do not have the physical embedding maps at our disposal (indeed they would have to be found by solving the RG flow equations), we instead use an ad hoc choice for embedding maps, which identify (kinematical) geometric quantities among different scales, such as spins. The degrees of freedom here are added by $\iota_{\Gamma\Gamma'}$ in such a way that e.g. fine areas add up to coarse areas. This condition is translated to a condition on the coupling of fine spins to coarse spins. Details can be found in [80].

6.2 Approximations

In order to solve the RG flow equation (6.10) we adopt a number of approximations

6.2.1 1st approximation: Reduced state sum

The partition function (4.12) is hardly usable to carry out predictions about transition probabilities and expectation values of observables. This fact has roots in the complexity of its expression which involves a sum over all the possible geometric configurations $\{j_f, \iota_e\}$. To overcome this issue we can restrict the state sum to a subset of symmetric configurations. A setting which has recently been proven successful in delivery the RG flow, consists of a discretization in terms of hypercuboids [81, 79, 80]. Using a set of approximations similar to the one described in this section, the highly symmetric hypercuboidal configuration allowed the evaluation of the RG flow of the parameter α appearing in the face amplitude (4.13). Also, the detection of a UV-attractive fixed point α_c showed an indication of invariance of the model under refinement. While opening the way to the numerical study of the continuum limit of restricted spin foams, the hypercuboid model stands on a severe restriction of d.o.f. which does not allow for curvature. The curvature is in fact vanishing everywhere and thus the theory is independent of other interesting parameters such as Newton's constant G and the cosmological constant Λ. This justifies the introduction of discrete structures able to support a basic concept of curvature and still simple enough to allow the exploration of the renormalization properties. The symmetric configurations studied in Chapter 5 and firstly introduced in the original work [42], provide such a working basis. To recap, they define a discretization of spacetime in which only a limited number of spins j_f is required to keep track of the geometric degrees of freedom, while all the intertwiners ι_e are confined into the shape of a *quantum frustum*. The typical grain of spacetime, defining the spin foam vertex, is the so called *hyperfrustum* F_n i.e., the four dimensional generalization of a truncated regular square pyramid. In the limit of large refinements, this 'pyramidal' discretization provides a natural description of a foliated manifold $\mathcal{M} = \Sigma \times \mathbb{R}$ in which the spatial hypersurfaces $\Sigma \sim T^3$ have the topology of a 3-torus, are flat, isotropic and homogeneous and can grow or contract at successive times.

6.2.2 2nd Approximation: Semiclassical limit

In the large spin limit the EPRL-FK vertex amplitude (4.11) has been proven to be connected to discrete GR, when built on a simplicial discretization [73]. This result was confirmed in [41] and [42] by a saddle point approximation of the reduced amplitude. In particular, as we have shown in Chapter 5, unlike the case of a general simplicial decomposition, the thinning of the state sum leads to an explicit asymptotic expression of the vertex amplitude as a function of the spins (5.64). This allows us to numerically evaluate the expectation values (5.65) for some geometric observables $\mathcal{O}_\Gamma$ on a given boundary graph Γ. Although the error one makes by replacing the amplitude with its

large-j-asymptotic expression is hard to estimate, it can be expected that the approximation is quite good already for small values of the spins [129, 42]. Since for large parts of the phase space the multi-vertex-amplitude appears to be suppressed for small spins [81], the error might in fact not be that large. Still, this point warrants further study.

6.2.3   3rd Approximation: Projection of the RG flow

In general, the cylindrical consistency equations (6.10) are very hard to solve, even though we restrict ourselves to specific lattices[6]. To simplify matters, one can instead consider amplitudes $\mathcal{A}_\Gamma^{(g_i)}$ on Γ, which are given in terms of few parameters g_i, called coupling constants. One then attempts to rewrite the flow of amplitudes in terms of a flow of coupling constants

$$g_i \;\longrightarrow\; g_i' \,. \tag{6.11}$$

The question whether a parametrization in terms of few coupling constants is feasible, depends on its renormalizability, i.e. on whether the effect of the integrated out degrees of freedom in (6.3) can be absorbed by a shift in the g_i. Whether quantum gravity is renormalizable or not, is still an open question. While it is often argued that the perturbative formulation is not [130], there are hints that there might exist a non-Gaussian fixed point, around which the flow might be renormalizable [131].

We have to leave this question open for now. To be able make computations, however, we truncate the flow to only finitely many parameters. That is, we make an ansatz for $\mathcal{A}_\Gamma = \mathcal{A}_\Gamma^{(g_i)}$ in terms of the EPRL-FK model described in Chapter 4. The asymptotic formulas are in (5.64), and the model has three free parameters

$$\{g_i\} \;=\; \{\alpha,\, G,\, \Lambda\}, \tag{6.12}$$

i.e. the parameter defined in the face amplitude (4.13), as well as Newton's constant G and the cosmological constant Λ. We specifically do not choose the Barbero-Immirzi parameter γ as a running coupling, since its connection to the allowed spins is rather pathological in the Euclidean EPRL-FK model. The precise range of allowed spins j_f sensitively depends on γ, by the condition that $j_f^\pm$ given by (4.6) are half-integers. In particular, changing γ by a tiny amount can make huge changes in the range. In particular, the chosen boundary data which works for one γ might not be allowed for another, which would spoil the RG flow equations. To avoid this complication, we fix the value to

$$\gamma \;=\; \frac{1}{2}. \tag{6.13}$$

---

[6]See [38] for the treatment of a case allowing for all possible lattices at the same time. In that case, there are uncountably many RG flow equations to solve.

Since the same pathology does not appear in the Lorentzian signature model, we surmise that, in that case, it would be prudent to also choose γ as a running coupling.

The projection of the flow will be achieved by requiring that the amplitudes $\mathcal{A}_\Gamma$ and $\mathcal{A}_{\Gamma'}$ weighting the expectation values (6.10) are of the EPRL-FK type (5.64).

6.2.4 4th Approximation: Numerical working point

If we truncate the theory space to amplitudes given in terms of few coupling constants g_i, we cannot expect (6.10) to hold for all observables any more exactly. Instead, we will only demand it to hold approximately, for a subset of all observables. In particular, we choose a finite set of observables $O_\Gamma^{(i)}$ (in general, as many as the number of coupling constants that are allowed to run), which we call *reference observables*, and demand that the error

$$\Delta_{\Gamma,\Gamma'}^{g,g'} := \sum_i \left| \langle \mathcal{O}_\Gamma^{(i)} \rangle_\Gamma^g - \langle \mathcal{O}_{\Gamma'}^{(i)} \rangle_{\Gamma'}^{g'} \right|^2, \tag{6.14}$$

is minimal[7]. This truncation of the RG flow obviously depends on the choice of observables, and a good flow requires that one finds observables which capture the dynamics of enough interesting degrees of freedom.

In this work, we choose a specific set of observables, depending on the situation we are in. We will describe these in more detail in the next chapter. In particular, we will, in some instances, truncate the flow further and keep some of the parameters in (6.12) fixed. Depending on which and how many, the choice for reference observables will be adapted.

6.2.5 Resolution algorithm

In order to deal with the resolution of the RG flow in the reduced setting, we developed in [83] a novel resolution strategy which eventually has been proven successful.

Let us choose a quantum gravity model which can be described by the EPRL-FK partition function on a coarse graph Γ or on a finer one Γ'. Also, suppose that we explicitly know the asymptotic expression of the respective amplitudes. Call $\{j\}$ and $\{j'\}$ the respective sets of free variables in the two systems. Then, we evaluate expectation values of i observables $\mathcal{O}^{(i)}$ by numer-

---

[7]To simplify notation we refer to all parameters by $g = (\alpha, G, \Lambda)$ and drop the subscript i.

ically integrating over these variables

$$\langle \mathcal{O}_\Gamma^{(i)} \rangle_\Gamma^g = \frac{1}{Z_\Gamma} \int \mathrm{d}j \; \mathcal{O}_\Gamma^{(i)} \; \mathcal{A}_\Gamma,$$
$$\langle \mathcal{O}_{\Gamma'}^{(i)} \rangle_{\Gamma'}^{g'} = \frac{1}{Z_{\Gamma'}} \int \mathrm{d}j' \; \mathcal{O}_{\Gamma'}^{(i)} \; \mathcal{A}_{\Gamma'}, \tag{6.15}$$

where g and g' are sets of parameters defining the theory. Observables should be cylindrically consistent, written as:

$$\langle \mathcal{O}_\Gamma^{(i)} \rangle_\Gamma^g = \langle \mathcal{O}_{\Gamma'}^{(i)} \rangle_{\Gamma'}^{g'} \qquad \forall n. \tag{6.16}$$

This defines the RG flow equation for our model. In fact, if one can solve it, for any point g' the equation returns a point g and we can connect them with an arrow $\mathrm{A}^{g' \to g}$ to draw the flow in the parameter space [8]. The existence of an exact solution to equation (6.16) depends on many factors. We already discussed the relevance of the choice of Γ and Γ' as well as the various approximations that may spoil the solution. A further technical obstacle is represented by the fact that the solution of (6.16) would require the knowledge of the values $\langle \mathcal{O}_\Gamma^{(i)} \rangle_\Gamma$ and $\langle \mathcal{O}_{\Gamma'}^{(i)} \rangle_{\Gamma'}$ in all the points of the parameter space. However, in our case these observables are evaluated numerically for every couple (g, g'). Therefore we must consider a finite number of points in the parameter space in order to perform a finite number of integrations. The solution of the flow equation is then approximated whereas for a point g' we cannot access all the points in its neighbor with infinite accuracy and, consequently, the point g cannot be defined exactly. In the light of this observations we impose the cylindrical consistency condition in (6.14) in the weak form

$$\Delta_{\Gamma,\Gamma'}^{g,g'} \overset{!}{=} \min. \tag{6.17}$$

Our plan consists in considering an adequate number of points in a 'large' region of the parameter space, draw the flow accordingly to the weak cylindrical consistency condition (6.17) and finally, for each arrow $\mathrm{A}^{g' \to g}$, check how small is the relative error

$$R_{\Gamma,\Gamma'}^{g,g'} \equiv \frac{\Delta_{\Gamma,\Gamma'}^{g,g'}}{\overline{\mathcal{O}}_{\Gamma,\Gamma'}^{g,g'}}, \tag{6.18}$$

---

[8]In analogy with the RG flows generated in the Asymptotic Safety scheme, where the arrows point from high to low energy, here the arrows start at g' associated to the fine observables, and point at g which is related to coarse observables. We recall that, in our context of background independent renormalization, there are no continuous labels tracing the energy scale. Instead, the shift of resolution happens in discrete steps and is associated to a change of discretization. This also equates to a change in the number of degrees of freedom that we keep when describing a physical process. Thus, in a 'Wilsonian' sense, the refinement of a discretization can be interpreted as a shift towards high energy regimes.

being

$$\overline{\mathcal{O}}^{g,g'}_{\Gamma,\Gamma'} \equiv \sum_i \left| \frac{\langle \mathcal{O}^{(i)}_\Gamma \rangle^g_\Gamma + \langle \mathcal{O}^{(i)}_{\Gamma'} \rangle^{g'}_{\Gamma'}}{2} \right|. \tag{6.19}$$

Eventually we will aim for an improved accuracy by zooming further into some regions of the parameter space where the arrows show the lowest relative errors and an overall 'interesting behavior'. During our analysis we encountered many regions of the parameter space where the cylindrical consistency condition is in fact violated and the RG flow cannot be trust. We concentrate on those regions where the error is small, and cylindrical consistency is satisfied up to only small errors.

6.3   Renormalization of reduced spin foam model

We are finally ready to apply the renormalization techniques introduced in the first part of this chapter to the asymptotic limit of the deformed and symmetry reduced Euclidean EPRL-FK model studied in Chapter 5. Refer to the summary section 5.4 for the important formulas. In what follows we are going to use these results to define and numerically solve the RG flow equation (6.17).

At this point, it is worthwhile to recap which degrees of freedom we are summing over when evaluating the expectation values of observables (6.15). Originally, the spin foam model depends on spins j and intertwiners ι. The truncation leaves us with a subset of variables j_n and k_n of spins (i.e. areas), which are assigned to space-like and time-like faces in the 4d lattice, where the first ones describe the geometry of the isotropic and homogeneous space-like Cauchy-surfaces, while the latter describe the transitions between hypersurfaces, i.e. time-steps.[9]

By going over to continuous areas, and because of the equivalence to length variables, this describes essentially a subsector of the state space of quantum Regge calculus. There are a few differences though: Firstly, the factor coming from the Hessian of the asymptotic formula induces a different measure. Secondly, the amplitude is not of the form $\exp(-S)$, but rather (5.64), i.e. $\cos(\tilde{S}) + \cos(S)$.

Also, it should be noted that the RG flow is defined slightly differently here, since we do not introduce a correlation length, but use, as ordering parameter, a different observable, usually certain volume fluctuations. These will be described in more detail in the following section. How to define a correlation length, other than in the pure combinatorial sense, is not obvious, but intriguing to explore in future research.

---

[9]Remember though, that the choice of time-direction is somewhat arbitrary at this point, since we deal with Riemannian geometries in this article.

In principle, the integral over degrees of freedom is unbounded, which could lead to divergences of the integral in the limit of large spins $j, k \to \infty$. However, depending on the value of the coupling constant α appearing in (5.64), the integrand goes to zero sufficiently fast in that limit, so the integral stays finite. This has been discussed for hypercuboids in [81], and a similar calculation is true for the frustum case, which we consider in this work. In particular, we only consider a flow of α well inside the region in which the large-j-region is not a problem.

The Hessian matrix which occurs in the measure factor of the path integral goes to zero in the limit of vanishing spins, which might a priori lead to divergences in the $j, k \to 0$ region as well. However, this is an artifact of the asymptotic formula, which does not hold for the small spin case. Indeed, the actual amplitude stays finite in that region, where the integral would have to be replaced by the sum anyway. Indeed, our numerical investigations show that there is usually only a very small region around $j, k \approx 0$ in which the amplitude diverges. Figure (6.4) is an example for this behavior, in which we find that the integrand itself tends to zero as spins approach small values, and only suddenly diverges very close to $j, k = 0$. We attribute this behavior to the breakdown of validity of the asymptotic formula, and remove it by introducing a small spin cutoff. As long as one does not enter the region in which the asymptotic formula breaks down anyway, the results appear not to be influenced by the precise position of the cutoff.

6.3.1   Renormalization setup

We work on a system Φ describing the time evolution of an isotropic and homogeneous universe. Such process is studied on a discretization given in terms of hyperfrusta. Thus, among all the possible paths in the state sum we are just focusing on those such that, at fixed time, the spatial geometry and its quantum fluctuations are represented by cubes.

Let us focus on the table in Figure 6.1 which catalogs some possible discretizations of Φ preserving the symmetries of the system. Each slot $(\mathcal{X}, \mathcal{Y})$ represents a discretization $\Phi_{(\mathcal{X}, \mathcal{Y})}$ of Φ in terms of $n = \mathcal{X}^3 \mathcal{Y}$ vertices.

In what follows we are considering the initial and final slices as our disconnected boundary. There exists a unique embedding map (6.1) which allows for using only and solely the hyperfrustum vertex at each refinement step. This is such that it maps a coarse boundary cube into the unique configuration of $\mathcal{X}^3$ smaller cubes, all of the same size. A posteriori, the interpretation that derives from the use of our special vertex can be summarized as follows: we are modeling a symmetry restricted quantum dynamics which is not allowed to fluctuate in a direction violating the Friedmann symmetries. In particular it does so not only globally, but also in any local region of space.

Figure 6.1: Catalog of some possible discretizations of Φ which preserve the homogeneity of the spatial hypersurfaces. The labels $\mathcal{X}$ refer to the number of links used to discretize each spatial direction. The labels $\mathcal{Y}$ refer to the number of time steps in which the transition occurs.

At the coarsest level the process is described by a single vertex i.e., a hyperfrustum $\Phi_{(1,1)}$ with boundary cubes of areas j_i and j_f. These labels fix the boundary geometry of $\Phi_{(1,1)}$ and determine the coarsest scale where there is a single degree of freedom available e.g., the height H. Shifting to the right in the picture (i.e. along $\mathcal{X}$) corresponds to a homogeneous split of the spatial discretizations, dictated by the embedding map. Thus, in the slot $(\mathcal{X}, 1)$ each spatial edge is split into $\mathcal{X}$ equal pieces. Correspondingly, each of the coarsest boundary cubes of areas j_i and j_f is respectively subdivided into $\mathcal{X}^3$ cubes of areas $j_i/\mathcal{X}^2$ and $j_f/\mathcal{X}^2$. Stepping down in the picture (i.e. along $\mathcal{Y}$) corresponds instead to refining the discretization in the time direction. As an example, at the slot $(1, \mathcal{Y})$ of Table 6.1 one has the transition of a single cube in $\mathcal{Y}$ time steps which is represented by a chain of $\mathcal{Y}$ hyperfrusta of heights $H_1, \ldots, H_{\mathcal{Y}}$ with $\sum_{i=1}^{\mathcal{Y}} H_i = H$. The variables of a discretization $\Phi_{(\mathcal{X},\mathcal{Y})}$ are the bulk spatial spins j_n and the time-like spins k_m, where $n = 1, \ldots, \mathcal{Y} - 1$, $m = 1, \ldots \mathcal{Y}$.

The flow is extrapolated from the comparison of the dynamics of two discretizations $\Gamma = \Phi_{(\mathcal{X},\mathcal{Y})}$ (coarse) and $\Gamma' = \Phi_{(\mathcal{X}',\mathcal{Y}')}$ (fine) defining a coarse graining step. One can choose whatever couple (Γ, Γ') in Table 6.1 with the condition that $\mathcal{X} \cdot \mathcal{Y} < \mathcal{X}' \cdot \mathcal{Y}'$. In general, the flow will depend on such a choice. However we expect that for highly discretized Γ and Γ' the dependence of the flow becomes negligible since the discretization is fine enough to capture the dynamics of the system.

Let us notice that all the configurations shown in Table 6.1 give rise to real

transition amplitudes in view of the fact that they are built as a product of real amplitudes $\widehat{\mathcal{A}}_v$ of the form (5.64). The discretizations laying in the even columns have positive amplitudes while the odd columns can take negative values since each time step comes with an odd power of vertex amplitudes. In what follows we restrict ourselves to discretizations with positive amplitudes only. This ensures in general a faster numerical evaluation of the expectation values of the observables.

6.3.2   One dimensional isochoric RG flow

First, we consider a restricted flow where all coupling constants are kept fixed, except for α. The RG flow in α is computed in the isochoric setting i.e., keeping fixed the total 4-volume of space-time. This is a generalization of a previous work, in which the discretization has been restricted to hypercuboids, and where it has been observed that the *RG* flow of α is intimately connected to the vertex displacement symmetry of the model [79].

In particular, in [81], it was observed that the EPRL-FK model breaks vertex displacement symmetry, which is the manifestation of diffeomorphisms on the lattice [132, 106, 133, 134, 81, 135]. While this breaking of symmetry is well-known in classical Regge calculus, where it appears whenever curvature is involved, the quantum theory breaks it even in the case of flat metrics.

If one restricts the state sum to only these flat metrics, by using hyper-cuboids, then it could be shown that the RG flow has an UV-attractive fixed point, on which vertex displacement symmetry is roughly restored. Since one only considers flat configurations, only the coupling constant α plays a role. Depending on the boundary state, the fixed point lies around $\alpha \approx 0.63$ [80]. In the following, we extend the RG flow to frusta geometries which also allow for curvature.

We consider the coarse-graining step of $\Gamma = 2 \times \Phi_{(1,2)}$ into $\Gamma' = 2 \times \Phi_{(2,4)}$ which are respectively discretizations with $n_\Gamma = 1^3 \times 2 \times 2 = 4$ and $n_{\Gamma'} = 2^3 \times 4 \times 2 = 64$ vertices (Figure 6.2). The lattice is doubled in one of the spatial directions, so that the amplitude is always positive. The initial and final boundary spins are fixed and equal $j_i = j_f = j_b$.

The RG flow is then evaluated in the isochoric regime, i.e. summing over all configurations which have identical total 4-volume V_{tot}. This is achieved by performing a transformation of the integral over spins (j_n, k_m) to an integral over (j_n, V_m), with the 4-volumes V_m of a vertex at time-step m. This adds a Jacobian determinant to the integration, after which the total volume is fixed by including a $\delta(\sum_m V_m - V_{\text{tot}})$ into the integral, which allows to express one of the volumes by the others and V_{tot}. For the coarse lattice Γ this results in two variables j_1, V_1, while for the fine lattice Γ' one has six variables j'_n, V'_n, with $n = 1, 2, 3$.
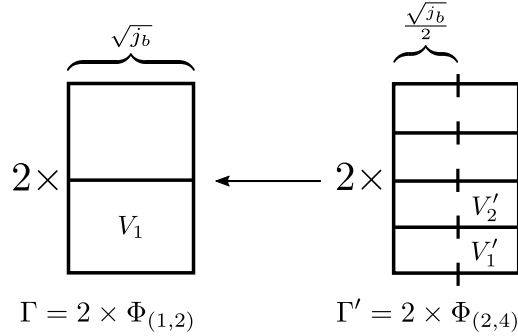
Figure 6.2: Coarse graining step used to generate the one-dimensional flow in the isochoric setting i.e., keeping the total 4-volume fixed.

We use the amplitude (5.64) and equation (5.65) to compute the expectation values of an observable corresponding to the fluctuation of half of the volume, i.e.

$$\langle O_\Gamma \rangle_\Gamma \quad \equiv \quad \langle (V_1 - V_{\text{tot}}/2)^2 \rangle, \tag{6.20}$$

$$\langle O_{\Gamma'} \rangle_{\Gamma'} \quad \equiv \quad \langle (V_1' + V_2' - V_{\text{tot}}/2)^2 \rangle. \tag{6.21}$$

To compare to the computation in [80], we fix $1/G = 1.5$, $\Lambda = 0.1$, and consider the amplitude depending only on the coupling constant α. For a given α' on the fine lattice, we compute the fine observable (6.21), and look for the value α on the coarse lattice, which leads to the same value for (6.20), i.e. the RG flow $\alpha' \to \alpha$ is given by the condition (6.10) i.e.,

$$\langle \mathcal{O}_\Gamma \rangle_\Gamma^\alpha \quad \overset{!}{=} \quad \langle \mathcal{O}_{\Gamma'} \rangle_{\Gamma'}^{\alpha'}. \tag{6.22}$$

The result can be seen in Figure 6.3. The intersection with the line of $\alpha = \alpha'$ lies at about

$$\alpha^* \quad \approx \quad 0.69, \tag{6.23}$$

which marks an unstable (i.e. UV-attractive) fixed point of this flow. This value is slightly above the one found in [80], but only differs by about 10%.

A plot of the path integrand for the coarse lattice (depending on the two free variables j_1, V_1) is depicted in Figure 6.4. It can be seen that for α at the fixed point, there is a plateau in the integrand, indicating that some symmetry among the variables is approximately realized in the path integral. This can be regarded as some vertex displacement symmetry. It should be noted, however, that in this case the connection to the diffeomorphisms is much less clear, due to the presence of non-trivial deficit angles. Numerical tests show indeed that the plateau depicted in Figure 6.4 vanishes, as soon as one moves α away from the fixed point α^*. All of this is in agreement with what has been found previously in the case of hypercuboids [80, 79].
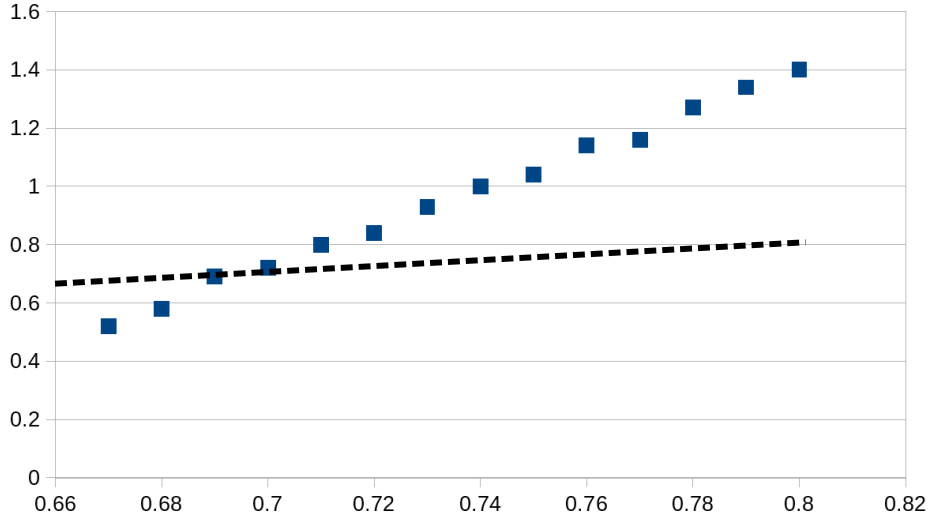
Figure 6.3:   RG flow $\alpha \to \alpha'$ in the isochoric case. The intersection with the dashed line $(\alpha\alpha')$ lies at about $\alpha \approx 0.69$, while the other coupling constants are fixed to $1/G = 1.5$, $\gamma = \frac{1}{2}$, and $\Lambda = 0.1$.
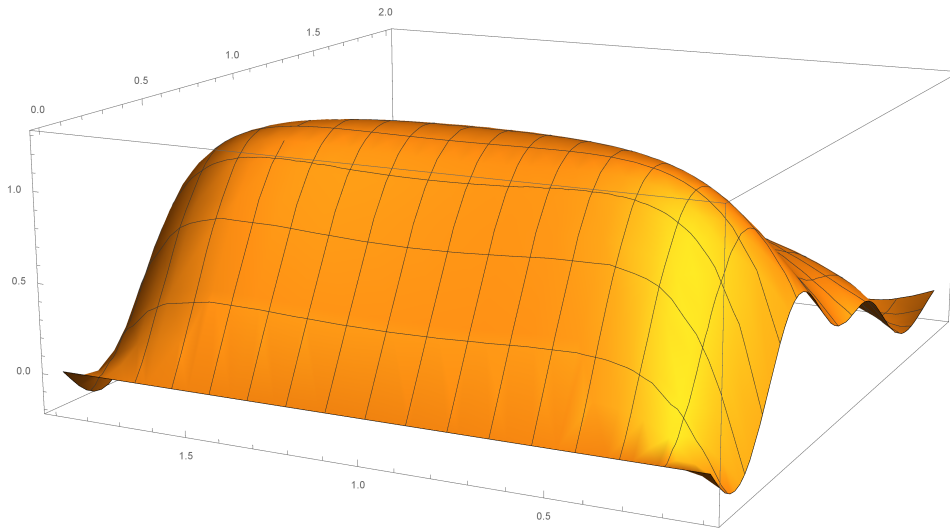
Figure 6.4:   Path integrand $\widehat{\mathcal{A}_1} \cdot \widehat{\mathcal{A}_2}$ for the coarse lattice at $\alpha = \alpha^*$, depending on the two variables j_1, V_1. The plateau indicates the presence of vertex displacement symmetry.

6.3.3 The isotemporal gauge

Let us now go beyond the one dimensional analysis and generate higher dimensional RG flow diagrams. In fact, the theory is also defined by the parameters G and Λ. We first look at a two dimensional flow in the space (Λ, G) while keeping fixed the value of α. Such analysis reveals a partial information being a projection of the three dimensional flow. Nonetheless we will see that it carries the traces of non trivial regions. We then extend this result to the entire parameter space generating a more detailed flow diagram in the space (α, G, Λ). As we will show, the flow has a fixed point with one attractive and two repulsive directions.

Here we relax the constraint which keeps fixed the total 4-volume and instead we fix the total height H. Furthermore, we work in an isotemporal gauge i.e., we demand that all the hyperfrusta in a given discretization have the same height. As an example, the slot $(1, \mathcal{Y})$ of Fig.6.1 is now interpreted as the transition of a single cube into the same cube in $\mathcal{Y}$ time steps which is represented by a chain of $\mathcal{Y}$ hyperfrusta of same height $H/\mathcal{Y}$.

In our analysis we consider the case of $\Gamma = \Phi_{(3,2)}$ and $\Gamma' = \Phi_{(4,3)}$ which respectively correspond to discretizations of Φ in terms of $n_\Gamma = 3^3 \times 2 = 54$ and $n_{\Gamma'} = 4^3 \times 3 = 192$ hyperfrusta (Figure 6.5). We also choose a fiducial set
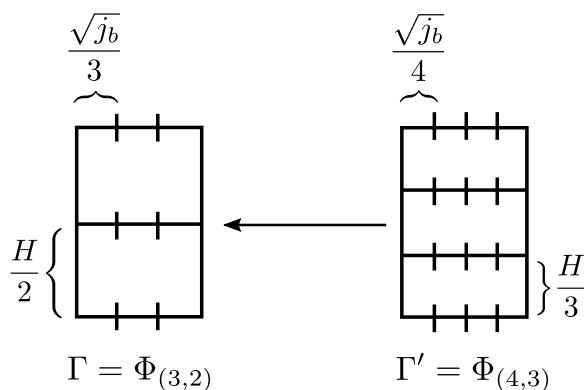
Figure 6.5: Coarse graining step used to generate the two- and three-dimensional flows in the isotemporal gauge, i.e. keeping fixed the height of the vertices in each discretization and imposing the total height H to be fixed

of boundary conditions $j_i = j_f = 1$ and we fix $H = 6$.

Let us note that the total amplitude of Γ' is always positive being given as a product of an even number of identical dressed vertex amplitudes for each time step. The coarse lattice Γ has instead an odd number of vertices contributing to each time step. However, thanks to the symmetry $\widehat{\mathcal{A}}_v(j_n, j_{n+1}, k_n) = \widehat{\mathcal{A}}_v(j_{n+1}, j_n, k_n)$ of (5.64), the chosen boundary conditions and the isotemporal gauge setting guarantee the positivity of the total amplitude as both time

steps carry the same amplitude.

In the large spin limit the partition functions associated to these two systems are respectively

$$Z_\Gamma = \int \mathrm{d}j_1 \mathrm{d}k_1 \mathrm{d}k_2 \ \widehat{\mathcal{A}}_v(\frac{j_i}{9}, j_1, k_1)^{27} \ \widehat{\mathcal{A}}_v(j_1, \frac{j_f}{9}, k_2)^{27},$$

$$Z_{\Gamma'} = \int \mathrm{d}j_1' \mathrm{d}j_2' \mathrm{d}k_1' \mathrm{d}k_2' \mathrm{d}k_3' \ \widehat{\mathcal{A}}_v^{64}(\frac{j_i}{16}, j_1', k_1') \tag{6.24}$$

$$\times \ \widehat{\mathcal{A}}_v^{64}(j_1', j_2', k_2') \ \widehat{\mathcal{A}}_v^{64}(j_2', \frac{j_f}{16}, k_3'),$$

where j_1, j_1', j_2' are internal space-like spins associated to square areas while $k_1, k_2, k_1', k_2', k_3'$ are internal 'time-like' spins associated to trapezoidal faces. To implement the isotemporal gauge we first perform a change of variables

$$\begin{aligned} k_1 &\to H_1, & k_2 &\to H_2, \\ k_1' &\to H_1', & k_2' &\to H_2', & k_3' &\to H_3'. \end{aligned} \tag{6.25}$$

Each of these substitutions generates a Jacobian factor. For an hyperfrustum $F_n(j_n, j_{n+1}, k_n)$ the Jacobian $J \equiv J(j_n, j_{n+1}, H_n)$ reads

$$\begin{aligned} J &= \frac{\partial H_n(j_n, j_{n+1}, k_n)}{\partial k_n} \\ &= \frac{H_n(\sqrt{j_n} + \sqrt{j_{n+1}})^2}{\sqrt{4H_n(\sqrt{j_n} + \sqrt{j_{n+1}})^2 + 2(j_n - j_{n+1})^2}}, \end{aligned} \tag{6.26}$$

and refers to the change of variables $k_n \to H_n$, the height H_n being given in terms of (5.12) by

$$H_n = \frac{2k_n}{\sqrt{j_{n+1}} + \sqrt{j_n}} \ K. \tag{6.27}$$

As a second step we insert in the coarse and fine partition functions respectively

$$\delta(H - H_1 - H_2)\delta(H_1 - H_2),$$

$$\delta(H - H_1' - H_2' - H_3')\delta(H_1' - H_2')\delta(H_1' - H_3'). \tag{6.28}$$

The partition functions then become

$$\begin{aligned} Z_\Gamma &= \int \mathrm{d}j_1 \ \mathcal{A}_\Gamma, \\ Z_{\Gamma'} &= \int \mathrm{d}j_1' \mathrm{d}j_2' \ \mathcal{A}_{\Gamma'}, \end{aligned} \tag{6.29}$$

where we have defined

$$
\begin{aligned}
\mathcal{A}_\Gamma &= J\Big(\frac{j_i}{9}, j_1, \frac{H}{2}\Big)\, J\Big(j_1, \frac{j_i}{9}, \frac{H}{2}\Big) \\
&\quad \times \widehat{\mathcal{A}}^{27}\Big(\frac{j_i}{9}, j_1, k_1\Big)\, \widehat{\mathcal{A}}^{27}\Big(j_1, \frac{j_i}{9}, k_2\Big), \\
\mathcal{A}_{\Gamma'} &= J\Big(\frac{j_i}{16}, j_1', \frac{H}{3}\Big)\, J\Big(j_1', j_2', \frac{H}{3}\Big) J\Big(j_2', \frac{j_f}{16}, \frac{H}{3}\Big) \\
&\quad \times \widehat{\mathcal{A}}^{64}\Big(\frac{j_i}{16}, j_1', k_1'\Big)\, \widehat{\mathcal{A}}^{64}\Big(j_1', j_2', k_2'\Big) \widehat{\mathcal{A}}^{64}\Big(j_2', \frac{j_f}{16}, k_3'\Big).
\end{aligned}
\tag{6.30}
$$

The 'time-like' spins in the expressions above must be understood as functions $k_n \equiv k_n(j_n, j_{n+1}, H_n)$.

Thus, in the coarse case we remain with a system with a single d.o.f. given by the intermediate spatial spin $j_1 \in [0, \infty]$. In the fine case there are two d.o.f. corresponding to the two intermediate spins $j_1', j_2' \in [0, \infty]$.

6.3.4 Two dimensional isotemporal RG flow

Let us look at the projection of the RG flow on the two dimensional parameter space (Λ, G). To do so we fix the value of $\alpha = 0.68$. We recall that the choice of α influences the convergence of the amplitude for large spins. In particular, the chosen value for α favors small spins. This allows us to set an upper spin cutoff during the Monte Carlo integrations so that the results will be independent of it. Furthermore, this value of α stands out in our analysis as a point where an interesting and consistent dynamics takes place.

In order to draw a flow diagram we proceed as follows

- Select a domain in the parameter space (Λ, G) and identify $n = 32 \times 32 = 1024$ points homogeneously distributed in this domain.

- In each point of the domain evaluate numerically the coarse and fine expectation values of three operators:

  1. the 3-volume at middle height $\langle \mathcal{O}^{(1)} \rangle \equiv \langle V_3 \rangle$
  2. its variance $\langle \mathcal{O}^{(2)} \rangle \equiv \langle V_3^2 \rangle - \langle V_3 \rangle^2$
  3. the total 4-volume $\langle \mathcal{O}^{(3)} \rangle \equiv \langle V_4 \rangle$.

- Starting from each $g' = (\Lambda', G')$ draw an arrow $\mathrm{A}^{g' \to g}$ pointing at $g = (\Lambda, G)$ such that, following the notation of (6.17), the distance $\Delta_{\Gamma, \Gamma'}^{g^\star, g'}$ is minimal for $g^\star = g$, where $g^\star$ is a point in the selected domain. This defines an RG flow diagram.[10]

---

[10]In the first plots we fix a maximum length for the arrows since we are interested in getting an idea about where to zoom next to satisfy equation (6.17) at best. Later, when we are in a region that we can trust, we will allow the arrows to have any length.

Figure 6.6:   RG flow with cylindrical consistency condition maximally and minimally violated with the respective relative errors $R_{red} = 4.0675$, $R_{blue} = 0.0169$.

- Assign a color to the arrows depending on the value of the relative errors $R_{\Gamma,\Gamma'}^{g,g'}$, where we have used the notation as in (6.18). Namely, draw in red the arrow that violates the most the cylindrical consistency condition (6.17) (w.r.t. the other arrows in the plot). On the contrary, color in blue the one which satisfies at best the condition. Report the corresponding values R_{red} and R_{blue} of the relative errors. Accordingly to the above classification, draw the other arrows in a tonal progression from red to blue.

The resulting RG flow in the region $\Lambda = (-0.04, 0.04)$ and $G = (-0.02, 0.02)$ is shown in Figure 6.6.

As the relative errors suggest, at the analyzed resolution the flow is hardly reliable in some regions. Still we notice that the arrows drawn in dark blue have a small relative error $R \sim 0.017$. Most notably, those in the first quadrant, close to $(\Lambda, G) = (0, 0)$, show an interesting behavior whereas they have a vanishing length (represented by dots). This is exactly what we would expect to happen at a fixed point. Let us then zoom into such region. The result for $\Lambda = (-0.01, 0.01)$ and $G = (-0.004, 0.004)$ is shown in Figure 6.7.

A first clear observation is that the overall relative errors have improved, reaching a top precision $R \sim 0.008$. In an angular region around $G = 0$ the flow is still unreliable. However, in correspondence to the interesting region (blue arrows), the relative errors are fairly small and the flow shows a more coherent behavior. In particular there are still some arrows with null distance.
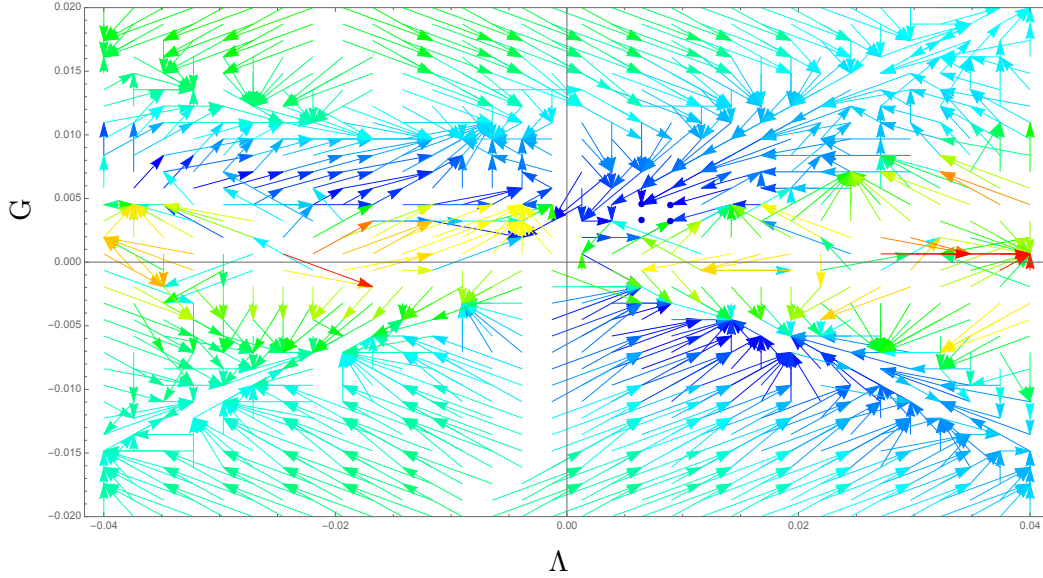
Figure 6.7: RG flow with cylindrical consistency condition maximally and minimally violated with the respective relative errors $R_{red} = 4.0675$, $R_{blue} = 0.0169$.

We then want to zoom further into the top right region of Figure 6.7. We do so by also unlocking the parameter α and let it vary slightly around $\alpha = 0.68$.

6.3.5 Three dimensional isotemporal RG flow

Using the same strategy as in the two dimensional case, it is possible to generate an RG flow in the space defined by the three couplings (α, G, Λ). Figure 6.8 shows the RG flow in the region $\Lambda = (0.006, 0.01)$, $G = (0.003, 0.0045)$ and $\alpha = (0.6765, 0.6775)$ in which we have selected $32 \times 32 \times 32$ points. All the arrows in the plot satisfy with a fine precision the cylindrical consistency condition, the smallest relative error being $R \sim 0.00017$ [11].

Remarkably, nestled at the center of this region there is the indication of a fixed point showing one attractive and two repulsive directions. At this order of precision, both the relevant and irrelevant directions seem to be associated with linear combinations of all three parameters. A better precision can be reached by further zooming. Our research suggest that this is a rare point of the parameter space. Whether this point is unique needs further analysis.

6.3.6 Expanding and contracting universes

We now investigate the dynamics described by the amplitudes, in order to gain an insight into the interpretation of the RG flow.

---

[11] For practical graphical reasons, we only draw the most reliable arrows in blue and green.
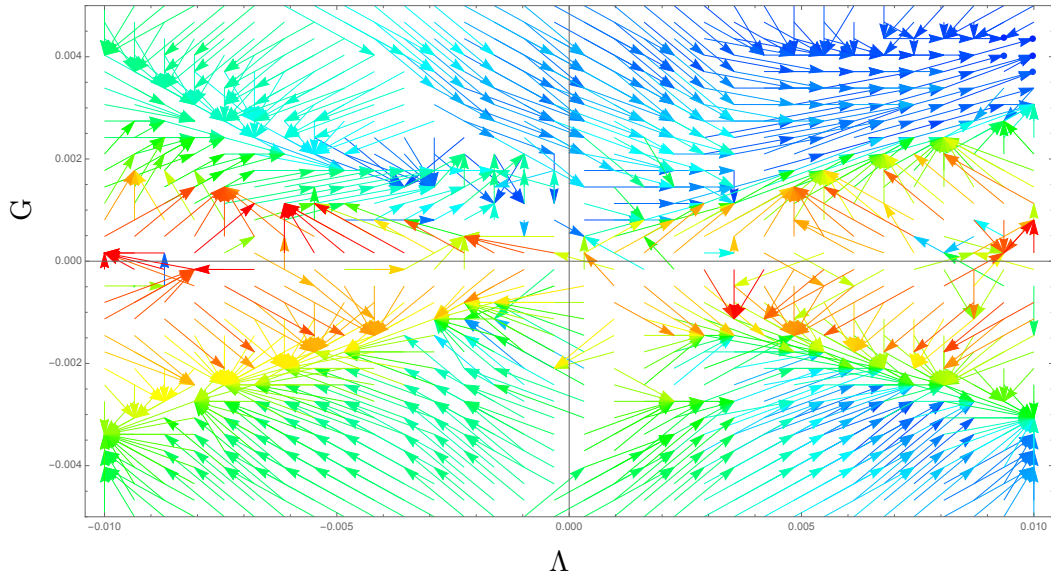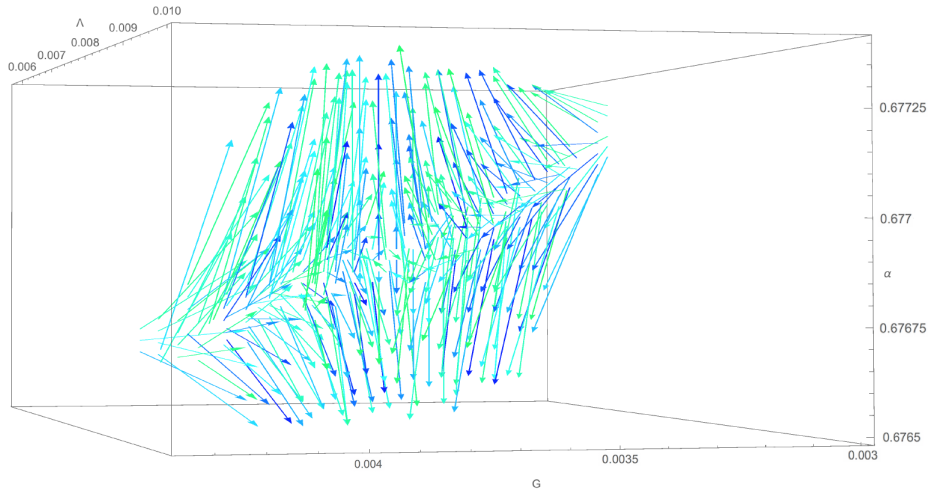
Figure 6.8:   Three dimensional RG flow with cylindrical consistency condition maximally and minimally violated with the respective relative errors $R_{green} = 0.004$, $R_{blue} = 0.00017$.

Frusta geometries are geared towards studying cosmological transitions. The spatial cubes essentially encode the scale factor a of the universe at a certain 'time step', and the 'time-like' frusta mediate between spatial cubes of different size[12]. Naturally the question arises which configurations are preferred in the path integral given by the EPRL-FK amplitudes. In particular we intend to examine how the parameters of the model, e.g. the cosmological constant Λ, influence the dynamics and whether familiar features of the classical theory emerge as well. In the case of our simple model this could be whether the universes expansion is accelerating or slowing down, depending on the sign of the cosmological constant.

To this end, we study again the expectation values of observables that we have used before to define and compute a renormalization group flow. More precisely, we consider the 3D volume for the coarse transition investigated before, as it essentially gives the intermediate scale factor between an initial and final state of the same size. Furthermore, studying an observable used for the renormalization group flow in more detail may reveal a few insights as to the form of the flow. We show its expectation value in fig. 6.9.

As a first striking feature, we recognize the 'X'-shape in the values of the observables similar to the 2D scans of the renormalization group flow. Inside this region, the 3D volume fluctuates significantly and can reach quite high values. These peaks appear to be slightly larger for negative cosmological

---

[12]The cuboid intertwiners we use are sharply peaked on the cuboid shape, yet they are undetermined in the extrinsic curvature, i.e. how the 3D cubes are embedded in a 4D geometry. In this sense the states are sharply peaked in a, but $\dot{a}$ is maximally uncertain.
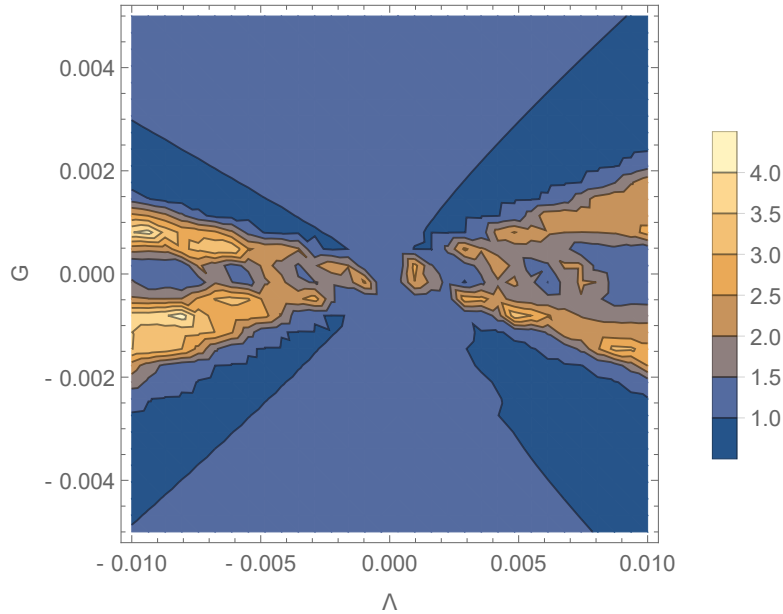
Figure 6.9: Expectation value for the 3D volume of the intermediate spin, $\langle j^{\frac{3}{2}} \rangle$, for $\alpha = 676855$. This is the case of the coarse transition with 54 hyperfrusta.

constant, but there also exist regions for positive Λ, in which the intermediate 3D volume is significantly larger compared to the initial / final state. Note that this is also the region in which the cylindrical consistency conditions for the observables of the RG flow are strongly violated, which implies that a similar behavior does not exist in a similar region for the fine observable. Judging from the plot, this behavior is due to the small size of $|G|$ and it appears to extend slightly as $|\Lambda|$ is increased. A possible explanation is that both parameters enhance the oscillatory behavior of the integral, resulting in a highly fluctuating expectation value.

Outside that region, more precisely for larger $|G|$, we observe a rather uniform behavior, where the 3D volume is around or slightly larger than 1, which is also the volume at the initial and final slice.

There is only little dependence on the sign of the cosmological constant: For negative Λ, we observe a slightly larger intermediate 3D volume already for smaller $|G|$. Thus, $\Lambda < 0$ appears to favor a larger intermediate 3D volume compared to $\Lambda > 0$, however in both cases we observe an intermediate volume that is larger than the initial and final one. Hence, we generically observe a transition in which the universe first expands and then contracts, or at most remains constant. A transition to a contracting and then expanding universe is not observed numerically.

Naturally, one would like to compare this behavior to classical dynamics.

However it is not clear to which discrete action we should compare our results to. In the vertex amplitude (5.64) several oscillating terms appear, containing different actions. While the cosine contains the (area) Regge action and a volume term times the cosmological constant, the other oscillating terms only contain the Regge action. Clearly the former term is the desired one, we will briefly compare our results to the classical, discrete dynamics.

Since we consider the transition for fixed heights, with $j_{\text{in}} = j_{\text{fin}} = 1$. There is one discrete equation of motion to solve depending on Λ[13]. For $\Lambda = 0$ the equations of motion are solved by $j = 1$, so there is no expansion or contraction as one would expect. For $\Lambda > 0$ we find $j < 1$ as the solution, while for $\Lambda < 0$ we find $j > 1$. So we see a first contracting, then expanding universe for positive cosmological constant and the opposite for negative cosmological constant. Something similar can be seen in the continuum, where $\Lambda > 0$ implies $\ddot{a} > 0$. Hence in order to arrive at the same scale factor a at a later time, the universe first contracts before expanding again. The behavior is reversed as $\Lambda < 0$ implies $\ddot{a} < 0$.

It seems that the behavior of the truncated SFM does not reproduce the classical dynamics. Instead we usually see $\langle j^{\frac{3}{2}} \rangle > 1$, no matter the sign of the cosmological constant. Nevertheless, we do observe generically larger expectation values $\langle j^{\frac{3}{2}} \rangle > 1$ for negative Λ compared to positive Λ. There are a few plausible explanations for these deviations: The vertex amplitude contains several oscillating functions, some contain the cosmological constant term, some do not. Moreover, the 'proper' action appears in the cosine, which might lead to unwanted interference of different bulk solutions. Additionally, the whole spin foam does not oscillate with the sum of Regge actions assigned to hyperfrusta, as the cosine is not additive. Another possible deviation might stem from the face amplitudes, which favor small or large spins depending on the value of the parameter α. If α is large, it puts emphasis on large spins, which generically results in larger expectations values for spins or volume etc.

A possibility to overcome the 'cosine' problem would be to consider states which are not just peaked on the shape of cuboids or frusta, but which are also peaked in the extrinsic curvature. This would roughly correspond to prescribing both a and $\dot{a}$ at the initial and final time. As a result, one of the two stationary and critical points in the asymptotic expansion might be suppressed, resulting in a quantum dynamics closer to its classical counterpart. We leave this for future research.

6.3.7   Free theory

In this chapter we consider the limit of the RG flow equations $G \to 0$ and $\Lambda \to 0$. This can be understood as the free theory, as the gravitational coupling

---

[13]As G is an overall constant, only Λ determines the classical dynamics in the absence of matter.

G, which governs the strength of the perturbative interaction in the linearized theory, vanishes. It should be noted that, due to its non-perturbative nature, the EPRL-FK model does not exist for $G = 0$ ($\Lambda = 0$ is no problem, though). We therefore approach this point in theory space asymptotically.

Considering the RG step of a lattice with $4 \times 4 \times 4 \times 3 = 192$ to one with $3 \times 3 \times 3 \times 2 = 54$ vertices, as described in section 6.2. We compute the observables V_3 and V_4 for the isotemporal case, i.e. when the time-steps are gauge-fixed, for $\Lambda = 0$ in the asymptotic limit $1/G \to \infty$. The initial and final boundary spins are fixed to the same (but ultimately arbitrary) value $j_i = j_f = j$.

We first consider not the full EPRL-FK model, but only its proper vertex, where the amplitude as replaced simply by the exponential of the Regge action. In that case, we have that

$$Z_{54} = \int_0^{J_{\max}} dj_1 \left(\hat{\mathcal{A}} \right)^{54}, \tag{6.31}$$

with

$$\hat{\mathcal{A}} = F(j_1) \frac{e^{54i/G\,S_R}}{|D|},$$

where D is the Hessian determinant, and $S_R = S_R(j_1, j, H)$ is the Regge action for one hyperfrustum with initial/final spin j, intermediate spin j_1, and height H. Also, $F(j_1)$ is a function depending on j_1 (and j and H), which are given by a collection of face- and edge-amplitudes.

To evaluate (6.31) in the limit $1/G \to \infty$, we can perform a stationary phase approximation. For this we simply observe that the condition

$$\frac{\partial S_R(j, j_1, k(j, j_1, H))}{\partial j_1} = 0 \tag{6.32}$$

has only $j_1 = j$ as solution. To compute expectation values, we perform the same calculation, but include another function $O(j, H, j_1)$ (in our case V_3 and V_4) into the integral, which we evaluate at the respective stationary point as well. We can immediately conclude that

$$\langle V_3 \rangle_{54}^{G \to 0, \Lambda = 0} = 27 j^{\frac{3}{2}}, \quad \langle V_4 \rangle_{54}^{G \to 0, \Lambda = 0} = 54 H \, j^{\frac{3}{2}}. \tag{6.33}$$

The computation for Z_{192} is only slightly more complicated. We have

$$Z_{192} = \int dj_1' dj_2' \left(\hat{\mathcal{A}}_1 \hat{\mathcal{A}}_2 \hat{\mathcal{A}}_3 \right)^{64}, \tag{6.34}$$

where the $\hat{\mathcal{A}}_i$, $i = 1, 2, 3$ denote the vertex amplitudes for the i-th time step. We get

$$\hat{\mathcal{A}}_1 \hat{\mathcal{A}}_2 \hat{\mathcal{A}}_3 \; = \; \frac{e^{i/G \left(S_1 + S_2 + S_3 \right)}}{|D_1 D_2 D_3|} \; , \tag{6.35}$$

with the Regge actions S_i for the i-th time step, and D_i the corresponding Hessian determinant. The variables for these are j_1' and j_2', and one can show that, again, the only solution to

$$\frac{\partial}{\partial j_1'}(S_1 + S_2 + S_3) \; = \; \frac{\partial}{\partial j_2'}(S_1 + S_2 + S_3) \; = \; 0 \tag{6.36}$$

is $j_1' = j_2' = j'$. This immediately leads to

$$\langle V_3 \rangle_{192}^{G \to 0, \Lambda = 0} \; = \; 64(j')^{\frac{3}{2}}, \quad \langle V_4 \rangle_{192}^{G \to 0, \Lambda = 0} \; = \; 192 H' \, (j')^{\frac{3}{2}}.$$

With $H' = \frac{2}{3}H$ and $\sqrt{j'} = \frac{3}{4}\sqrt{j}$, we can conclude that

$$\langle V_3 \rangle_{192}^{G \to 0, \Lambda = 0} \; = \; \langle V_3 \rangle_{54}^{G \to 0, \Lambda = 0},$$
$$\langle V_4 \rangle_{192}^{G \to 0, \Lambda = 0} \; = \; \langle V_4 \rangle_{54}^{G \to 0, \Lambda = 0}.$$

This demonstrates that the point $G = 0$, $\Lambda = 0$ is a fixed point of the discussed RG flow of the reduced amplitude.

It is notable that this analysis rests on using the reduced amplitude, i.e. where only one term in the exponential expression for EPRL-FK amplitude (the one containing the exponential of the Regge action) is kept. As soon as this is replaced with the full EPRL-FK amplitude, the analysis does not hold any more. This can be traced back to the presence of the cosine, as well as the weird terms. Indeed, in the case where these terms are present, the path integral is a sum over different possibilities, in which different vertices contribute the same parts of the Regge action with different signs. This allows for several terms in which the individual contributions of vertices identically cancel, irrespective of the configuration. As a result, the stationary phase approximation is dominated by those terms, which do not only contribute the classical solutions, but many non-classical configurations as well. For instance, all transitions via arbitrary intermediate (bulk) spin j contribute. Since the quantum theory is not dominated by the classical solutions in this case, it seems unlikely that the free theory is a fixed point in this case.

Incidentally, the problem, can be avoided when using only the cosine, as well as an odd number of vertices per time step. This is an indication that, for Lorentzian signature and an odd number of vertices, the free theory might indeed be a fixed point.

Chapter 7

Summary and conclusions

In this thesis we investigate the renormalization of a symmetry reduced spin foam model in its semiclassical limit. Let us recap each section and make a linear short story of this work.

7.1 A linear story

Many faces of classical General Relativity

In Chapter 2 we give a brief review about the classical (Action and Hamiltonian) formulations of GR. The most important for the development of the quantum theory are the Plebanski formulation, in which GR is described as a topological BF theory with constraints (Section 2.1.3), and the canonical formulation in terms of the Ashtekar variables (Section 2.1.5). Then we introduce to discrete gravity à la Regge, a theory that approximates GR on a simplicial discretization of spacetime. The Regge action (2.59) appears multiple times throughout the work e.g., in the semiclassical limit (4.19) of the quantum theory studied in later chapters. Eventually, we prepare the working basis of the quantum formulations by distributing the classical variables on discrete structures. To introduce the covariant quantum formulation we define BF theory on a 2-complex dual to a 4d triangulation. To prepare the canonical formulation, we distribute instead the Ashtekar variables on a graph dual to a 3d triangulation.

Canonical and Covariant Quantum Gravity

In Chapter 3 we give the quantization algorithms defining the Canonical theory, also called Loop Quantum Gravity (LQG), and the covariant theory which comes with different configurations called Spin Foam Models (SFMs). The two frameworks have many features in common.

Roughly speaking, LQG defines the kinematical Hilbert space of the theory, whose states (3.8) are cylindrical functionals of the holonomy of the Ashtekar connection (2.77). A basis in this space is given in terms of Spin Networks (3.27), representable as (directed) graphs whose links are associated with irreducible representations of a compact Lie group and whose nodes are associated with intertwiners of the link representations adjacent to it.

A SFM defines the quantum dynamics in terms of a path integral over states. The partition function (3.49) of a spin foam model is generated from a BF action (2.63). This can be expressed as a product of amplitudes associated to each element of a 2-complex. The most important are the vertex amplitudes. A partition function ultimately defines the transition probabilities among different spin network states.

In the covariant approach we introduce the coherent state representation, fundamental in the study of the semiclassical (i.e., large spin) limit of SFMs.

The 4d Euclidean EPRL-FK Spin Moam Model

In Chapter 4, we define the EPRL-FK spin foam model which is used in its Euclidean formulation throughout this work (4.12), (4.13), (4.14), (4.15).

One nice characteristics of this model is its link with discrete classical gravity in the semiclassical limit i.e., in the limit of large spins of the vertex amplitude where we recover the Regge action (4.19). Although promising, the resulting formula is hard to handle given that it depends on complex functions of the spins, the first of which is a certain determinant D of a Hessian matrix.

In the final sections of Chapter 4, we have discussed a deformation of the Euclidean EPRL-FK model, so to introduce a cosmological constant term. This is an original work published in [41] and generalizes Han's formulation [76] to arbitrary vertices i.e., not only those dual to a 4-simplex. The deformation amounted to introducing an operator for each crossing C of the graph Γ in the formula for the amplitude (see section 4.3.1). Such operator depends on a parameter ω, and we have considered the definition for arbitrary graphs as well as the corresponding asymptotic expression of the deformed amplitude $\mathcal{A}_\Gamma^\omega$.

The main statement is that the deformed amplitude $\mathcal{A}_\Gamma^\omega$ has a close connection to $\mathcal{A}_\Gamma$, the undeformed one. Firstly, the equations for the stationary critical points in the asymptotic analysis are in one-to-one correspondence. Also, we could show that the Hessian determinant (the one appearing in the general formula (4.18) so to speak) can be treated, and is just a multiple of the undeformed one. This led to an expression of the asymptotic expression in terms of the original Regge action. In particular, the original expression (4.19) consists of the so-called weird terms W (4.20), as well as the cosine of the Regge action. Our analysis (4.59) shows that the weird terms remain un-

changed, while the Regge action is replaced by a term ΛV, where $\Lambda = -12\omega$, and V is an expression which, if the boundary data is that of a convex, non-degenerate polyhedron, is equal to its volume.

Spin Foam state sum reduced to Frustum geometries

In Chapter 5 we present an original work in which we investigate the Euclidean EPRL-FK model by cutting off most degrees of freedom of the theory and leaving in only some very symmetric ones. In particular, we work on a hypercubic lattice in which all the vertices are dual to a 4d truncated pyramid with cubic bases (hyperfrustum). Furthermore we restrict the state sum by considering only coherent intertwiners which in the large-spin limit reproduce the geometry of a 3d pyramidal frustum. The reduced state sum allows us to investigate the semiclassical structure of the Euclidean EPRL-FK model and in particular to compute explicitly the asymptotic formula of the vertex amplitude $\mathcal{A}_{\Gamma_v}$ (5.64). We show that the final expression contains the correct Regge action (5.19) describing the classical properties of our model. Starting from these results one can perform a numerical analysis of the semiclassical features of the model. This opens a path to study the renormalization of a symmetry reduced model of quantum gravity, which is notoriously difficult to access in the full state sum setting due to the intricacy of the formulas. Further developments are possible in studying the diffeomorphism symmetry which is usually broken by the discretization of the spacetime manifold. In fact, knowing the full analytic expression of the partition function (4.12) and gauging the parameters in the theory one can look for configurations in which this symmetry is restored. Such perspectives can potentially shed a new light on a sector of the EPRL-FK model which still has many unknown features. This research line has been originally paved by a series of works on hypercuboidal geometry and non-trivial results have been found in the case of flat spacetime [81, 79, 80]. Our analysis provides a step further in this direction. In particular, in the purely flat case only the parameter α, as set in the face amplitude (4.13), is a running coupling constant, while the inclusion of hyperfrusta also offers Newton's constant and the cosmological constant as nontrivial coupling. This makes the renormalization computation more general.

In the second part 5.3 of Chapter 5, taking inspiration from a series of works on cosmological modeling with Regge calculus [92, 94, 93, 101, 102, 103, 104, 95], we have completed the study of our model by focusing on its classical description. We have first shown that the discretization of spacetime in terms of hyperfrusta have a clear classical interpretation. In fact, a hyperfrustum can be pictured as the time evolution of its boundary cubes, each of them tessellating a flat Cauchy surface. The regular geometry of the cubes and their

even distribution on the lattice reproduce an isotropic and homogeneous space. Moreover, the change in size of the cubes in the boundary of a hyperfrustum mimic an expansion of the universe. These facts enable us to compare the dynamics of our model to the FLRW one. We do it in three different cases: In vacuum, in presence of a cosmological constant and by coupling dust particles to the lattice. The simplicity of our model allows us to consider the spins as the main variables instead of the edge lengths which are usually adopted in Regge calculus. Notably, the results do not change and an analogue of the Schläfli identity is proved to be satisfied. Indeed, with a numerical analysis of the Regge equations (for the spins), we show that in the continuum time limit the evolution of the model universe resembles the one predicted by the standard Friedmann dynamics in the case of fine discretization of the manifold. Furthermore, for small deficit angles this resemblance becomes exact and we find the Friedmann equations as the limit of the Regge equations.

A crucial open question is, of course, in what way this model can be used to perform actual quantum cosmological computations. Apart from the signature issues, the first quantum correction of this model comes from the Hessian matrix. This matrix is, in general, complex, such that its phase would give quantum corrections to the Regge action, while its modulus provides the path integral measure. It would be quite interesting to see whether these corrections have a classical limit which can be interpreted as higher order terms in the Einstein-Hilbert action. To probe the deep quantum regime in order to derive e.g. statements about singularity avoidance, however, one would have to depart from the large-j asymptotics, and consider the full amplitude in the regime of small spins.

The last section 5.4 of Chapter 5 summarizes the results of the semiclassical limit of the deformed vertex amplitude and more in general of the EPRL-FK partition function. Here we also make a clarification on the physical dimensions of areas, volumes and coupling constants. Finally, all the asymptotic formulas used to evaluate the RG flow in Chapter 6 are listed in a compact form.

Renormalization of the reduced model

In chapter 6, we review the concept of background independent renormalization. This is a fundamental tool to deal with spin foams, given that the absence of a background metric makes the standard QFT and Lattice gauge theories techniques not usable. In fact, in standard Wilsonian renormalization one associates the scale of the flow with a value of maximal energy or minimal length, which are introduced as cutoff. Then, for a given background geometry, a finer and finer regular lattice leads to an ever-decreasing value of lattice spacing. However, in our background independence case these two notions (of

refinement and of lattice spacing) are disentangled, in that on coarse or fine lattices both small and large spins occur. The reason is that on both lattices the geometry is not fixed, but rather the path integral sums over all of them. Hence, the notion of refinement of lattices is the only one that remains in this particular way of dealing with the sum over geometries. As a consequence, notions of UV and IR limit are not associated to e.g., small and large spins, but rather to fine and coarse lattices.

In order to deal with actual calculations of the RG flow, several approximations and truncations are employed 6.2.

First, we use the reduced state sum and semiclassical limit introduced in Chapter 5. Previous investigations [79][80] only allowed for quasi-local geometric fluctuations which are, in the semiclassical limit, expected to turn to gauge degrees of freedom. It can be expected that these appear in theory as spurious degrees of freedom, since it is well-known that the gauge symmetry of GR is broken in the EPRL-FK model [132][81]. The crucial innovation in our work (see also [83]) is to relax previous truncations to allow for quantum frustal geometries [42]. This allows, for the first time, to also treat some curved configurations, which are not just pure gauge. Also, the model restricted to frusta is an extension of previous settings, which allow for degrees of freedom which are local (in time).

Also, we project the RG flow so to use the same type of amplitudes at all scales. In fact, in general, given a theory defined by a set of couplings g_i, the dimension of the parameter space can grow or decrease when one looks at the physics at different scales. In other words, new parameters may arise during the coarse graining process. Here we truncate the RG flow by considering the system as self-similar at all the scales. Thus, at each renormalization step we project the amplitude down to the reduced Euclidean EPRL-FK model.

The interesting coupling constants of this model are the gravitational and cosmological constants G and Λ, as well as a parameter in the path integral measure α, which is connected to the 4-volume in the measure, and has been shown to play a crucial role in the restoration of broken diffeomorphism symmetry [79].

In our analysis, we have worked on hypercubic lattices, which provide discretizations of a torus universe. These are depicted in figure 6.1. The RG flow was considered for various coarse graining steps of finer to coarser discretizations.

To define a flow in terms of coupling constants G, Λ, α, it was necessary to choose a couple of reference observables, which we compared on the coarse and the fine lattice. Here, we mostly restricted ourselves to 3- and 4-volumes, as well as their fluctuations. Different choices are possible, but we expect those to yield only qualitatively minor changes to the results, as long as one considers observables which are diverse enough as to separate the space of considered

path integral measures. See also discussion in [38].

Furthermore, we employed a novel system which made the RG flow much more accessible to us (see Section 6.2.5). By relaxing the condition for cylindrical consistency, but allowing only slight changes in the coupling constants, we were able to produce a much smoother flow. As a drawback, not all of the flow diagrams can be trusted, but with the deviation R from cylindrical consistency (6.18), we had a control parameter to judge the quality of the resulting flow in that region. This allowed for quick scanning of parts of the phase space, since in the region of fixed points it can be expected that the value of R has to be small. It is in the vicinity of these regions that one can trust the flow images the most.

7.2   Our findings

Our results are as follows:

- Firstly, the employed approximations (see Section 6.2) allow us to generate images of the RG flow. The introduction of the R-parameter allowed us to quickly decide which regions of the phase space are more likely to contain fixed points, and were worthwhile to concentrate our analysis around. This is in general very encouraging, and we believe that this method can also be used more generally in other RG applications, possibly even beyond the spin foam context.

- We have considered three main flows. One in the parameter α, which was taken to be isochoric, i.e. with fixed total 4-volume. This was a direct generalization of the flow computed in [79], where the non-trivial fixed point was found. Our analysis revealed that the fixed point was still present, albeit with a slightly changed numerical value. We found that in the case of frusta, that the fixed point lies at

$$\alpha^* \approx 0.69, \tag{7.1}$$

  which is slightly increased from $\alpha^* \approx 0.62$ in the case of hypercuboids.

- For considering the RG flow in more parameter, we considered a 2d flow in G and Λ, keeping $\alpha \approx 0.67$ fixed. We used this to scan the parameter space for regions likely containing the fixed points, using the procedure describe above. We the considered a 3d flow in the parameters (G, Λ, α) within that region. This is one of the main results of this work and it is summarized by Figure 6.8.

  We found that there appears to be a fixed point at

$$\alpha^* \approx 0.677, \quad G^* \approx 0.037, \quad \Lambda^* \approx 0.008. \tag{7.2}$$

Numerical evidence shows that the fixed point has one repulsive and two attractive directions.

- We also considered the *free theory*, i.e. the point on which the coupling constant $G = 0$. This point plays an important role in the perturbative renormalization of GR, which is defined by perturbations around it. The EPRL-FK model is defined non-perturbatively, which is seen as one of the strengths of the (loop) quantum gravity approach. This, however, makes it difficult to draw comparisons to more traditional forms of the analysis.

  In particular, this point is not part of the range of EPRL-FK amplitudes. However, with our methods of defining the flow via observables, we can investigate this point at least asymptotically, since it sits on the infinite boundary of the EPRL-FK theory space., and expectation values of some observables converge when approaching this point.

  In particular, we could approach this point both numerically and analytically by asymptotic methods. We found that, contrary to our assumptions, the free theory appears *not* to be a fixed point of the Riemannian EPRL-FK model. If we replace the EPRL-FK amplitude by the exponential of the Regge action, however (with measure factors from the asymptotic EPRL-FK amplitude), we however can show that the free theory is a fixed point.

7.3 Discussion

The main goal of our analysis was to learn more about the RG flow of the EPRL-FK model. Indeed, there are several lessons one might draw from our findings.

- The stability of existence of fixed point under extension of the parameters, and relaxing of truncations, fosters hope that this sort of fixed point is an actual feature of the model, rather than an artifact of the approximation. Of course, further study needs to be taken before this point can be settled decidedly. At this instance, it is unclear whether this fixed point is the only interesting one of its kind in the considered phase space. It is also not clear whether this point bears any relation to the non-Gaussian fixed point discussed in the Asymptotic Safety Scenario [131].

- The fact that the free theory (i.e. where $G = 0$, $\Lambda = 0$) is not a fixed point of the EPRL-FK model, but becomes one when replacing it with simply the exponential of the Regge action, was an unexpected feature (see Section 6.3.7). It can be understood by the form of the EPRL-FK

amplitude: Apart from the exponential of the Regge action, it also contains its sign-reversed part (commonly referred to as the *cosine problem*), as well as other, non-geometric terms (colloquially called *weird terms*).

It is the presence of these additional terms which spoil the fixed point properties. In the free theory, it should be expected that quantum fluctuations around the classical solution are suppressed, since the prefactor in front of the Regge action oscillates rapidly for even minor deviations from the classical trajectory. However, in the EPRL-FK amplitude, the situation changes, since terms with opposite signs can cancel each other in the action. Fluctuations in these directions are therefore not suppressed since they do not change the value of the amplitude. These highly curved contributions are quite different numerically on different lattices, which is why the fixed point properties are spoiled.

The main message one might take away from this is that the Riemannian EPRL-FK model can be expected, in general, to be quite a different theory from (Riemannian signature) quantum gravity. This in itself is not surprising, but, to our knowledge, this is the first instance where this fact has been observed explicitly. It should be noted that in the Lorentzian-signature version of the EPRL-FK model, the weird terms are absent. Also, there is work on the so-called proper vertex, which aims at resolving the cosine issue, even for the Lorentzian amplitude [136, 137].

The question of whether the two terms in the cosine interfere with one another has not been decisively settled by our analysis, but the question appears to be answered in the affirmative. There are, however, some caveats which might, in the long run, change this point of view:

Firstly, if the weird terms are absent (as happens in the Lorentzian theory), one can make the free theory into a fixed point by only considering lattices with an *odd* number of vertices. This prevents precise cancellation of contributions from vertices with differing signs. Still, this restriction appears slightly artificial to us, but it illustrates an important point: the cancellations also happen because of the large amount of symmetries we consider, i.e. by using frusta. In the unrestricted theory where all fluctuations are considered, the states in which precise cancellation among all vertices happens might be dominated by those where it does not. This kind of entropic argument could resolve the issue for the Lorentzian amplitude.

Secondly, our choice of coherent states might influence the result as well. In general, it is expected that one can restrict to either sign of the action by prescribing the proper extrinsic curvature on the boundary. The Livine-Speziale intertwiners used in our analysis are maximally uncertain

in the extrinsic curvature, so that both signs of the Regge action are excited equally. It is feasible to assume that by choosing boundary states which suppresses one sign, one can effectively implement the proper vertex (with minor fluctuations), which would turn the free theory into a fixed point.

This point certainly warrants further investigations in the future.

Appendix A

Groups and Bivectors

A.1   The group SU(2)

The Lie group $SU(2)$ is the group of 2×2 complex valued unitary matrices with determinant 1. Its Lie algebra $\mathfrak{su}(2)$ is given by the set of three generators J_i, which satisfy the commutation relations

$$[J_i, J_j] = i\epsilon_{ijk}J_k. \tag{A.1}$$

A group element $g \in SU(2)$ is then given by

$$g = \exp(iX_i J^i), \tag{A.2}$$

where the coordinates X_i are real. The condition $\det g = 1$ and the unitarity $g^\dagger g = 1$ are satisfied if the generators J_i are Hermitian and traceless i.e.,

$$J_i^\dagger = J_i, \qquad \text{Tr}(J_i) = 0. \tag{A.3}$$

Working in the fundamental representation, the generators are $J_i = \sigma_i/2$ where we use the Pauli matrices

$$\sigma_1 = \begin{pmatrix} 0 & 1 \\ 1 & 0 \end{pmatrix}, \quad \sigma_2 = \begin{pmatrix} 0 & -i \\ i & 0 \end{pmatrix}, \quad \sigma_3 = \begin{pmatrix} 1 & 0 \\ 0 & -1 \end{pmatrix}. \tag{A.4}$$

They satisfy the relation

$$\sigma_i \sigma_j = \delta_{ij} + i\epsilon_{ijk}\sigma_k. \tag{A.5}$$

Also, the following formula holds

$$e^{i\alpha \hat{n} \cdot \hat{\sigma}} = \mathbb{1}\cos\alpha + i\hat{n} \cdot \hat{\sigma} \sin\alpha. \tag{A.6}$$

A generic element $g \in SU(2)$ has the form

$$g = \begin{pmatrix} p & -\bar{q} \\ q & \bar{p} \end{pmatrix} \tag{A.7}$$

with $p, q \in \mathbb{C}$ such that $|p|^2 + |q|^2 = 1$. Equivalently, we can write it in terms of the independent basis elements $(\mathbb{1}, J_1, J_2, J_3)$ as

$$g = a_0 \mathbb{1} + a_i J^i, \tag{A.8}$$

with $a_0, a_i \in \mathbb{R}$ such that $(a_0)^2 + \sum_i (a_i)^2 = 1$.

For all integers N there exists an irreducible representation of the algebra $\mathfrak{su}(2)$ i.e., there is always a set of matrices $N \times N$ satisfying (A.1). Since $SU(2)$ is compact and simply connected, these are also all the representations of the group.
A generic irreducible representation ρ_j is labeled by an half-integer $j \in \mathbb{N}/2$ and has dimension $N = 2j + 1$. Since J_3 is Hermitian it can be diagonalized. Also, according to Schur's lemma the unique $SU(2)$ Casimir $J^2 = \sum_i J_i^2$, which by definition commutes with all the generators, has a diagonal form. The corresponding basis of eigenvectors is given by the states $|j\ m\rangle$ with $m = -j, -j+1 \cdots, j$ satisfying

$$
\begin{aligned}
J_3 |j\ m\rangle &= m|j\ m\rangle, \\
J^2 |j\ m\rangle &= j(j+1)|j\ m\rangle.
\end{aligned}
\tag{A.9}
$$

Let V_j be the base vector space on which the representation ρ_j is realized. The states $|j\ m\rangle$ provide an orthonormal basis such that we can write the resolution of the identity acting on states of V_j as

$$\mathbb{1}_j = \sum_j |j\ m\rangle\langle j\ m|. \tag{A.10}$$

In terms of the generators we can also write a 3d rotation operator as

$$R(\alpha, \beta, \gamma) = e^{-i\alpha J_3} e^{-i\beta J_2} e^{-i\gamma J_3}, \tag{A.11}$$

where (α, β, γ) are the Euler angles. Then we can define the *Wigner matrices*

$$D^j_{mn} = \langle jm|R(\alpha, \beta, \gamma)|jn\rangle. \tag{A.12}$$

An $SU(2)$ invariant state in the tensor product of L elements $|j_1 m_1\rangle \otimes \cdots \otimes |j_L m_L\rangle$ is called an intertwiner $|\iota\rangle$. Let us take for example the tensor product of three states $|j_1 m_1\rangle \otimes |j_2 m_2\rangle \otimes |j_3 m_3\rangle \in \bigotimes_i V_{j_i}$, with $i = 1, 2, 3$. The invariant space $\mathrm{Inv}_{SU(2)} \bigotimes_i V_{j_i}$ is spanned by a unique intertwiner which is a tensor with three indices such that any invariant state is proportional to the following

$$|\iota\rangle = \sum_{m_1, m_2, m_3} \iota^{m_1 m_2 m_3} |j_1 m_1\rangle \otimes |j_2 m_2\rangle \otimes |j_3 m_3\rangle, \tag{A.13}$$

where we use the Wigner 3j-symbols

$$\iota^{m_1 m_2 m_3} = \begin{pmatrix} j_1 & j_2 & j_3 \\ m_1 & m_2 & m_3 \end{pmatrix} \equiv \frac{(-1)^{j_1 - j_2 - m_3}}{\sqrt{2j_3 + 1}} \langle j_1 m_1 j_2 m_2 | j_3 - m_3 \rangle, \qquad (A.14)$$

written in terms of the Clebsh-Gordan coefficients. The invariant contraction of four Wigner 3j-symbols defines a Wigner 6j-symbol

$$\begin{Bmatrix} j_1 & j_2 & j_3 \\ j_4 & j_5 & j_6 \end{Bmatrix} = \sum_{m_1, \ldots, m_6} (-1)^{\sum_{k=1}^{6}(j_k - m_k)} \begin{pmatrix} j_1 & j_2 & j_3 \\ -m_1 & -m_2 & -m_3 \end{pmatrix} \begin{pmatrix} j_1 & j_5 & j_6 \\ m_1 & -m_5 & m_6 \end{pmatrix}$$
$$\times \begin{pmatrix} j_4 & j_2 & j_6 \\ m_4 & m_2 & -m_6 \end{pmatrix} \begin{pmatrix} j_4 & j_5 & j_3 \\ -m_4 & m_5 & m_3 \end{pmatrix}.$$
$$(A.15)$$

In Chapter 3 a fundamental step, which realizes the first appearance of the spins in the quantum theory of gravity, is determined by the application of the *Peter-Weyl theorem*. It states that the Wigner matrix elements (A.12), seen as functions of $SU(2)$, are orthogonal with respect to the scalar product defined by the Haar measure

$$\int \mathrm{d}g = \frac{1}{16\pi^2} \int_0^{2\pi} \mathrm{d}\alpha \int_0^{\pi} \sin\beta \mathrm{d}\beta \int_0^{4\pi} \mathrm{d}\gamma, \qquad (A.16)$$

which is an invariant measure such that for $g, h \in SU(2)$ and given a test function $F(g)$ the following relations hold

$$\int \mathrm{d}g F(g) = \int \mathrm{d}g F(g^{-1}) = \int \mathrm{d}g F(g \cdot h) = \int \mathrm{d}g F(h \cdot g). \qquad (A.17)$$

Explicitly, the Wigner matrices satisfy

$$\int \mathrm{d}g \overline{D_{m'n'}^{j'}(g)} D_{mn}^j(g) = \frac{1}{2j+1} \delta^{jj'} \delta_{mm'} \delta_{nn'}. \qquad (A.18)$$

Then they form an orthogonal basis in the Hilbert space

$$\mathcal{H} = L_2[SU(2), \mathrm{d}g], \qquad (A.19)$$

of square integrable functions of $SU(2)$ with the Haar measure $\mathrm{d}g$. Given such Hilbert space, we can decompose it into finite dimensional subspaces of spin j spanned by the matrix elements of $D^j(g)$.

A.2   The group Spin(4)

This appendix extends the informations provided in section 4.1.1. The group of four dimensional rotations $SO(4)$ can be realized as $SU(2) \times SU(2)$ in the following way: given a vector $x^I \in \mathbb{R}^4$ one can build the matrix $\hat{x} \equiv x^I \tau_I$ with $\tau_0 = \mathbb{1}$ and $\tau_i = i\sigma_i$ (using the Pauli matrices (A.4)) i.e.,

$$\hat{x} = \begin{pmatrix} x^0 + ix^3 & ix^1 + x^2 \\ ix^1 - x^2 & x^0 - ix^3 \end{pmatrix}. \tag{A.20}$$

We also require that

$$\det \hat{x} = \|x\|^2. \tag{A.21}$$

Then, we can use two $SU(2)$ elements (g_1, g_2) to act as a rotation in the following way

$$g_1 \hat{x} g_2^{-1} = \hat{y}, \qquad \text{and} \qquad \det \hat{x} = \det \hat{y}. \tag{A.22}$$

Since (g_1, g_2) and $(-g_1, -g_2)$ have the same effect on $\hat{x}$, one has the isomorphism

$$SO(4) \simeq SU(2) \times SU(2)/\mathbb{Z}^2. \tag{A.23}$$

The group Spin (4) is the double cover of SO(4) and they have the same algebra.

Let us call $|j^+ \ j^- \ m^+ \ m^-\rangle$ a vector in the base space $V_{(j^+,j^-)}$ where the Spin(4) representations act. This vectors are eigenstates of the two Casimirs $C_1 = J_+^2 + J_-^2$, $C_2 = J_+^2 - J_-^2$ and of the two angular momenta operators $J_{3,\pm}$ such that

$$\begin{aligned} C_1|j^+ \ j^- \ m^+ \ m^-\rangle &= (j^+(j^+ + 1) + j^-(j^- + 1))|j^+ \ j^- \ m^+ \ m^-\rangle, \\ C_2|j^+ \ j^- \ m^+ \ m^-\rangle &= (j^+(j^+ + 1) + j^-(j^- + 1))|j^- \ j^- \ m^+ \ m^-\rangle, \\ J_{3,\pm}|j^+ \ j^- \ m^+ \ m^-\rangle &= m^\pm|j^- \ j^- \ m^+ \ m^-\rangle. \end{aligned} \tag{A.24}$$

The algebra of $spin(4)$ can be completely described in terms of generators of the subgroups of rotations L_i and of boosts K_i. Let us call $L_\pm = L_1 \pm iL_2$ and $K_\pm = K_1 \pm iK_2$. The algebra then is

$$\begin{aligned} &[L_3, L_\pm] = \pm L_\pm, \quad [L_3, K_\pm] = \pm K_\pm, \quad [L_+, L_-] = 2L_3, \quad [K_+, K_-] = 2L_3, \\ &[K_3, L_\pm] = \pm K_\pm, \quad [L_\pm, K_\mp] = \pm 2K_3, \quad [K_3, K_\pm] = \pm L_\pm, \\ &[L_+, K_+] = [L_-, K_-] = [L_3, K_3] = 0. \end{aligned} \tag{A.25}$$

The Casimirs become $C_1 = L^2 + K^2$ and $C_2 = \vec{K} \cdot \vec{L}$. The action of the

generators on the basis $|j^+ \ j^- \ j \ m\rangle$ is

$$
\begin{aligned}
L_3 \, |j^+ \ j^- \ j \ m\rangle &= m \, |j^+ \ j^- \ j \ m\rangle, \\
L_\pm \, |j^+ \ j^- \ j \ m\rangle &= \sqrt{(j \pm m + 1)(j \mp m)} \, |j^+ \ j^- \ j \ m \pm 1\rangle, \\
K_3 \, |j^+ \ j^- \ j \ m\rangle &= \alpha_j \sqrt{j^2 - m^2} \, |j^+ \ j^- \ j - 1 \ m\rangle \\
&\quad - \alpha_{j+1} \sqrt{(j+1)^2 - m^2} \, |j^+ \ j^- \ j + 1 \ m\rangle \\
&\quad + \gamma_j m |j^+ \ j^- \ j \ m\rangle, \\
K_\pm \, |j^+ \ j^- \ j \ m\rangle &= \pm \alpha_j \sqrt{(j \mp m)(j \mp m - 1)} \, |j^+ \ j^- \ j - 1 \ m \pm 1\rangle \\
&\quad \pm \alpha_{j+1} \sqrt{(j \pm m + 1)(j \pm m + 2)} \, |j^+ \ j^- \ j + 1 \ m \pm 1\rangle \\
&\quad + \gamma_j \sqrt{(j \mp m)(j \pm m + 1)} \, |j^+ \ j^- \ j \ m \pm 1\rangle.
\end{aligned}
\tag{A.26}
$$

having defined

$$
\begin{aligned}
\alpha_j &= \sqrt{\frac{(j^2 - (j^+ + j^- + 1)^2))(j^2 - (j^+ - j^-)^2)}{j^2(4j^2 - 1)}}, \\
\gamma_j &= \frac{j^+(j^+ + 1) - j^-(j^- + 1)}{j(j + 1)}.
\end{aligned}
\tag{A.27}
$$

A.3 Bivector conventions

A bivector $B_{ab} = -B_{ba} \in \bigwedge^2 \mathbb{R}^4$, $a, b = 0, 1, 2, 3$, can be dualized via the Hodge operator

$$
(*B)_{ab} := \frac{1}{2} \epsilon_{abcd} B_{cd},
\tag{A.28}
$$

where indices are raised and lowered with the Kronecker delta δ_{ab}. The Killing form on $\bigwedge^2 \mathbb{R}^4$ is taken to be positive definite as

$$
\langle B_1, B_2 \rangle := -\frac{1}{4} \text{tr}(B_1 B_2).
\tag{A.29}
$$

The isomorphism $\bigwedge^2 \mathbb{R}^4 \simeq \mathbb{R}^3 \oplus \mathbb{R}^3$

$$
B \leftrightarrow (\vec{b}^+, \vec{b}^-),
\tag{A.30}
$$

is given by

$$
b^{\pm,I} = \frac{1}{2} \left(B_{0I} \pm \frac{1}{2} \epsilon_{IJK} B_{JK} \right),
\tag{A.31}
$$

with $I = 1, 2, 3$. The wedge product of two bivectors B and C is defined to be

$$(B \wedge C)_{abcd} = \frac{1}{24} \epsilon_{abcd} \epsilon^{efgh} B_{ef} C_{gh}. \tag{A.32}$$

Acting with the Hodge dual on this yields a number which is

$$\begin{aligned} *(B \wedge C) &= \frac{1}{24} \epsilon^{efgh} B_{ef} C_{gh} \\ &= \frac{1}{12} \left(\vec{b}^+ \cdot \vec{c}^+ - \vec{b}^- \cdot \vec{c}^- \right), \end{aligned}$$

and which can be regarded as the expression for the 4d volume in the volume simplicity constraint [39, 72].

Appendix B

Matrices and determinants of deformed amplitude

The Hessian matrix of a term at level n of the expansion (4.26) is rather involved, and needs to be treated with care. Its matrix elements are given by (4.38), (4.39), (4.41), (4.43), (4.44), and (4.45). In all that follows, remember that the indices a, b, a', b' are not free, but (ab) and $(a'b')$ label the links in the graph which are crossing. If we need free indices from the beginning of the alphabet to indicate nodes, we'll begin with $c, d, \ldots$.

With this, we get that the final Hessian matrix is of the form

$$H = \begin{pmatrix} A & B \\ B^T & C \end{pmatrix}, \tag{B.1}$$

where C is the same Hessian matrix as in the undeformed case, B is the matrix of mixed X_c^I and angle variables, and A is the quadratic matrix of two angle derivatives. We have

$$\det(H) = \det(A) \det(C - B^T A^{-1} B). \tag{B.2}$$

First, we consider the matrix $4(n-1) \times 4(n-1)$-dimensional matrix A. It is of the form

$$A = \begin{pmatrix} D & 0 \\ 0 & D' \end{pmatrix}, \tag{B.3}$$

where the order of the indices is as:

$$\phi_1, \ldots, \phi_{n-1}, \theta_1, \ldots, \theta_{n-1}, \xi_1, \ldots, \xi_{n-1}, \chi_1, \ldots, \chi_{n-1}. \tag{B.4}$$

D is therefore the $2(n-1) \times 2(n-1)$-dimensional matrix which has the form

$$D = \frac{j_{ab}}{2} \begin{pmatrix} E & F \\ -F & E \end{pmatrix}, \qquad D' = \frac{j_{a'b'}}{2} \begin{pmatrix} E & F \\ -F & E \end{pmatrix},$$

with E and F being $(n-1) \times (n-1)$-dimensional matrices, with

$$E_{rr} = -2, \qquad r = 1, \ldots, n-1,$$

$$E_{r,r+1} = E_{r+1,r} = 1, \qquad r = 1, \ldots, n-2,$$

$$F_{r,r+1} = i \qquad r = 1, \ldots, n-2,$$

$$F_{r+1,r} = -i, \qquad r = 1, \ldots, n-2,$$

and all other entries being equal to zero. One readily computes

$$\det(D) = j_{ab}^{2(n-1)}, \qquad \det(D') = j_{a'b'}^{2(n-1)}, \tag{B.5}$$

as well as

$$D^{-1} = \frac{1}{2j_{ab}} \begin{pmatrix} K & L \\ -L & K \end{pmatrix}, \tag{B.6}$$

$$(D')^{-1} = \frac{1}{2j_{a'b'}} \begin{pmatrix} K & L \\ -L & K \end{pmatrix},$$

with

$$K_{rs} = -\delta_{rs} - 1, \qquad L_{rs} = \begin{cases} i & r < s \\ 0 & r = s \\ -i & r > s \end{cases} \tag{B.7}$$

with $r, s = 1, \ldots, n-1$. With this, we get

$$\det(A) = (j_{ab}j_{a'b'})^{2(n-1)}. \tag{B.8}$$

Next we are turning our attention to the part $B^T A^{-1} B$. We note that the matrix B is of dimension $4(n-1) \times 3N$, where $3N$ is the number of different values of the multi-index (cI), i.e. N is the number of nodes in the graph. Out of these $3N$ columns, only twelve contain (potentially) nonzero entries, namely $aI, bI, a'I$, and $b'I$, with $I = 1, 2, 3$. These columns are (u runs from 1 to $4(n-1)$, in the order (B.4) given above):

$$B_{u,(aI)} = x^I \delta_{u,1} - ix^I \delta_{u,n},$$

$$B_{u,(bI)} = -x^I \delta_{u,1} + ix^I \delta_{u,n},$$

$$B_{u,(a'I)} = y^I \delta_{u,2n-1} - iy^I \delta_{u,3n-2},$$

$$B_{u,(b'I)} = -y^I \delta_{u,2n-1} + iy^I \delta_{u,3n-2},$$

with $x^I = j_{ab}\left(iV_2^I - V_1^I\right)$ and $y^I = j_{a'b'}\left(i(V')_2^I - (V')_1^I\right)$. Denote

$$M := B^T A^{-1} B, \tag{B.9}$$

then it is clear that M is a $3N \times 3N$ matrix, which has zero entries until both row and column index are equal to one of the twelve combinations $(aI), \ldots (b'I)$ above. Now it is straightforward to show that also

$$M_{(aI)(a'J)} = M_{(aI)(b'J)} = M_{(bI)(a'J)} = M_{(bI)(b'J)} = 0,$$

and similarly for other mixed combinations. This is clearly the case, since A^{-1} is block-diagonal, as can be seen from (B.3). The potentially nonzero entries are

$$
\begin{aligned}
M_{(aI)(aJ)} &= \sum_{u,v=1}^{2(n-1)} B_{u,(aI)} B_{v,(aJ)} (D^{-1})_{uv} \\
&= \frac{1}{2j_{ab}}\left(x^I x^J K_{11} - 2i x^I x^J L_{11} + (ix^I)(ix^J)K_11\right) \\
&= 0,
\end{aligned}
$$

as can be seen from (B.6) and (B.7). We also get

$$
\begin{aligned}
M_{(aI)(bJ)} &= \sum_{u,v=1}^{2(n-1)} B_{u,(aI)} B_{v,(bJ)} (D^{-1})_{uv} \\
&= \frac{1}{2j_{ab}}\left(- x^I x^J K_{11} + 2i x^I x^J F_{11} + (-ix^I)(ix^J)K_{11}\right) \\
&= 0.
\end{aligned}
$$

Similar relations hold for $M_{(a'I)(a'J)}$, etc., which lets us conclude that

$$M = 0. \tag{B.10}$$

With (B.2) and (B.8), this immediately leads to

$$\det(H) = (j_{ab}j_{a'b'})^{2(n-1)} \det(C), \tag{B.11}$$

where C is the Hessian matrix of the undeformed case.

Appendix C

Geometric properties of Hyperfrustum

Here we derive some geometric properties of the hyperfrustum introduced in Chapter 5. Although all the formulas that we are going to derive can be found by assigning a set of four dimensional coordinates to the elements in the boundary of the hyperfrustum, we will propose different solutions which do not require this labeling.

C.1 Dihedral angles

The dihedral angles Θ_{ab} between the couples of hexahedra in the boundary of a hyperfrustum (as depicted in figure 5.4) can be found from the critical points in table 5.1 using the following formula (see [73])

$$\cos\Theta_{ab} = N_a \cdot N_b = \frac{\chi_{ab}}{2}\mathrm{tr}\Big[g_a(\Sigma_1)g_a(\Sigma_2)^{-1}g_b(\Sigma_2)g_b(\Sigma_1)^{-1}\Big], \qquad (C.1)$$

being N_a and N_b the four dimensional outward-pointing normals to the hexahedra a and b and

$$\chi_{ab} = \begin{cases} 1 & \text{if } a,b \in [0,3] \\ 1 & \text{if } a,b \in [4,7] \\ -1 & \text{if } a \in [0,3] \wedge b \in [4,7] \\ -1 & \text{if } a \in [4,7] \wedge b \in [0,3] \end{cases}$$

Notice that this prefactor is necessary since imposing the condition (5.1) we have chosen outward-pointing normals to describe the hexahedra $a = 0,1,2,3$ and inward-pointing normals to describe the hexahedra $a = 4,5,6,7$. We find six dihedral angles $\Theta = \theta$ associated to hexahedra which meet along the faces of the cube 0, six dihedral angles $\Theta' = \pi - \theta$ associated to hexahedra meeting

along the faces of the cube 7 and twelve dihedral angles $\Theta'' = \arccos(\cos^2 \theta)$ corresponding to boundary frusta meeting along their side faces. These angles are the four dimensional analogue of the one represented in figure C.1 on the left.
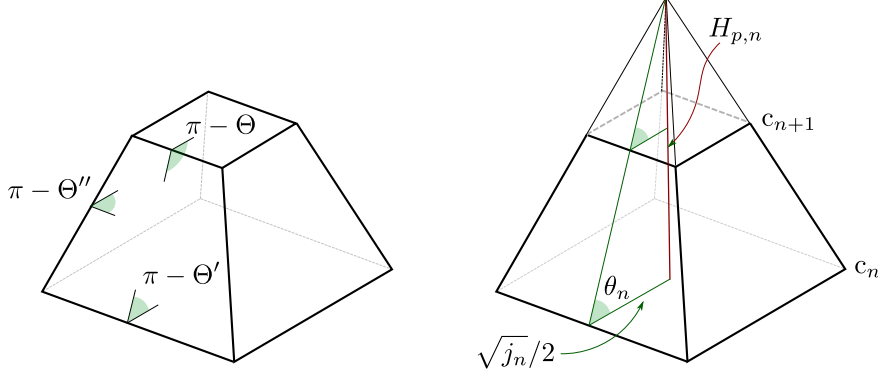

Figure C.1: A 3d representation of a 4d hyperfrustum. The top and bottom square faces represent cubes. The side faces represent squared pyramidal frusta.

C.2 Volume of a hyperfustum

For the following analysis we refer to figure 5.8. The volume V_n of the hyperfrustum F_n that appears in equation (5.40) can be computed as the difference of the volumes of two four dimensional pyramids with base cubes c_n and c_{n+1}. A comparison with the three dimensional representation in figure C.1 on the right may be helpful to get an intuitive understanding. The volume of the four dimensional pyramids with base cubes c_n and c_{n+1} are

$$V_{p,n} = \frac{1}{4} H_{p,n} j_n^{3/2}, \qquad V_{p,n+1} = \frac{1}{4} H_{p,n+1} j_{n+1}^{3/2}. \tag{C.2}$$

being $H_{p,n}$ and $H_{p,n+1}$ the heights of the pyramids. These have to be determined in order to ensure that the 'slope' of the hyperpiramidal sides is the same as for the hyperfrustum. Their values are

$$H_{p,n} = \frac{1}{2} \sqrt{j_n} \tan \theta_n, \qquad H_{p,n+1} = \frac{1}{2} \sqrt{j_{n+1}} \tan \theta_n, \tag{C.3}$$

and they are constrained so that their difference gives the height of the hyperfrustum (5.25). Finally, the four dimensional volume of the hyperfrustum is given by

$$V_n = V_{p,n} - V_{p,n+1} = \frac{1}{8} (j_n^2 - j_{n+1}^2) \tan \theta_n. \tag{C.4}$$

Using equation (5.30) for the angle θ_n, one can easily find the expression (5.40) of the volume of the hyperfrustum in terms of the spin variables.

Appendix D

Numeric integration method

The vital ingredient of this article is the calculation of expectation values of geometrical observables in the spin foam state sum. Since we are working in the large j-limit, we can replace the sums over irreducible representations by integrals and assume the spins to be continuous. However since the spin foam amplitudes are intricate functions of the spins j, these integrations generically cannot be performed analytically. As in a similar analysis for cuboid-shaped spin foams REF. we will perform these integrations numerically.

We perform our numerical simulations in the programming language `Julia` REF and use algorithms suitable for higher-dimensional integration from the `Cuba` package REF. See REF for the package and documentation how to use these algorithms in `Julia`.

While the `Cuba` package contains several algorithms, most of which employ Monte Carlo techniques, we use a *deterministic* algorithm called `Cuhre`. It roughly works as follows: Similar to Monte Carlo algorithms, the integrand is evaluated at several points. `Cuhre` then attempts to approximate the integrand by a polynomial in the integration variables and estimates the error. If the error is larger than requested, the region with the largest error gets subdivided and the algorithm is iterated. Once this procedure has sufficiently converged, or the maximum number of iterations has been reached, the polynomials are used to deterministically evaluate the integral.

For our purposes this algorithm is particularly useful since it is more efficient for integrating oscillatory integrands than ordinary Monte Carlo techniques, at least if the dimensionality of the integrand is not too high[1]. Indeed, as Frusta configurations allow for curvature, the vertex amplitude is a sum of several oscillating terms, which marks an important generalization compared to the pure cuboid case. Fortunately Hyperfrusta are prescribed by only three spins, compared to six of a hypercuboid, which. Together with the large

---

[1]To approximate higher dimensional regions by polynomials requires considerably more sample points rendering the algorithm less efficient.

amount of symmetry in these configurations, we can study discretizations containing many spin foam vertices, which only depend on a few spins. Indeed most of the integrations performed in this article are two dimensional, which can be efficiently performed.

Another generalization compared to the cuboid case is the necessity of introducing a cut-off on the spins. While in the cuboid case we implemented an embedding map fixing the total area of a coarse face, we a priori cannot enforce such a restriction onto the hyperfrusta. To efficiently perform the integrals, an upper cut-off on the spins is necessary. Usually one then has to carefully check that the result does not change under gradually increasing the cut-off. In our case this question is closely tied to the value of the parameter α as it determines whether large or small spins are preferred. Generically if α is too large the result is cut-off dependent as the amplitudes diverge for growing spins. We have performed our simulations in a regime of α where the results converge for relatively small cut-off $j_{\max} \sim 10$. Fortunately this is also the regime of interesting dynamics.

Thus the difficulty of the numerics stems less from the integrand itself but from the fact that we have to scan a 3-dimensional parameter space. To quickly generate the results we have used the local HPC at Perimeter Institute, e.g. to perform 1024 one- and two-dimensional integrations took roughly 12 hours on a single core. This can be further accelerated as the `Cuba` package in `Julia` can be straightforwardly vectorized and parallelized.

Bibliography

[1] G. Aad *et al.*, "Observation of a new particle in the search for the Standard Model Higgs boson with the ATLAS detector at the LHC," *Phys. Lett.*, vol. B716, pp. 1–29, 2012.

[2] B. P. Abbott *et al.*, "Observation of Gravitational Waves from a Binary Black Hole Merger," *Phys. Rev. Lett.*, vol. 116, no. 6, p. 061102, 2016.

[3] D. J. Griffiths, *Introduction to elementary particles; 2nd rev. version.* Physics textbook, New York, NY: Wiley, 2008.

[4] C. W. Chou, D. B. Hume, T. Rosenband, and D. J. Wineland, "Optical Clocks and Relativity," *Science*, vol. 329, p. 1630, Sept. 2010.

[5] R. M. Wald, *General Relativity.* Chicago, USA: Chicago Univ. Pr., 1984.

[6] T. Aoyama, M. Hayakawa, T. Kinoshita, and M. Nio, "Tenth-Order QED Contribution to the Electron g-2 and an Improved Value of the Fine Structure Constant," *Phys. Rev. Lett.*, vol. 109, p. 111807, 2012.

[7] N. Ashby, "Relativity in the global positioning system," *Living Reviews in Relativity*, vol. 6, p. 1, Jan 2003.

[8] G. 't Hooft, "Naturalness, chiral symmetry, and spontaneous chiral symmetry breaking," *NATO Sci. Ser. B*, vol. 59, pp. 135–157, 1980.

[9] M. E. Peskin, "Beyond the standard model," in *1996 European School of High-Energy Physics, Carry-le-Rouet, France, 1-14 Sep 1996: Proceedings*, pp. 49–142, 1997.

[10] S. Weinberg, *Gravitation and Cosmology: Principles and Applications of the General Theory of Relativity.* New York: Wiley, 1972.

[11] E. Komatsu, K. M. Smith, J. Dunkley, C. L. Bennett, B. Gold, G. Hinshaw, N. Jarosik, D. Larson, M. R. Nolta, L. Page, D. N. Spergel, M. Halpern, R. S. Hill, A. Kogut, M. Limon, S. S. Meyer, N. Odegard,

G. S. Tucker, J. L. Weiland, E. Wollack, and E. L. Wright, "Seven-year wilkinson microwave anisotropy probe (wmap) observations: Cosmological interpretation," *The Astrophysical Journal Supplement Series*, vol. 192, no. 2, p. 18, 2011.

[12] A. H. Guth, "The Inflationary Universe: A Possible Solution to the Horizon and Flatness Problems," *Phys. Rev.*, vol. D23, pp. 347–356, 1981. [Adv. Ser. Astrophys. Cosmol.3,139(1987)].

[13] A. D. Linde, "Inflation and string cosmology," *Prog. Theor. Phys. Suppl.*, vol. 163, pp. 295–322, 2006.

[14] S. Carlip, "Black Hole Thermodynamics," *Int. J. Mod. Phys.*, vol. D23, p. 1430023, 2014.

[15] S. Weinberg, *Dreams of a Final Theory*. Pantheon Books, 1992.

[16] G. 't Hooft and M. J. G. Veltman, "One loop divergencies in the theory of gravitation," *Ann. Inst. H. Poincare Phys. Theor.*, vol. A20, pp. 69–94, 1974.

[17] M. H. Goroff and A. Sagnotti, "The Ultraviolet Behavior of Einstein Gravity," *Nucl. Phys.*, vol. B266, pp. 709–736, 1986.

[18] S. Weinberg, *The Quantum theory of fields. Vol. 1: Foundations*. Cambridge University Press, 2005.

[19] S. L. Adler, "Axial-vector vertex in spinor electrodynamics," *Phys. Rev.*, vol. 177, pp. 2426–2438, Jan 1969.

[20] Yu. V. Kuzmin, "Finite nonlocal gravity," *Sov. J. Nucl. Phys.*, vol. 50, pp. 1011–1014, 1989. [Yad. Fiz.50,1630(1989)].

[21] K. S. Stelle, "Renormalization of Higher Derivative Quantum Gravity," *Phys. Rev.*, vol. D16, pp. 953–969, 1977.

[22] D. Anselmi, "On the quantum field theory of the gravitational interactions," *JHEP*, vol. 06, p. 086, 2017.

[23] D. Anselmi and M. Piva, "The Ultraviolet Behavior of Quantum Gravity," *JHEP*, vol. 05, p. 027, 2018.

[24] P. A. R. Ade *et al.*, "Planck 2015 results. XX. Constraints on inflation," *Astron. Astrophys.*, vol. 594, p. A20, 2016.

[25] K. Becker, M. Becker, and J. H. Schwarz, *String theory and M-theory: A modern introduction*. Cambridge University Press, 2006.

[26] L. Susskind, "The Anthropic landscape of string theory," pp. 247–266, 2003.

[27] M. R. Douglas, "The Statistics of string / M theory vacua," *JHEP*, vol. 05, p. 046, 2003.

[28] L. Smolin, "The Case for background independence," pp. 196–239, 2005.

[29] J. C. Baez, "An Introduction to spin foam models of quantum gravity and BF theory," *Lect. Notes Phys.*, vol. 543, pp. 25–94, 2000.

[30] A. Perez, "The Spin Foam Approach to Quantum Gravity," *Living Rev. Rel.*, vol. 16, p. 3, 2013.

[31] C. Rovelli, *Quantum gravity*. Cambridge Monographs on Mathematical Physics, Cambridge, UK: Univ. Pr., 2004.

[32] H. Nicolai, K. Peeters, and M. Zamaklar, "Loop quantum gravity: An Outside view," *Class. Quant. Grav.*, vol. 22, p. R193, 2005.

[33] M. Rocek and R. M. Williams, "Quantum Regge Calculus," *Phys. Lett.*, vol. 104B, p. 31, 1981.

[34] D. Oriti, "The Group field theory approach to quantum gravity," pp. 310–331, 2006.

[35] J. Ambjorn, J. Jurkiewicz, and R. Loll, "Dynamically triangulating Lorentzian quantum gravity," *Nucl. Phys.*, vol. B610, pp. 347–382, 2001.

[36] M. E. Peskin and D. V. Schroeder, *An Introduction to quantum field theory*. Reading, USA: Addison-Wesley, 1995.

[37] A. Codello, R. Percacci, and C. Rahmede, "Investigating the Ultraviolet Properties of Gravity with a Wilsonian Renormalization Group Equation," *Annals Phys.*, vol. 324, pp. 414–469, 2009.

[38] B. Bahr, "On background-independent renormalization of spin foam models," 2014.

[39] J. Engle, E. Livine, R. Pereira, and C. Rovelli, "LQG vertex with finite Immirzi parameter," *Nucl. Phys.*, vol. B799, pp. 136–149, 2008.

[40] L. Freidel and K. Krasnov, "A New Spin Foam Model for 4d Gravity," *Class. Quant. Grav.*, vol. 25, p. 125018, 2008.

[41] B. Bahr and G. Rabuffo, "Deformation of the Engle-Livine-Pereira-Rovelli spin foam model by a cosmological constant," *Phys. Rev.*, vol. D97, no. 8, p. 086010, 2018.

[42] B. Bahr, S. Kloser, and G. Rabuffo, "Towards a Cosmological subsector of Spin Foam Quantum Gravity," *Phys. Rev.*, vol. D96, no. 8, p. 086009, 2017.

[43] B. Bahr, G. Rabuffo, and S. Steinhaus, "Renormalization in symmetry restricted spin foam models with curvature," 2018.

[44] S. W. Hawking and G. F. R. Ellis, *The Large Scale Structure of Space-Time.* Cambridge Monographs on Mathematical Physics, Cambridge University Press, 2011.

[45] S. Deser, R. Jackiw, and G. 't Hooft, "Three-dimensional einstein gravity: Dynamics of flat space," *Annals of Physics*, vol. 152, no. 1, pp. 220 – 235, 1984.

[46] R. De Pietri and L. Freidel, "so(4) Plebanski action and relativistic spin foam model," *Class. Quant. Grav.*, vol. 16, pp. 2187–2196, 1999.

[47] T. Thiemann, *Modern canonical quantum general relativity.* Cambridge University Press, 2008.

[48] P. Dona and S. Speziale, "Introductory lectures to loop quantum gravity," in *Gravitation Theorie et Experience.Proceedings, Troisieme ecole de physique theorique de Jijel: Jijel, Algeria, September 26 October 03, 2009*, pp. 89–140, 2013.

[49] T. Regge, "General Relativity Without Coordinates," *Nuovo Cim.*, vol. 19, pp. 558–571, 1961.

[50] R. M. Williams, "Discrete quantum gravity: the Regge calculus approach," p. 12 p, Sep 1991.

[51] C. Rovelli and F. Vidotto, *Covariant Loop Quantum Gravity.* Cambridge Monographs on Mathematical Physics, Cambridge University Press, 2014.

[52] A. Ashtekar and R. S. Tate, "An Algebraic extension of Dirac quantization: Examples," *J. Math. Phys.*, vol. 35, pp. 6434–6470, 1994.

[53] A. Ashtekar, J. Lewandowski, D. Marolf, J. Mourao, and T. Thiemann, "Quantization of diffeomorphism invariant theories of connections with local degrees of freedom," *J. Math. Phys.*, vol. 36, pp. 6456–6493, 1995.

[54] B. Dittrich, C. Guedes, and D. Oriti, "On the space of generalized fluxes for loop quantum gravity," *Class. Quant. Grav.*, vol. 30, p. 055008, 2013.

[55] J. Lewandowski, A. Okolow, H. Sahlmann, and T. Thiemann, "Uniqueness of diffeomorphism invariant states on holonomy-flux algebras," *Commun. Math. Phys.*, vol. 267, pp. 703–733, 2006.

[56] B. Fauser, ed., *Quantum gravity: Mathematical models and experimental bounds.* 2007.

[57] A. Ashtekar and J. Lewandowski, "Representation theory of analytic holonomy C* algebras," 1993.

[58] B. Dittrich, "From the discrete to the continuous: Towards a cylindrically consistent dynamics," *New J. Phys.*, vol. 14, p. 123004, 2012.

[59] B. Dittrich and S. Steinhaus, "Time evolution as refining, coarse graining and entangling," *New J. Phys.*, vol. 16, p. 123041, 2014.

[60] A. Ashtekar and J. Lewandowski, "Quantum theory of geometry. 2. Volume operators," *Adv. Theor. Math. Phys.*, vol. 1, pp. 388–429, 1998.

[61] C. Rovelli and L. Smolin, "Discreteness of area and volume in quantum gravity," *Nucl. Phys.*, vol. B442, pp. 593–622, 1995. [Erratum: Nucl. Phys.B456,753(1995)].

[62] J. W. Barrett and I. Naish-Guzman, "The Ponzano-Regge model," *Class. Quant. Grav.*, vol. 26, p. 155014, 2009.

[63] E. R. Livine and S. Speziale, "A New spinfoam vertex for quantum gravity," *Phys. Rev.*, vol. D76, p. 084028, 2007.

[64] A. M. Perelomov, *Generalized coherent states and their applications.* 1986.

[65] L. Freidel and J. Hnybida, "A Discrete and Coherent Basis of Intertwiners," *Class. Quant. Grav.*, vol. 31, p. 015019, 2014.

[66] J. C. Baez and J. W. Barrett, "The Quantum tetrahedron in three-dimensions and four-dimensions," *Adv. Theor. Math. Phys.*, vol. 3, pp. 815–850, 1999.

[67] J. W. Barrett and L. Crane, "Relativistic spin networks and quantum gravity," *J. Math. Phys.*, vol. 39, pp. 3296–3302, 1998.

[68] J. W. Barrett, R. J. Dowdall, W. J. Fairbairn, F. Hellmann, and R. Pereira, "Lorentzian spin foam amplitudes: Graphical calculus and asymptotics," *Class. Quant. Grav.*, vol. 27, p. 165009, 2010.

[69] A. Riello, "Self-energy of the Lorentzian Engle-Pereira-Rovelli-Livine and Freidel-Krasnov model of quantum gravity," *Phys. Rev.*, vol. D88, no. 2, p. 024011, 2013.

[70] V. Bonzom and B. Dittrich, "Bubble divergences and gauge symmetries in spin foams," *Phys. Rev.*, vol. D88, p. 124021, 2013.

[71] W. Kaminski, M. Kisielowski, and J. Lewandowski, "Spin-Foams for All Loop Quantum Gravity," *Class. Quant. Grav.*, vol. 27, p. 095006, 2010. [Erratum: Class. Quant. Grav.29,049502(2012)].

[72] B. Bahr and V. Belov, "On the volume simplicity constraint in the EPRL spin foam model," 2017.

[73] J. W. Barrett, R. J. Dowdall, W. J. Fairbairn, H. Gomes, and F. Hellmann, "Asymptotic analysis of the EPRL four-simplex amplitude," *J. Math. Phys.*, vol. 50, p. 112504, 2009.

[74] H. M. Haggard, M. Han, W. Kamiński, and A. Riello, "SL(2,C) Chern-Simons Theory, a non-Planar Graph Operator, and 4D Loop Quantum Gravity with a Cosmological Constant: Semiclassical Geometry," *Nucl. Phys.*, vol. B900, pp. 1–79, 2015.

[75] W. J. Fairbairn and C. Meusburger, "Quantum deformation of two four-dimensional spin foam models," *J. Math. Phys.*, vol. 53, p. 022501, 2012.

[76] M. Han, "Cosmological Constant in LQG Vertex Amplitude," *Phys. Rev.*, vol. D84, p. 064010, 2011.

[77] H. M. Haggard, M. Han, W. Kaminski, and A. Riello, "SL(2,C) Chern-Simons Theory, Flat Connections, and Four-dimensional Quantum Geometry," 2015.

[78] B. Dittrich, "Cosmological constant from condensation of defect excitations," 2018.

[79] B. Bahr and S. Steinhaus, "Numerical evidence for a phase transition in 4d spin foam quantum gravity," *Phys. Rev. Lett.*, vol. 117, no. 14, p. 141302, 2016.

[80] B. Bahr and S. Steinhaus, "Hypercuboidal renormalization in spin foam quantum gravity," 2017.

[81] B. Bahr and S. Steinhaus, "Investigation of the Spinfoam Path integral with Quantum Cuboid Intertwiners," *Phys. Rev.*, vol. D93, no. 10, p. 104029, 2016.

[82] P. Donï¿½$\frac{1}{2}$, M. Fanizza, G. Sarno, and S. Speziale, "SU(2) graph invariants, Regge actions and polytopes," *Class. Quant. Grav.*, vol. 35, no. 4, p. 045011, 2018.

[83] B. Bahr, "Volume of 4-polytopes from bivectors," 2018.

[84] B. Bahr, "On knottings in the physical Hilbert space of LQG as given by the EPRL model," *Class. Quant. Grav.*, vol. 28, p. 045002, 2011.

[85] C. Rovelli and L. Smolin, "Knot Theory and Quantum Gravity," *Phys. Rev. Lett.*, vol. 61, p. 1155, 1988.

[86] P. Dona and G. Sarno, "Numerical methods for EPRL spin foam transition amplitudes and Lorentzian recoupling theory," *Gen. Rel. Grav.*, vol. 50, p. 127, 2018.

[87] G. Sarno, S. Speziale, and G. V. Stagno, "2-vertex Lorentzian Spin Foam Amplitudes for Dipole Transitions," *Gen. Rel. Grav.*, vol. 50, no. 4, p. 43, 2018.

[88] E. Alesci and F. Cianfrani, "A new perspective on cosmology in Loop Quantum Gravity," *Europhys. Lett.*, vol. 104, p. 10001, 2013.

[89] V. Bonzom, "Spin foam models for quantum gravity from lattice path integrals," *Phys. Rev.*, vol. D80, p. 064028, 2009.

[90] F. Hellmann and W. Kaminski, "Holonomy spin foam models: Asymptotic geometry of the partition function," *JHEP*, vol. 10, p. 165, 2013.

[91] J. Rennert and D. Sloan, "A Homogeneous Model of Spinfoam Cosmology," *Class. Quant. Grav.*, vol. 30, p. 235019, 2013.

[92] P. A. Collins and R. M. Williams, "Dynamics of the friedmann universe using regge calculus," *Phys. Rev. D*, vol. 7, pp. 965–971, Feb 1973.

[93] L. Brewin, "Friedmann cosmologies via the regge calculus," *Classical and Quantum Gravity*, vol. 4, no. 4, p. 899, 1987.

[94] S. M. Lewis, "Two cosmological solutions of Regge calculus," *Phys. Rev.*, vol. D25, pp. 306–312, 1982.

[95] A. P. Gentle, "A cosmological solution of Regge calculus," *Class. Quant. Grav.*, vol. 30, p. 085004, 2013.

[96] J. W. Barrett, M. Rocek, and R. M. Williams, "A Note on area variables in Regge calculus," *Class. Quant. Grav.*, vol. 16, pp. 1373–1376, 1999.

[97] J. Makela, "On the phase space coordinates and the Hamiltonian constraint of Regge calculus," *Phys. Rev.*, vol. D49, pp. 2882–2896, 1994.

[98] J. Makela, "Variation of area variables in Regge calculus," *Class. Quant. Grav.*, vol. 17, pp. 4991–4998, 2000.

[99] J. Makela and R. M. Williams, "Constraints on area variables in Regge calculus," *Class. Quant. Grav.*, vol. 18, p. L43, 2001.

[100] B. Dittrich and S. Speziale, "Area-angle variables for general relativity," *New J. Phys.*, vol. 10, p. 083006, 2008.

[101] R. G. Liu and R. M. Williams, "Regge calculus models of closed lattice universes," *Phys. Rev.*, vol. D93, no. 2, p. 023502, 2016.

[102] R. G. Liu and R. M. Williams, "Regge calculus models of the closed vacuum Λ-FLRW universe," *Phys. Rev.*, vol. D93, p. 024032, 2016.

[103] R. G. Liu and R. M. Williams, "Cosmological modelling with Regge calculus," 2015.

[104] R. Tsuda and T. Fujiwara, "Expanding Polyhedral Universe in Regge Calculus," 2016.

[105] I. Rivin and J.-M. Schlenker, "On the schlafli differential formula," 2000.

[106] B. Bahr and B. Dittrich, "Improved and Perfect Actions in Discrete Gravity," *Phys. Rev.*, vol. D80, p. 124030, 2009.

[107] B. Bahr and B. Dittrich, "Regge calculus from a new angle," *New J. Phys.*, vol. 12, p. 033010, 2010.

[108] H. Coxeter, "Regular polytopes," *(Methuen and Company, Ltd, London)*, 1948.

[109] K. G. Wilson and J. B. Kogut, "The Renormalization group and the epsilon expansion," *Phys. Rept.*, vol. 12, pp. 75–200, 1974.

[110] R. Oeckl, "Renormalization of discrete models without background," *Nucl. Phys.*, vol. B657, pp. 107–138, 2003.

[111] B. Bahr, "Operator Spin Foams: holonomy formulation and coarse graining," *J. Phys. Conf. Ser.*, vol. 360, p. 012042, 2012.

[112] B. Bahr, B. Dittrich, F. Hellmann, and W. Kaminski, "Holonomy Spin Foam Models: Definition and Coarse Graining," *Phys. Rev.*, vol. D87, no. 4, p. 044048, 2013.

[113] B. Dittrich, "The continuum limit of loop quantum gravity - a framework for solving the theory," 2014.

[114] Z.-C. Gu and X.-G. Wen, "Tensor-Entanglement-Filtering Renormalization Approach and Symmetry Protected Topological Order," *Phys. Rev. B*, vol. 80, p. 155131, 2009.

[115] M. Levin and C. P. Nave, "Tensor renormalization group approach to 2d classical lattice models," *Phys. Rev. Lett.*, vol. 99, p. 120601, 2007.

[116] B. Dittrich, F. C. Eckert, and M. Martin-Benito, "Coarse graining methods for spin net and spin foam models," *New J. Phys.*, vol. 14, p. 035008, 2012.

[117] H. W. Hamber, "Critical behavior in simplicial quantum gravity," *Nucl. Phys. Proc. Suppl.*, vol. 20, pp. 728–732, 1991.

[118] H. W. Hamber, "Phases of simplicial quantum gravity in four-dimensions: Estimates for the critical exponents," *Nucl. Phys.*, vol. B400, pp. 347–389, 1993.

[119] H. W. Hamber and R. M. Williams, "Renormalization group running of Newton's G: The Static isotropic case," *Phys. Rev.*, vol. D75, p. 084014, 2007.

[120] J. Ambjorn, A. Görlich, J. Jurkiewicz, A. Kreienbuehl, and R. Loll, "Renormalization Group Flow in CDT," *Class. Quant. Grav.*, vol. 31, p. 165003, 2014.

[121] T. Thiemann, *Modern Canonical Quantum General Relativity*. Cambridge: Cambridge University Press, 2008.

[122] G. Evenbly and G. Vidal, "Tensor Network Renormalization," *Phys. Rev. Lett.*, vol. 115, p. 180405, 2015.

[123] B. Dittrich, M. Martin-Benito, and E. Schnetter, "Coarse graining of spin net models: dynamics of intertwiners," *New J. Phys.*, vol. 15, p. 103004, 2013.

[124] B. Dittrich, M. Martin-Benito, and S. Steinhaus, "Quantum group spin nets: refinement limit and relation to spin foams," *Phys. Rev.*, vol. D90, p. 024058, 2014.

[125] S. Steinhaus, "Coupled intertwiner dynamics: A toy model for coupling matter to spin foam models," *Phys. Rev.*, vol. D92, no. 6, p. 064007, 2015.

[126] B. Dittrich, E. Schnetter, C. J. Seth, and S. Steinhaus, "Coarse graining flow of spin foam intertwiners," *Phys. Rev.*, vol. D94, no. 12, p. 124050, 2016.

[127] B. Dittrich, S. Mizera, and S. Steinhaus, "Decorated tensor network renormalization for lattice gauge theories and spin foam models," *New J. Phys.*, vol. 18, no. 5, p. 053009, 2016.

[128] M. C. Banuls, K. Cichy, J. I. Cirac, K. Jansen, S. Kühn, and H. Saito, "Towards overcoming the Monte Carlo sign problem with tensor networks," 2016. [EPJ Web Conf.137,04001(2017)].

[129] V. Bayle, F. Collet, and C. Rovelli, "Short-scale Emergence of Classical Geometry, in Euclidean Loop Quantum Gravity," 2016.

[130] M. H. Goroff and A. Sagnotti, "Quantum Gravity at Two Loops," *Phys. Lett.*, vol. B160, pp. 81–86, 1985.

[131] M. Niedermaier and M. Reuter, "The Asymptotic Safety Scenario in Quantum Gravity," *Living Rev. Rel.*, vol. 9, pp. 5–173, 2006.

[132] B. Bahr and B. Dittrich, "(Broken) Gauge Symmetries and Constraints in Regge Calculus," *Class. Quant. Grav.*, vol. 26, p. 225011, 2009.

[133] B. Dittrich, "How to construct diffeomorphism symmetry on the lattice," *PoS*, vol. QGQGS2011, p. 012, 2011.

[134] B. Dittrich, W. Kaminski, and S. Steinhaus, "Discretization independence implies non-locality in 4D discrete quantum gravity," *Class. Quant. Grav.*, vol. 31, no. 24, p. 245009, 2014.

[135] S. K. Asante, B. Dittrich, and H. M. Haggard, "The Degrees of Freedom of Area Regge Calculus: Dynamics, Non-metricity, and Broken Diffeomorphisms," 2018.

[136] J. Engle, "Proposed proper Engle-Pereira-Rovelli-Livine vertex amplitude," *Phys. Rev.*, vol. D87, no. 8, p. 084048, 2013.

[137] J. Engle and A. Zipfel, "Lorentzian proper vertex amplitude: Classical analysis and quantum derivation," *Phys. Rev.*, vol. D94, no. 6, p. 064024, 2016.

Acknowledgments

I want to thank first of all my supervisor Benjamin, my collaborators Sebastian S., Sebastian K., Vadim, Robin and the all the research group at DESY.

The PIER team for the huge support during these three years.

The research group at CPT in Marseille for hosting me.

My closest friends from the years of University Marco, Paco, Tiziano e Andrea. The Hamburg friends that I greet, those in Marseille that I can not wait to meet again, and all those scattered around the world.

A special thanks to my mother, my father, my little sister Claudia and to all my big family.

Un pensiero affettuoso a mio zio Franco.

Declaration

Eidesstattliche Versicherung / Declaration on oath

Hiermit versichere ich an Eides statt, die vorliegende Dissertationsschrift selbst verfasst und keine anderen als die angegebenen Hilfsmittel und Quellen benutzt zu haben.

Die eingereichte schriftliche Fassung entspricht der auf dem elektronischen Speichermedium.

Die Dissertation wurde in der vorgelegten oder einer ähnlichen Form nicht schon einmal in einem früheren Promotionsverfahren angenommen oder als ungenügend beurteilt.

Hamburg, den October 4th 2018

_____

Giovanni Rabuffo